Glycolytic Oscillations in Yeast Cells

The nonlinear dynamics of metabolism studied in living yeast cells.

Sune Danø

Chaos and Turbulence Studies
Department of Chemistry, H. C. Ørsted Institute
University of Copenhagen, Denmark

June 1999

Preface

This thesis contains the major part of my work as a master student at Chemistry Laboratory III at the Department of Chemistry at the University of Copenhagen.

I would like to thank my supervisors Preben Graae Sørensen and Finn Hynne for the opportunities that I have been given to try out my own ideas. – Both when I was working with the experiments presented here, and when I found other projects interesting. This freedom and your kindness made it all worthwhile.

Without the excellent technical skills of Torben Hansen and Aage Nissen, the experiments presented in this thesis would never have worked out. Equally important was the friendly help on the growth and handling of the yeast cells, which Bas Teusink provided during my short stay at the E. C. Slater Institute, University of Amsterdam. I would also like to thank everybody in the group of Per Amstrup Pedersen at the August Krogh Institute for discussions, good advise, and access to laboratory facilities. Good advise was also given by Bjørn Quistorff at the NMR center at the Panum Institute. At the Chemistry Laboratory IV, I would like to thank Jens Christian Poulsen for frequent use of the autoclave. The staff at the Department of Genetics kindly provided the yeast strain.

My fellow students created a good atmosphere at the laboratory, and Morten Garkier Hendriksen, Henrik Skødt, Anders Bisgaard, and Thomas Lorenzen even gave valuable advise after having read parts of this thesis. A special thank should be given to Mette Hoffmann and Henrik Skødt for sharing this office with me. You both made this a very pleasant place to work.

Finally, I would like to thank my mother; not for any sentimental reasons, but for providing competent help with the English language at all times of the day. Without your help, this thesis would have been a whole lot murkier.

Sune Danø
Copenhagen, June 1999

Contents

1
Introduction

Biology has changed from being a strictly descriptive science into being a dynamic science, dealing with control, regulation and evolution of highly complicated systems. Examples include the control and regulation of gene transcription, the hierarchy of eukaryotic compartmentation, the maintenance of cellular homoeostasis, and the pathways of intercellular communication.

All of these examples, and many more which I could equally well have mentioned, only work because the chemical reactions governing the systems are far from thermodynamic equilibrium. This allows the systems to have highly nonlinear responses when exposed to the actions of the environment or internal factors. The molecular basis of such biological systems is, in many cases, understood in impressive detail. Nevertheless, understanding the dynamics of such living systems is still a challenge.

If you consider the complexity of such systems, it is easy to see why. The chemical reaction systems, which define the dynamics, consist of many different substances, and the reactions often take place in an heterogenic environment. In principle, it is possible to calculate the development of such systems from their chemical and physical basis. But the computations are in practice too big to be performed even when using state of the art computers. On top of this comes the problem of determining the correct parameters for the modelling.

Consider the interactions among a set of chemicals in a homogeneous environment. Now, increase the complexity of the system by adding more chemical species. These species might undergo reactions with several of the other species at different rates. These rates might again depend on the instantaneous chemical composition of the system, e.g. some of the species might catalyse the reaction of some of the other species. Therefore, in the typical case the computational complexity increases in a polynominal way, when more species are added.

The computational complexity is also polynominally increased by the spatial heterogeneity found in almost all biological systems. Even though we disregard all such spatial effects, and limit our description to a small subset of the cellular metabolism, you will se in chapter 6, that this increase in complexity, as more and more details are added to the description of our experimental system, does in fact become a major practical problem.

Thus, it turns out that even though one might know all the chemical and physical details of the biological system, it is still an impossible job to calculate, from the chemical and physical basis, how it will evolve.

A similar situation is seen in other fields of science. From quantum mechanics one could in principle calculate all of the phenomena of chemistry, but in practice this cannot be done. Therefore, the problems are dealt with at a higher level of organization, which we call chemistry. At an even higher level of organization, chemistry is no longer practical, and the entities are now animals, populations and ecosystems.

Dynamics can also be described at a higher level of organization than the underlying chemical kinetics. This is done by focusing on the geometry of the phase space as described in chapter 3. Our group has been working towards experimental and theoretical approaches to this geometric description of dynamical systems for many years, and the extension of this into living sytems is the overall goal of the work presented here.

1.1 Glycolytic Oscillations

In more practical terms, the aim of my thesis work was to provide an experimental setup, in which stable metabolic oscillations in living cells can be monitored, controlled and chemically perturbed.

The organism chosen for these experiments is *Saccharomyces cerevisiae*, baker's yeast. In these cells, oscillations in the concentration of glycolytic metabolites can be measured, and the individual yeast cells are capable of synchronizing these oscillations with each other by means of acetaldehyde, which diffuses readily in and out of the cells (see chapter 4 for details on the oscillations and the synchronization mechanism).

Working with these oscillating yeast cells, one question seemed inevitable to me: Does the glycolytic oscillations fulfil a purpose, or are they just a peculiarity provoked by the special experimental conditions?

Richter and Ross (1981) show that the oscillations might in theory increase the efficiency of glycolysis by reducing the dissipation of free energy in glycolysis. Whether this is reality or just speculations, can only be judged sometime in the future when, hopefully, a detailed and accurate model of glycolysis is avaliable. In a first attempt to do such an investigation from a comprehensive glycolytic model, Termonia and Ross (1981) calculate that the oscillations in fact reduce the dissipation of free energy.

In any case, this gives no explanation why the yeast cells should synchronize their oscillations. Taking into account that they are basically unicellular organisms when living in their natural environment, this might very well be a coincidence caused by the intrinsic dynamics of glycolysis. Paradoxically, this could turn out to be the most interesting thing about the synchronization: Even though it serves no purpose, it is there ready and working[1]. Therefore, this synchronization mechanism could very well have been utilized for cell communication in multicellular organisms.

Indeed, glycolytic oscillations have been found in extracts of many other cell types, notably smooth muscle cells (Frenkel, 1968), skeletal muscle cells (Tornheim and Lowenstein, 1973), pancreatic $\beta-$cells (Chou *et al.*, 1992), tumor cells (Ibsen and Schiller, 1967), and heart cells (O'Rourke *et al.*, 1994, 1995). References to reports of glycolytic oscillations in plants and insects are given by Teusink *et al.* (1996b).

As pointed out by Betz and Chance (1965b), the oscillations in the ATP concentration make it possible for other cellular processes to couple to the glycolytic oscillations, since hydrolysis of ATP drives many biochemical reactions. This mechanism has been suggested for the pulsatory insulin secretion of $\beta-$cells (Tornheim, 1997; Civelek *et al.*, 1997), or in the spatio-temporal regulation of blood flow (Siegel *et al.*, 1997). Such couplings are even more interesting in the light of the synchronization mechanism of the yeast cells. A similar mechanism could work through the blood in order to synchronize cells of multicellular organisms; this could explain the existence of bulk oscillations of insulin concentrations, which is seen in the blood of healthy people. In Mammalians, acetaldehyde cannot be the mediator of the synchronization, since mammalian cells ferment pyruvate to lactate instead of ethanol (cf. page 9).

[1]This is an example of neutral evolution: Since many realisations of glycolysis are equally fit, new properties – that do not presently serve any purposes – can evolve from it within the limitation that the glycolytic fitness should not be compromised.

But, as it is seen from the experiments[2] cited in chapter 4, pyruvate can do the job as well if it is allowed to pass the cell membrane. With this in mind, the finding that the activity of lactate dehydrogenase is about 100-fold lower in the β-cell than in any other mammalian cell type examined thus far (Prentki (1996) and references therein), is striking. In mammals, lactate dehydrogenase is analogous to alcohol dehydrogenase in yeast. As described in chapter 4 the reaction catalyzed by this enzyme is important for the synchronization mechanism in yeast.

The value of such speculations can only be assessed through experiments. My hope is that the yeast cell will – once again – show its value as a model organism of eukaryotic cells (cf. page 6). As you will see in chapter 5, my investigations have already given new insights into the mechanism of cell synchronization, by showing that glucose – and not just acetaldehyde – can mediate the synchronization. In my mind, this makes the possible connection to insulin secretion even more interesting.

[2] In particular, the experiments which show that yeast cells respond to extracellular pyruvate perturbations at low pH values.

2
The Biological System

In this chapter, I will introduce the biological system which I have been working on. Special focus will, of course, be given to the reactions investigated. A more general description will also be given, so that other parts of the system, interacting with the part of the system under study, are also described. As general references to this chapter, please see Walker (1998) and Mathews and van Holde (1990).

In order to describe the biological system in a short and precise way, a lot of common biochemical abbreviations are used. They are not all explained in the text, but you will find a listing of abbreviations in appendix A on page 137.

2.1 Yeast

In broad terms, the system under study is yeast cells metabolising sugar. Yeasts form a vast and diverse group of organisms, that has great biotechnological and scientific importance. In fact, it is probably the only group of microorganisms, that has a cultural history dating back to prehistoric time. From the childhood of biochemistry, this use of yeast for baking and, especially, brewing, has encouraged research in yeast metabolism.

These investigations, starting with the discovery by Louis Pasteur of yeast's role in alcohol fermentation, have given much of the basic understanding of metabolism. In fact the word "enzyme" originates from Greek "en-", meaning "in", and "zyme" which means 'yeast'.

Yeast cells are eukaryotes, having cellular organelles like mitochondria, a nucleus, an endoplasmic reticulum, etc. The genome organization and the

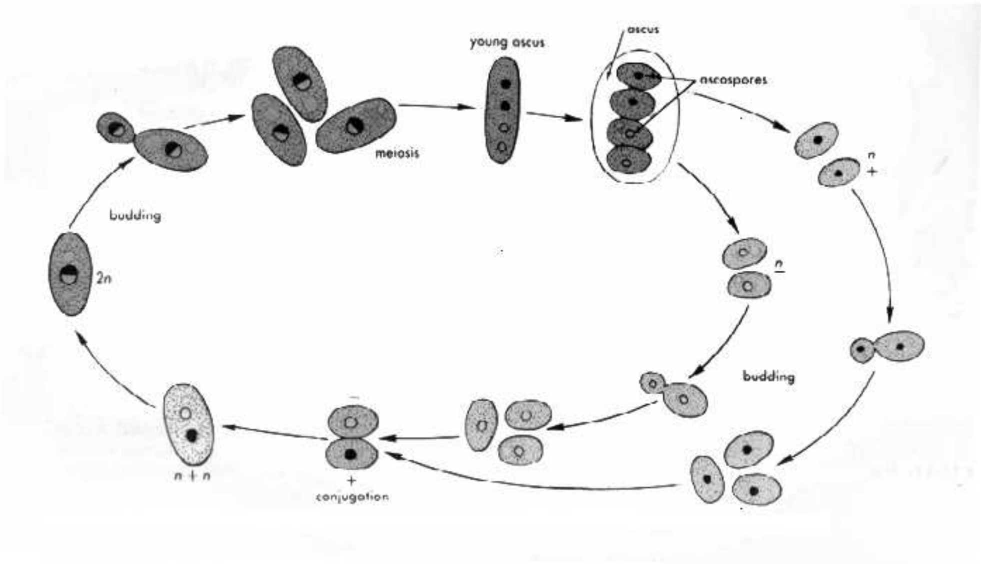

Figure 2.1: The life cycle of wild-type *Saccharomyces cerevisiae*. Reproduced from Rost *et al.* (1984).

mechanisms for transcription (DNA → mRNA), translation (mRNA → protein) and DNA replication are also similar to those of other eukaryotes. Still, yeast cells are easy to handle in the laboratory, and standard methods from microbiology can be used. Therefore, yeast cells are at the core of many new discoveries in molecular biology and cell biology.

Benefitting from this, commercial interests in yeast have grown further, because genetically engineered yeast cells are used to produce a whole range of medically and industrially important proteins. For example, the Danish medical company Novo Nordisk uses a strain of *Saccharomyces cerevisiae* to produce insulin. Insulin needs posttranslational modifications, and therefore this protein must be produced by an eukaryote.

Classification

Since the pioneering work of Emil Christian Hansen who was the first to isolate pure strains of yeast (Hansen, 1886), more than 700 species have been described. Still, it is estimated that only one out of thousand yeast species has been described.

Classical taxonomy divides yeasts into three main groups (subdivisions) according to their sexuality: Ascomycotina, Basidiomycotina and Deuteromycotina. The most common of these is the Ascomycotina, which after meiosis forms ascospores in a common sac called an ascus (figure 2.1). Basidiomycotina produces individual spores following meiosis. The last group, Deuteromycotina, consists of yeasts with no known sexual reproduction. Subdivisions are further divided into families, subfamilies, genera, species and strains.

Yeast is a very diverse group of organisms. They are all mostly unicellular, but some species have a multicellular form as well. A prominent feature of all yeasts is the cell wall on the outside of the plasma membrane. It is mostly made up of polysaccharides, and gives strength and rigidity to the yeast cells.

Yeasts can be found living with plants or animals, in water or in soils. Most yeasts live of soluble nutrients from vascular plants, but more exotic yeasts can also be found. For example, *Candida albicans* is an opportunistic pathogen yeast, causing severe problems for AIDS patients, and the Dutch elm disease – presently causing many problems in European cities – is caused by the yeast-like organism *Opiostoma ulmi*.

Saccharomyces cerevisiae

For my studies, I use a specific strain of the ascomycotic species *Saccharomyces cerevisiae* . This species is the best known and most studied species of yeast. As such, it is one of the best known organisms at all, and *Saccharomyces cerevisiae* was the first eukaryote to have its entire genome sequenced (Goffeau *et al.*, 1996). *Saccharomyces* means "sugar fungi", and indeed it is characteristic of *Saccharomyces* species that they grow well in high concentrations of sugar, which is often toxic to other microorganisms. They are fermentative yeasts, which means that they ferment the sugar into ethanol instead of oxidizing it, even though plenty of oxygen is avaliable. The resulting ethanol is toxic to most other microorganisms, but *Saccharomyces* species themselves are tolerant to ethanol concentrations of up to about 10–15%. The cells of *Saccharomyces cerevisiae* are ellipsoidal in shape, and their size is 5–10μm on the longest diameter. They divide by budding, which normally results in a small daughter cell and a larger mother cell. Each budding produces a bud scar and by counting these, mother cells have been found which have produced up to 100 daughter cells (Bartholomew and Mittwer, 1953).

In biotechnological applications, it is often of interest to know the exact strain. For our purpose, it mainly serves to insure reproducibility of the exper-

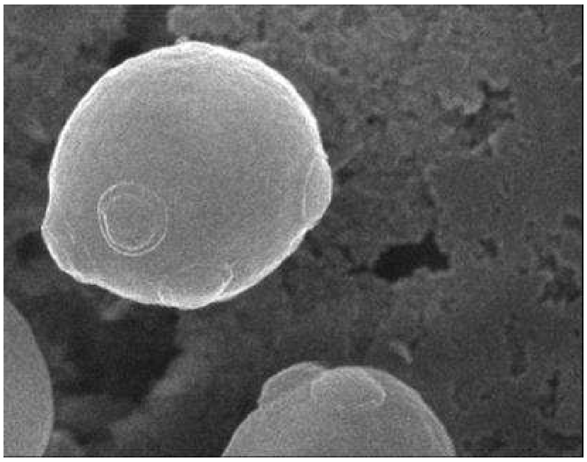

Figure 2.2: *Saccharomyces cerevisiae* as seen through the electron microscope. Notice the bud scars. The picture was found at the website of the Electron Microscopy Group, Institute of Microbiology, Academy of Sciences of the Czech Republic, Department of Biotechnology and Production of Natural Compounds, Laboratory of Mathematical and Physical Methods.

iments. Considerations on the choice of yeast are given in chapter 5.1.

2.2 Metabolism

Metabolism is a vast subject, and I shall not attempt to give a thorough coverage, since this could easily fill this thesis. In *Saccharomyces cerevisiae*, almost 600 metabolites are known, and they are interchanged by approximately ten times as many enzymes (including isozymes, which are different variants of enzymes catalysing the same reaction).

Instead I will try to give a quick overview of metabolism in *Saccharomyces cerevisiae*, leaving basic biochemistry, and subjects not directly linked to this thesis, to textbooks. In my opinion, a good basic coverage is given by Mathews and van Holde (1990).

The central biochemical reaction system of this thesis is glycolysis and the subsequent fermentation. Glycolysis, which is also known as the Embden-Meyerhof pathway, takes place in the cytoplasm of all cells of plants, fungi, and animals, and in most bacteria. It is central to energy metabolism, because it is the first steps in converting the chemical energy of sugar into chemical energy in the form of ATP, which is the form needed by the cell.

In few words, glycolysis is the oxidation of glucose to the key metabolite pyruvate:

$$\mathrm{Glc} + 2\mathrm{ADP} + 2\mathrm{P_i} + 2\mathrm{NAD^+} \longrightarrow 2\mathrm{Pyr} + 2\mathrm{ATP} + 2\mathrm{NADH} + 2\mathrm{H^+} + 2\mathrm{H_2O}$$

Pyruvate is a precursor for several parts of anabolism (see table 2.4), but most pyruvate is degraded further, in order to provide energy for the cell.

Normally, the catabolic faith of pyruvate depends on the availability of molecular oxygen. If the catabolism is aerobic, further degradation of pyruvate takes place in the mitochondria, where it is oxidized primarily by NAD^+ in the citric acid cycle.

The NADH from this oxidation is oxidized by oxygen in the electron transport chain, finally producing ATP. During anaerobiosis, some other means of re-oxidising NADH must be found, in order for the cell to maintain homeostasis. In most organisms, this problem is solved by fermentation of pyruvate itself. In yeast, this fermentation leads to the formation of ethanol:

$$\mathrm{Pyr} + \mathrm{NADH} + 2\mathrm{H}^+ \quad \longrightarrow \quad \mathrm{EtOH} + \mathrm{CO}_2 + \mathrm{NAD}^+$$

In other organisms, other fermentation products can be found. Mammalians produce lactic acid, and different microorganisms produce a wide range of small organic molecules like butyrate, acetate, formate, succinate, etc. The ethanol and CO_2 formed by the yeast are the basis of the classical commercial use of yeast for brewing and baking. Fermentation products from other microorganisms are sometimes responsible for the specific flavour of the fermented product. For example, Scotch malt whiskey is flavoured by lactic acid bacteria as well as by the yeast.

2.2.1 Glycolysis and the Subsequent Fermentation

As described above, glycolysis is at the heart of classical biochemistry, and the details of the pathway have been thoroughly investigated. The overall picture is presented in figure 2.3, where I have drawn it as a “biochemical cartoon”. In the upper part of glycolysis, the sugar is phosphorylated twice by hexokinase (HK) and phosphofructokinase (PFK). Then the sugar is cleaved into two 3-carbon substances. Oxidation of glyceraldehyde 3-phosphate (GAP) by NAD^+ is coupled to another phosphorylation, so that we now have four phosphorylations for each degraded glucose molecule. In the subsequent steps, these phosphorylations are used to produce four ATP’s from ADP in the reactions catalyzed by phosphoglycerate kinase and pyruvate kinase.

The question asked is what determines the dynamics of this sequence of reactions? The answer has several layers to it.

First of all, all the reactions are catalyzed by enzymes. Since the cytoplasmic concentration of a specific enzyme is limited, there is a maximal velocity

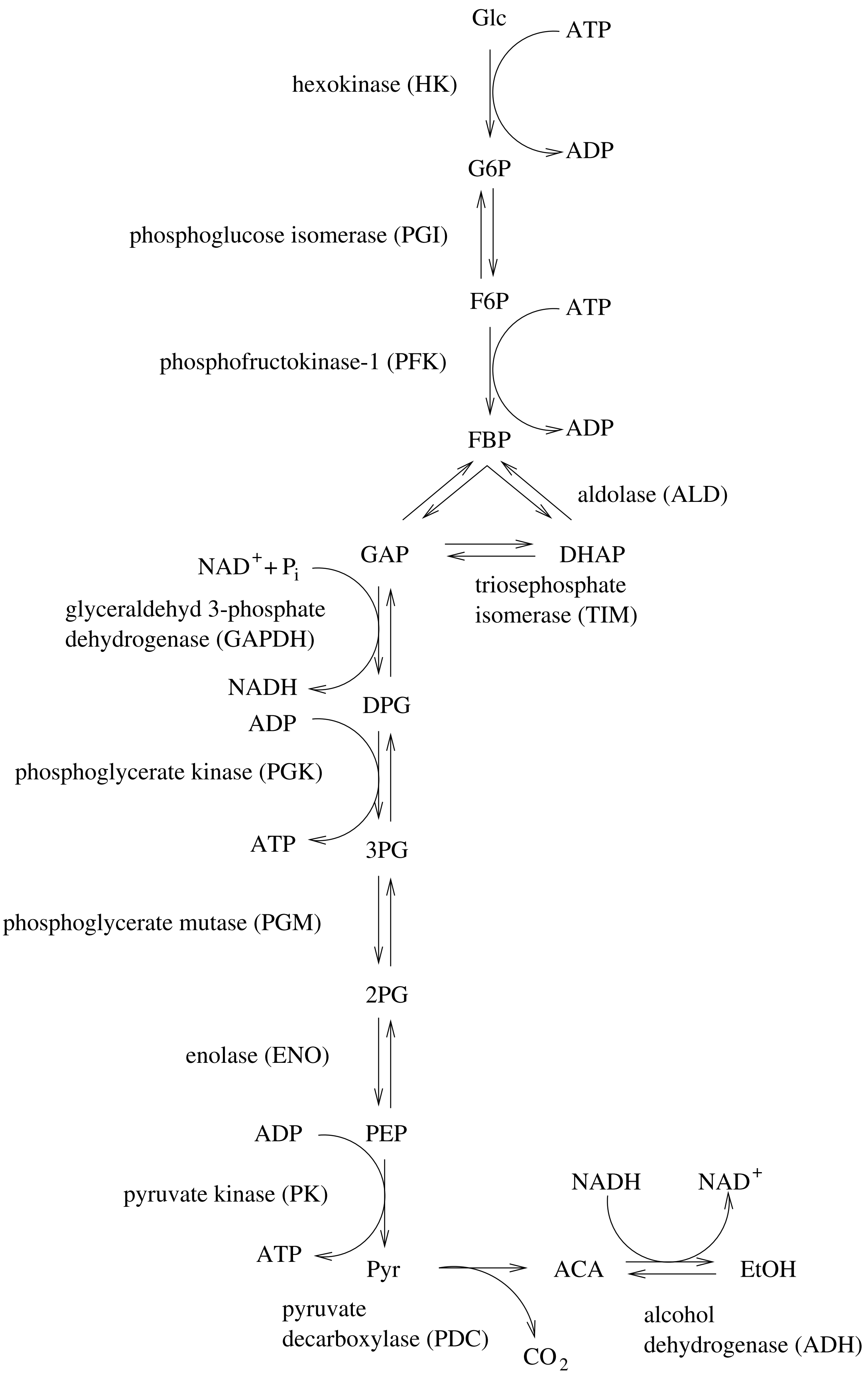

Figure 2.3: Glycolysis and the subsequent fermentation in the cytoplasm of the yeast cell.

for each reaction, independent of the concentrations of the substrates and products. This might not be true for all of the glycolytic enzymes, since some of the enzymes have high concentrations themselves (Hess *et al.*, 1973). In any case, such considerations have led to the concept of the "rate-limiting step" of an entire pathway, being the enzyme with the lowest V_{max}. In an attempt to quantify this concept, simple models of glycolysis have been analysed using metabolic control analysis (MCA), which is a kind of sensitivity analysis of the steady state. (See Fell (1997) for a nice introduction to MCA). The conclusion is, not surprisingly[1], that there is generally not any single "rate-limiting step" in glycolysis. Also, the oscillations are not controlled by a single enzyme (Bier *et al.*, 1996; Teusink *et al.*, 1996a).

More importantly, a whole range of enzymes have been overexpressed in yeast and the above conclusion holds: There is no single rate-limiting step in glycolysis (Heinisch, 1986; Schaaff *et al.*, 1989; Davis and Brindle, 1992).

There are also some stoichiometric constraints on the pathway. An obvious one is the fact that the NADH produced by GAPDH must be reoxidized, if the reactions are not to stop at GAP. In anaerobic catabolism, this is primarily done by the ADH reaction, although glycerol production oxidizes NADH too (as described on page 20). This gives a stoichiometric feedback loop, which implies that flux through the lower part of glycolysis must balance the fermentative flux to within the total amount of NAD^+ and NADH at all times.

Since ATP is "invested" in the upper part of glycolysis, something similar applies in special situations. The flux in the upper part can be limited by the availability of ATP, produced in the lower part. But since glycolysis produces two moles of ATP per mole of glucose, this only applies to transients with sudden increases in the glycolytic flux. This effect might therefore not seem to be of any practical importance, but in fact mutant strains of *Saccharomyces cerevisiae* have been found, which lack a regulatory mechanism which prevents this way of ATP exhaustion in wild type *Saccharomyces cerevisiae.* These mutants grow poorly in high concentrations of glucose (see Teusink *et al.* (1998) and references therein). This regulatory mechanism is described further below.

Apart from the enzyme kinetics and stoichiometric constraints, some of the

[1]At least four of the five models investigated were minimal models, meant to give the simplest possible description of the system. If such models were to have unimportant steps, they wouldn't be minimal models.

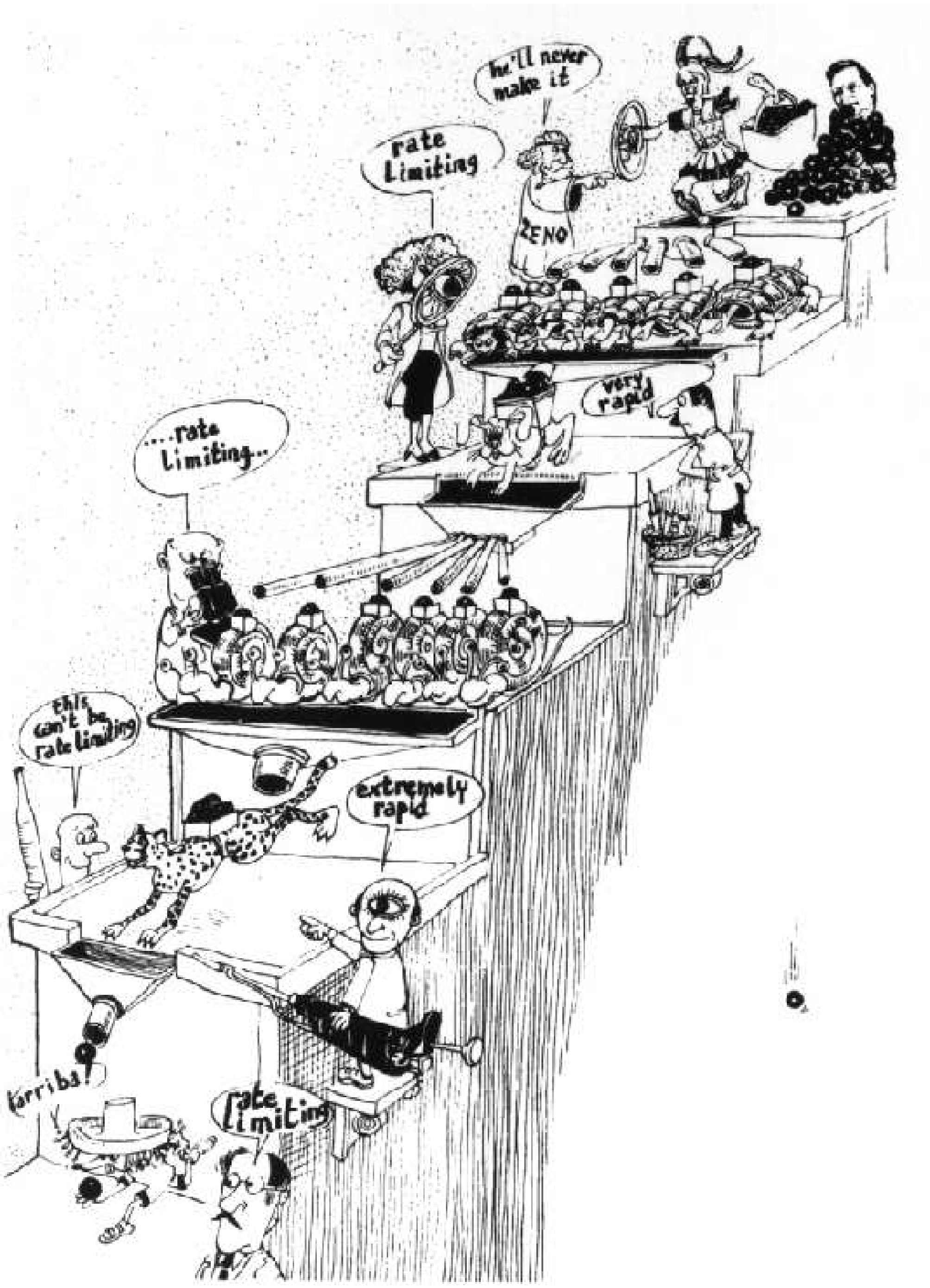

Figure 2.4: The quest for the rate-limiting step. Reproduced from A. B. Tulp (1986) Trends Biochem. Sci. **11**, 13.

glycolytic enzymes are allosterically[2] regulated by specific metabolites, often termed effectors. It is, of course, easiest to realize effectors internal to glycolysis, since such effectors are more likely to be present in the *in vitro* experiments actually performed. As a consequence, such internal glycolytic effectors were the first to be described. HK is allosterically inhibited by G6P

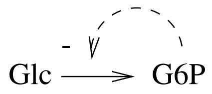

PFK is allosterically activated by AMP, ADP and its product FBP. Furthermore, it is allosterically inhibited by its substrate ATP

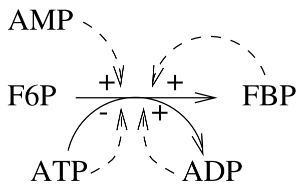

At high concentrations, FBP is an inhibitor instead of an activator. In low concentrations, fructose and fructose 1-phosphate are also activators of PFK; at high concentrations they are competitive inhibitors (Kreuzberg, 1978). Finally, PK is allosterically inhibited by its product ATP and activated by FBP

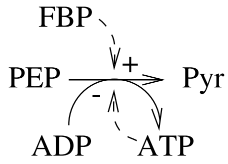

In the early 1980s it was found, that fructose 2,6-bisphosphate (F2,6BP) is a strong allosteric activator of PFK. F2,6BP is produced from F6P in a reaction catalyzed by phosphofructokinase-2 (PFK2):

$$\mathrm{F6P} + \mathrm{ATP} \quad \stackrel{\mathrm{PFK2}}{\longrightarrow} \quad \mathrm{F2,6BP} + \mathrm{ADP} + \mathrm{H}^+$$

It is now believed that F2,6BP is the fysiological most important regulator of glycolysis, because it regulates glycolysis and glyconeogenesis at the same time.

[2]From Greek “allo-” meaning “other” and “stereos” meaning “firm”, “physical” or “spatial”. That is, an allosteric effector interacts with the enzyme in some other place than the active site.

Changes in the F2,6BP level is often mediated by the second messenger cAMP. In glucose stimulated *Saccharomyces cerevisiae* the level of both cAMP[3] and F2,6BP rises and causes a strong activation of PFK and at the same time a profound inhibition of fructose 1,6-bisphosphatase, which catalyses one step in the production of glucose from pyruvate. Thus gluconeogenesis is shut down (François *et al.*, 1984). F2,6BP is also an important regulator of glycolysis and gluconeogenesis in many other cell types. As an example, in mamalian liver cells F2,6BP is lowered in response to the hormone glucagon through a phosphorylation cascade initiated by cAMP. This is an important part of our blood-sugar regulation.

Other external allosteric effectors have been found as well. Acetyl CoA and citrate from the citric acid cycle, decrease the glycolytic flux by inhibiting PK and PFK, respectively. As mentioned, there is also a regulation which prevents ATP exhaustion in the upper part of glycolysis. This is accomplished by trehalose 6-phosphate, which inhibits HK (Blazquez *et al.*, 1993). Along the same lines, the actual transport of glucose into the cell is inhibited by G6P, the product of HK.

This complicated net of regulations is shown in figure 2.5. It looks quite complicated, but the regulations can be rationalised by looking at glycolysis teleologically. Since glycolysis is responsible for the energy production in the cell, it should slow down when there is plenty of ATP avaliable, and it should speed up when ATP is needed, that is when the concentration of ADP or AMP is high. This is exactly what happens at PFK and PK. The inhibition by the metabolites from the citric acid cycle can be reasoned the same way. As already discussed, the regulation of the glucose transporter and HK serve to prevent ATP exhaustion due to overloading of the upper part of glycolysis. The role of F2,6BP then seems to be as an overall regulator, which regulates glycolysis in response to external stimuli of the cell. The FBP product activation of PFK is not easy to rationalise, but nevertheless it is important in the generation of the oscillations which I have studied. Maybe it activates PFK by binding to the same site as F2,6BP does, because the two metabolites are similar.

In accordance with biochemical tradition, some of the reactions of figure 2.3 are drawn as reversible reactions, and some are drawn as irreversible. In fact, the only truly irreversible reaction is the one catalyzed by PDC. The other reactions which are drawn irreversible, are the HK, PFK and PK reactions.

[3]In deep contrast with what is known of the liver enzyme, yeast PFK2 is activated by phosphorylation instead of being inactivated.

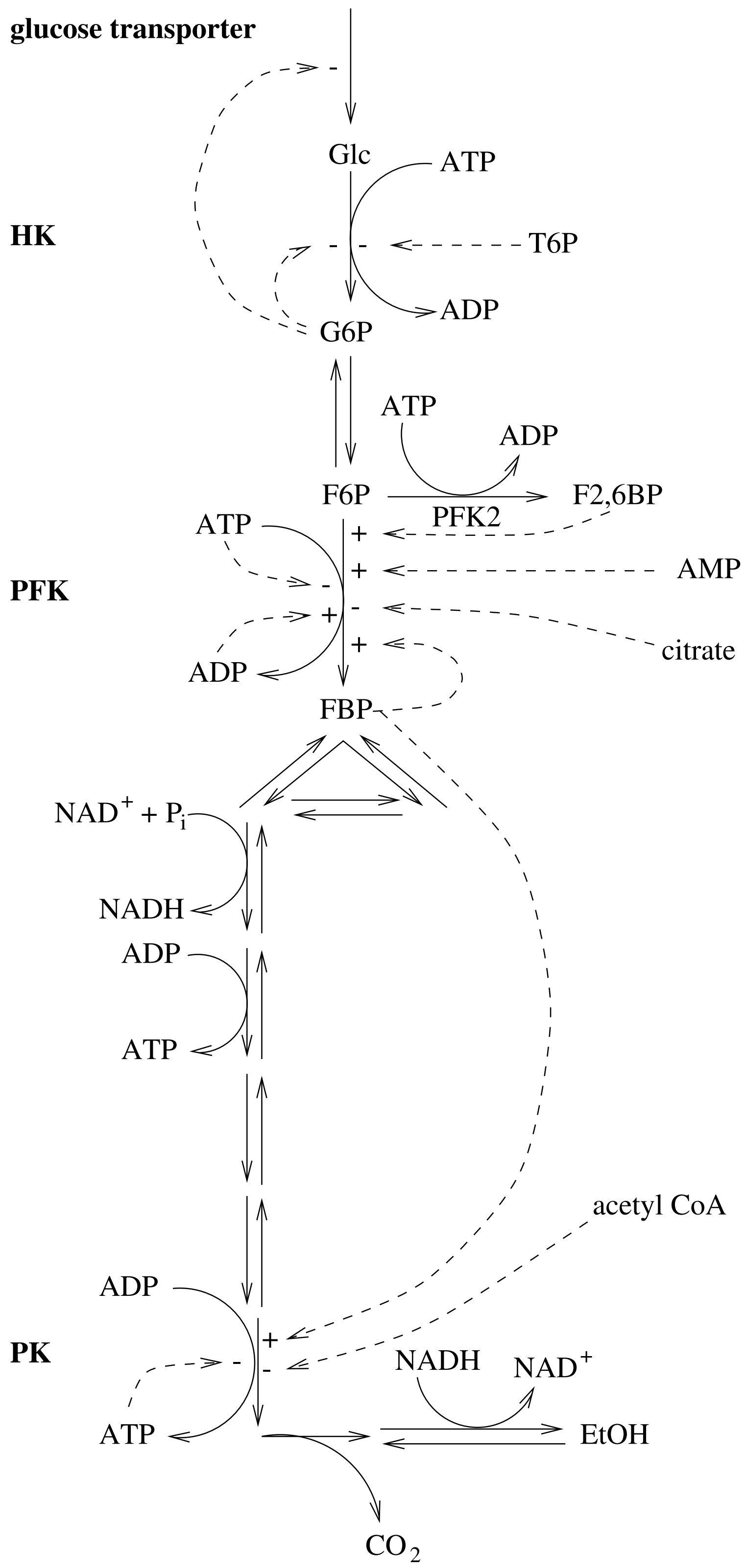

Figure 2.5: Regulation of glycolysis. Solid lines symbolise reactions, dashed lines represent regulation. Enzyme abbreviations are in boldface. See text for further details.

Each of these reactions has a large negative ΔG under the conditions inside the cell and therefore, the reactions always run from substrates to products. Such estimates can be made from ΔG°, but should of course be corrected for the actual concentrations of the metabolites[4].

In table 2.3 I present such calculations, based on measurements of intracellular metabolites in oscillating *Saccharomyces cerevisiae* in a closed reactor (Richard *et al.*, 1996b). In these experiments, the reactions inside the cells were stopped immediately by spraying the cells into methanol at a temperature of $-40°$C. The metabolite concentrations were then determined enzymatically. Samples were taken every 5 seconds. This allows for 8 samples within the period of the oscillations, which was 41 s. Sinusoidal oscillations were assumed *a priori* for all metabolites investigated, and an amplitude and a phase were fitted in a window of 23 data points. The results of this fitting and the measurements themselves are reprinted in table 2.1. Measurements of extracellular metabolite concentrations under similar experimental conditions (Richard *et al.*, 1994, 1996a) are cited in table 2.2.

The ΔG calculations show, that the standard picture given in figure 2.3 is also valid for oscillating yeast cells, even though there are some differences compared to the ΔG values from rabbit skeletal muscle and human erythrocytes cited in Mathews and van Holde (1990). The most striking difference is that $-\Delta G_{PDC}$ is large compared to lactate dehydrogenase in the other cell types. This is partly caused by the large intracellular concentration of pyruvate in the yeast cells (compare 8.7 mM in the yeast with 51 μM in the erythrocyte). The large value of $-\Delta G_{\mathrm{PDC}}$ even holds for conservative estimates of [ACA] and p_{CO_2}. With ten times the extracellular concentration of ACA and 1% of CO_2 in the air, $-\Delta G_{\mathrm{PDC}}$ is still the largest in the pathway ($\Delta G' = -37$kJ/mol). A comparison also reveals that $-\Delta G_{\mathrm{PFK}}$ in the yeast is only half the value found in the skeletal muscle and in the erythrocyte.

Even though one should be careful when interpreting such thermodynamic data, I will note that it is remarkably from a biochemical point of view that the decarboxylation, which is not known to be allosterically regulated, has such a large $-\Delta G$. This is, as described above, in contrast to the other exergonic reactions catalyzed by HK, PFK and PK. As discussed on page 22, this might be a consequence of the experimental procedure, but it might also be a consequence of the two different types of fermentation.

[4]Further corrections should be added to compensate for the high ionic strength of the cytosol and complexes formed between metabolites and metal ions, etc. However, this is not doable with the present experimental results.

Metabolite	Average concentration (mM)	Fitted relative amplitude (%)	Computed mean relative amplitude $\pm$ standard error of that mean (%)	Phase (°)
G6P	4.1	40	48 ± 13	-100
F6P	0.5	52	52 ± 11	-110
FBP	5.1	46	48 ± 7	70
F2,6BP	0.02	n.f.	2 ± 5	-
DHAP	2.5	n.f.	2 ± 3	-
GAP	0.12	n.f.	3 ± 28	-
DPG	n.d.	n.d.	n.d.	-
3PG	0.3	n.f.	2 ± 9	-
2PG	n.d.	n.d.	n.d.	-
PEP	0.04	n.f.	17 ± 11	-
Pyr	8.7	n.f.	8 ± 7	-
ATP	2.1	28	36 ± 9	180
ADP	1.5	56	60 ± 10	0
AMP	0.33	101	104 ± 18	0
P_i	11	12	10 ± 2	-100
NADH	0.33	32	29 ± 6	0
NAD^+	0.65	9	9 ± 6	180
ATP/ADP	2.04	75	88 ± 14	180
NADH/NAD^+	0.51	39	37 ± 7	0

Table 2.1: Intracellular concentrations of glycolytic metabolites in oscillating yeast cells as reported by Richard *et al.* (1996b). Samples were taken every 5 s for 115 s starting 9 min after a 20 mM glucose pulse followed 4 min later by a 3 mM cyanide pulse. "Fitted relative amplitude" is $\frac{1}{2}$ of the peak to peak amplitude, obtained from a least square fit of a sine function to the data. "Computed mean relative amplitude" is the mean value of the amplitude, fitted point by point. Phase is relative to the phase of NADH. Abbreviations: n.f.: not fitted, n.d.: not detected. The temperature is 25°C. There are some minor discrepancies in the data: AMP has a relative amplitude of 101%, and the average ratio of ATP and ADP does not fit the average concentrations of the two substances.

Metabolite	Average concentration (mM)	Relative amplitude (%)	Phase (°)	Rate of accumulation (μM/s)
ACA	0.07	43	-160	-
EtOH	7.1	-	-	18
Glycerol	1.3	-	-	1.9

Table 2.2: Extracellular concentrations of ACA, EtOH and glycerol in a suspension of oscillating yeast cells. Measurements were done 9 min after a 20 mM glucose pulse, followed 4 min later by a cyanide pulse. Phase is relative to NADH fluorescence. The ACA measurements are from Richard *et al.* (1996a) and were performed at 20°C with a cyanide concentration of 3 mM. The samples for EtOH and glycerol determination were taken with 2 min interval, so oscillations cannot be detected. The temperature is 25°C, and the cyanide concentration is 8 mM. The values are estimated from measurements in Richard *et al.* (1994).

Enzyme	Reaction	$\Delta G^{\circ\prime}$ (kJ/mol)	$\Delta G'$ (kJ/mol)
HK	$\mathrm{Glc + ATP \rightarrow G6P + ADP + H^+}$	-16.7	-
PGI	$\mathrm{G6P \rightarrow F6P}$	1.7	-3.5
PFK	$\mathrm{F6P + ATP \rightarrow FBP + ADP + H^+}$	-14.2	-9.3
ALD	$\mathrm{FBP \rightarrow GAP + DHAP}$	23.8	-0.3
TIM	$\mathrm{DHAP \rightarrow GAP}$	7.5	0.0
GAPDH	$\mathrm{GAP + NAD^+ + P_i \rightarrow DPG + NADH + H^+}$	6.3	-
PGK	$\mathrm{DPG + ADP \rightarrow 3PG + ATP}$	-18.8	-
PGM	$\mathrm{3PG \rightarrow 2PG}$	4.6	-
ENO	$\mathrm{2PG \rightarrow PEP + H_2O}$	1.7	-
PK	$\mathrm{PEP + ADP + H^+ \rightarrow Pyr + ATP}$	-31.4	-17
PDC	$\mathrm{Pyr + H^+ \rightarrow ACA + CO_2(g)}$	-19.0	-50
ADH	$\mathrm{ACA + NADH + H^+ \rightarrow EtOH + NAD^+}$	-23.7	-11

Table 2.3: $\Delta G'$ (ΔG at pH = 7) and $\Delta G^{\circ\prime}$ of the glycolytic reactions and the alcohol fermentation. The $\Delta G'$ values have been calculated from the average intracellular concentrations of metabolites in oscillating yeast cells as reported by Richard *et al.* (1996b) and listed in table 2.1. Intracellular EtOH and ACA concentrations are taken to the extracellular concentrations measured by Richard *et al.* (1994) and Richard *et al.* (1996a) and presented in table 2.2. $p_{\mathrm{CO_2}}$ is estimated to $4 \cdot 10^{-4}$ atm (Holtzclaw *et al.*, 1991). No experimental values for [Glc], [DPG] and [2PG] were avaliable. The $\Delta G^{\circ\prime}$ values are from Mathews and van Holde (1990), Nielsen (1994) and Lehninger (1975).

So far I have given an account of glycolysis and fermentation as it is usually viewed. But the dynamics of the pathway might also be influenced by other things. The simple effect of H^+ is usually neglected, because the cytosol is a strongly buffered solution. It might, however, be of some significance, since H^+ is involved in many of the glycolytic reactions. This is evident from table 2.3. Reactions in the upper part of glycolysis (catalyzed by HK, PFK and GAPDH) acidify the cytosol, while the reactions catalyzed by PK, PDC and ADH consume H^+. Overall, glycolysis and the subsequent fermentation consume two H^+, but at the same time CO_2, which acts as a weak acid, is produced:

$$\mathrm{Glc} + 2\mathrm{ADP} + 2\mathrm{P_i} \quad \longrightarrow \quad 2\mathrm{EtOH} + 2\mathrm{ATP} + 2\mathrm{HCO_3^-}$$

Even though this seems to balance, the "compartmentation" into H^+ production in the upper part and removal in the lower part, might give rise to pH fluctuations, which could in term affect the kinetics of individual enzymes. Indeed, pH transients have been measured *in vivo* in yeast cells in response to glucose pulses (Haworth *et al.*, 1991), and in yeast extracts pH oscillations have been seen (Hocker *et al.*, 1994). In unstirred yeast extract travelling proton waves have been observed along with travelling NADH waves (Mair and Müller, 1996). Such effects could be important, since many membrane transport processes in yeast are driven by a proton gradient across the cell membrane. This, however, does not involve any metabolites directly involved in glycolysis in *Saccharomyces cerevisiae*.

The concentration of inorganic phosphate P_i will also affect the dynamics, presumably by changing ΔG of reactions involving phosphorylations and dephosphorylations. My fellow student, Mette Hoffmann, has given a direct demonstration of this in her work with yeast extracts (Hoffmann, 1999). Indeed, Richard *et al.* (1996b) have measured oscillations in the concentration of P_i in oscillating yeast cells.

Glycolysis is also affected by the presence of some metal ions, since they are essential for the function of several of the enzymes. Mg^{2+} forms complexes with phosphates. This "activates" ATP and other phosphorylated metabolites, and thus it is essential to HK, PGI, PFK, GAPDH, ENO and PK. In ENO and PK Mg^{2+} can be substituted by Mn^{2+}. PK also has a requirement for K^+, and ALD and ADH have Zn^{2+} requirements.

Metabolite	Biosynthesis	
G6P	pentose phosphates	nucleotides reduction equivalents
F6P	amino sugars	glycolipids, glycoproteins
DHAP	2-glycerophosphate	lipids
DPG	2,3-bisphosphoglycerate	
3PG	serine	
PEP	aromatic amino acids	
	aspartate	pyrimidines
	asparagine	
Pyr	alanine	
	TCA cycle intermediates	fatty acids, sterols amino acids heme, chlorophyl purines, pyrimidines

Table 2.4: Glycolytic precursors for biosynthesis.

2.2.2 Glycolysis and the Rest of Metabolism

In this work I consider the dynamics of glycolysis and the subsequent fermentation as a whole. But things are even more complicated, since glycolysis does not function on its own in the yeast cell.

Many of the metabolites in glycolysis are anabolic precursors (see table 2.4). How this affects glycolysis will of course depend on the amount of biosynthesis taking place. In the experiments, the yeast cells are suspended in a phosphate buffer without any nitrogen source avaliable. This should make protein synthesis impossible, and thus ensure that growth does not take place. This minimises the drain of glycolytic intermediates, but drainage is not completely avoided.

In table 2.2 I cited experimental results showing the production of glycerol by glycolysis under the experimental conditions that I use. Glycerol is produced from DHAP and NADH in two reactions catalyzed by DHAP reductase and glycerol phosphatase:

$$\begin{aligned} \mathrm{DHAP} + \mathrm{NADH} + \mathrm{H}^+ &\longrightarrow \mathrm{glycerol\ 3-phosphate} + \mathrm{NAD}^+ \\ \mathrm{glycerol\ 3-phosphate} &\longrightarrow \mathrm{glycerol} + \mathrm{P_i} \end{aligned}$$

Because the formation of NAD^+ must be balanced by the NADH consumption, glycerol production is equivalent to a drain of metabolites between GAPDH and ADH. An obvious candidate when no cell growth occurs is ACA, since this metabolite easily diffuses across the cell membrane, and since it is found extracellularly. Such a drain should be 1:1 with the glycerol production. From table 2.2 this seems not to be the case, but according to Richard *et al.* (1994) this is due to the presence of cyanide, which reacts with ACA to form lactonitril. The reason why there is cyanide in the suspension is described below, and some consequences of this is discussed on page 64. It is concluded that the total ACA drain matches the glycerol production, and thus the drain from cyanide-induced glycolysis and fermentation is mostly in the form of ACA leaking from the cells. From table 2.2 it can be seen that the drain and glycerol production is quite substantial, amounting to 17 % of the total flux. From the glycerol and ethanol measurements in Richard *et al.* (1994) it seems that the magnitude of this drain is directly determined by the extracellular cyanide concentration as described on page 64. Indeed, the glycerol production is not always so high; according to Boiteux and Hess (1973) it amounts to round 1.5 % in oscillating yeast extracts, where ACA cannot be drained to the extracellular medium.

Even if no growth takes place, some ATP have to be produced to maintain basic cellular functions, such as the membrane potential of the plasma membrane. It has also been reported that the starved yeast cells – which I use in my experiments – build large amounts of glucose into glycogen (or some other storage carbohydrate) when glucose is administered (Betz and Hinrichs, 1968; Becker and Betz, 1972). This amounts to almost half of the glucose used, and therefore this incorporation will use almost all the ATP produced by glycolysis[5]. Thus, there will be a catabolic flux through glycolysis. The pyruvate will then either be fermented to ethanol or oxidized in the TCA cycle and the electron transport chain. Again, we want to concentrate on glycolysis and the subsequent fermentation. This is done by adding cyanide to the suspension of yeast cells, since cyanide is a potent inhibitor of cytochrome C oxidase, which is the enzyme catalyzing the last step in the electron transport chain. By blocking the electron transport chain, and thereby indirectly the TCA cycle, the catabolic fate of pyruvate will be fermentation to ethanol. In a way, this simulates anaerobic metabolism, but plugging the flow through the TCA cycle in this way is of course different from growing the yeast under anaerobic conditions.

[5]ATP is not used directly, but in the form of UTP.

When grown anaerobically, the yeast adjusts the activity of the relevant enzymes accordingly, but this cannot be done when the electron transport chain is suddenly blocked, and no nitrogen source is avaliable for protein synthesis. This might explain the differences between the ΔG values of the oscillating yeast cells and the skeletal muscle cells or the erythrocytes, that I discussed on page 16. The enzymatic make-up of the yeast cells are determined by the conditions under which they were grown, and at that time there might very well have been a substantial flux through the TCA cycle as well as through the alcohol fermentation. Thus, the enzyme activities are adjusted to a branching of the pathway at pyruvate. Now, when we force the whole flux through the fermentation branch, the enzyme activities of PDC and ADH are too small to handle the pyruvate produced in glycolysis. This would result in saturation of PDC , and give both the high concentration of pyruvate and the large $-\Delta G_{\mathrm{PDC}}$ which we observe. Because of the stoichiometric feedback loop of $\mathrm{NAD}^+/\mathrm{NADH}$ (described on page 11), this might also lower the reaction rate of the GAPDH reaction. As a result both GAP, DHAP and FBP would accumulate, because the reactions catalyzed by TIM and ALD both have $\Delta G \approx 0$ kJ/mol. This way, the relatively low $-\Delta G_{\mathrm{PFK}}$ of the oscillating yeast cells, as compared to that of the erythrocytes or the rabbit skeletal muscle, might also be a consequence of the cyanide addition.

Since I do experiments with intact yeast cells, the processes related to membrane transport are very important. As with the ACA drain discussed above, this can influence the dynamics in itself, but it also determines which substances I can use to perturb the system by extracellular additions. In fact this is somewhat disappointing, since most of the relevant metabolites are phosphorylated, and therefore cannot pass the lipid bilayer of the plasma membrane. This leaves us with glycerol, ACA and EtOH which will definitely pass the cell membrane by diffusion, and glucose which is transported through the membrane. Cyanide and pyruvate can pass the membrane in their protonated form, but for pyruvate this process is expected to be quite slow, since the protonated form of pyruvate has a low $\mathrm{pK_A}$ value of 2.49. In *Saccharomyces cerevisiae* glucose is transported by facilitated diffusion. According to Azam and Kotyk (1969) the membrane protein that binds glucose binds G6P as well, and therefore the glucose transport is inhibited by G6P.

No other means of transport than simple diffusion is known for ACA and EtOH, but under certain conditions facilitated glycerol diffusion takes place (Luyten *et al.*, 1995). The protein responsible for this facilitation is not believed to be expressed under the conditions I have used, so I will treat the glycerol transport along with that of ACA and EtOH. As a first approximation, we can think of the passing of the cell membrane as composed of three steps:

- Transition from the aqueous phase to the lipid phase.
- Diffusion across the membrane.
- Transition from the lipid to the aqueous phase.

If the diffusion of the three water-soluble substances is about equal, which is reasonable here since they are of approximately the same size, then the membrane permeability can be estimated from the partitioning coefficients of the substances. From empirical formulas in Jain and Wagner (1980) the relative permeabilities can be calculated to 13 : 8.8 : 1 (given as ACA : EtOH : Glyc). I conclude that ACA can permeate the membrane even faster than EtOH, which on the other hand is known to permeate cell membranes readily. However, glycerol permeates the plasma membrane one order of magnitude slower than the other two metabolites.

Another reaction, which seems to be important for the glycolytic oscillations, is the reaction catalysed by adenylate kinase (AK), which catalyses the interconversion of AMP, ADP and ATP:

$$2\text{ADP} \quad \overset{\text{AK}}{\rightleftharpoons} \quad \text{AMP} + \text{ATP}.$$

As a summary of this discussion, I have drawn the glycolytic pathway once more (figure 2.6); this time with the intention to give a picture as complete as possible.

The Make-up of the Yeast Cell

The enzymatic make-up of the yeast cells is another important aspect. This is a very complicated subject, but when concerned with sugar metabolism in *Saccharomyces cerevisiae*, one effect – termed the Crabtree effect – is not to be overlooked. This phenomenon relates glucose concentration with the particular catabolic route adopted by the yeast cell when grown under aerobic conditions. When extracellular glucose concentration is high (typically above 5 mM), respiratory and gluconeogenic enzymes are repressed at the level of transcription, so that the yeast, as mentioned on page 7, has fermentative catabolism even though plenty of oxygen is avaliable. On a shorter timescale

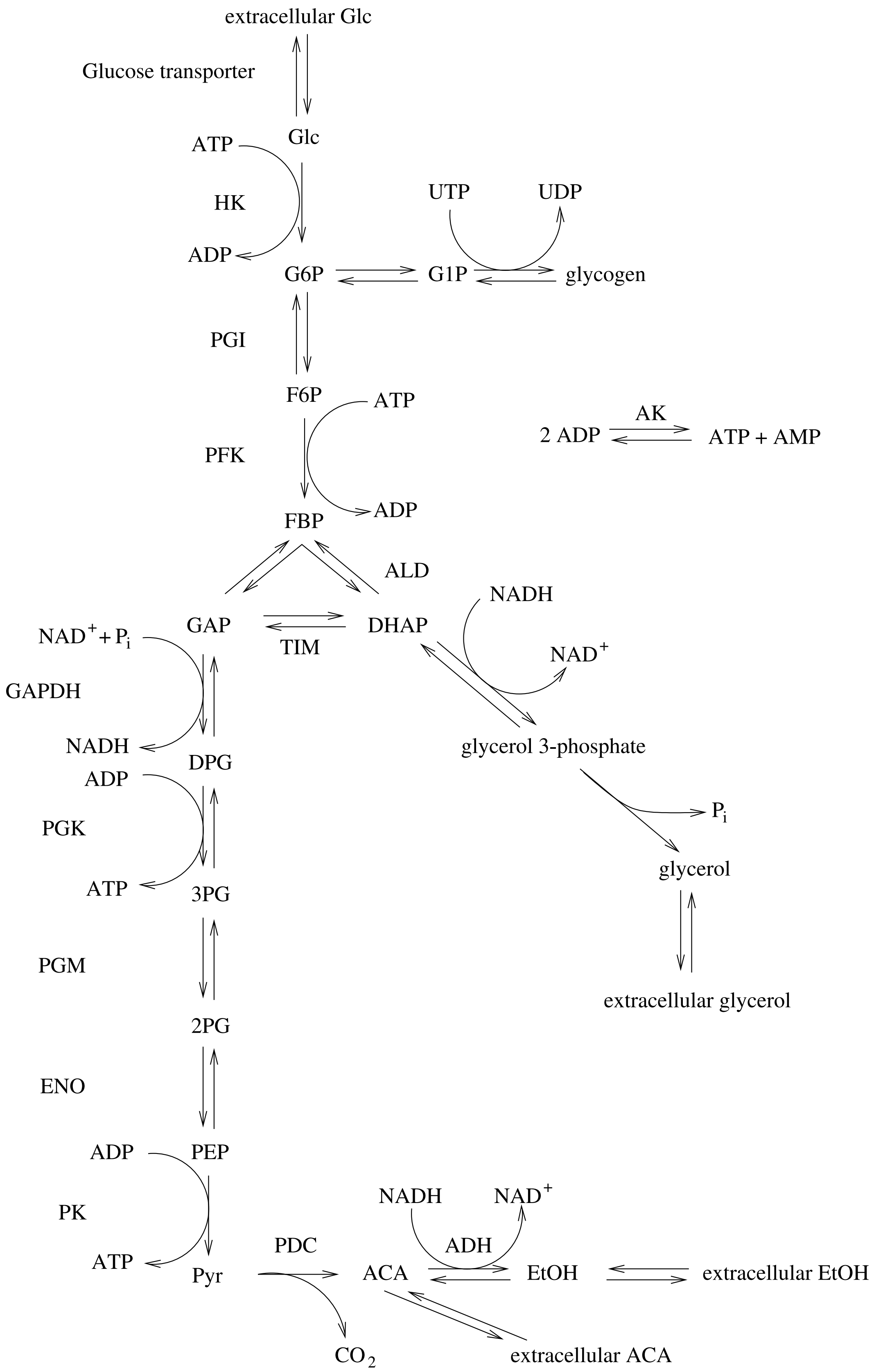

Figure 2.6: Glycolysis, the subsequent fermentation and other reactions known to influence the dynamics of glycolysis.

a similar effect is seen. Here, the Crabtree effect is not mediated by regulation of the transcription, but by cAMP and F2,6BP as described on page 14.

The consequence of the Crabtree effect when *Saccharomyces cerevisiae* is grown in an aerobic batch culture is, that the yeast grows in two phases[6]. First most of the glucose is fermented to EtOH and CO_2. Then, when no more glucose is left and the yeast cells start to metabolise the EtOH, the fermentative and gluconeogenetic enzymes are derepressed. This marks the beginning of the second (slower) growth phase known as the diauxic phase, where the EtOH produced in the first phase is oxidized via the TCA cycle and the respiratory chain. The enzymatic changes at this diauxic shift are drastic, and affects the glucose transport and many of the enzymes of glycolysis and the subsequent fermentation. For example, Walsh *et al.* (1994) report that, although the maximal uptake rate does not change, the glucose transporter changes its glucose affinity from a low affinity (K_m = 25 mM) when growing on glucose to a high affinity (K_m = 1.5 mM) after the shift. Richard *et al.* (1994) measured an increase of the HK activity by a factor three at the diauxic shift, but found constant PDC, PFK, ALD and ADH activities around it. This is contrary to the general understanding of the phenomenon, which states that at least the ADH activity should increase at least an order of magnitude. This discrepancy might arise from complications in the experimental determination af ADH activity (Bas Teusink, personal communication).

Another famous "effect" which can be seen in *Saccharomyces cerevisiae* is the Pasteur effect. It makes glycolysis run faster under anaerobic conditions than under aerobic. It can also be viewed as the opposite of the Crabtree effect, since it works through suppression of fermentation by oxygen. It works on a short time scale, and can be understood from the regulation of PFK and PK. When oxygen is avaliable, oxidative phosphorylation can produce 36 moles of ATP from each mole of glucose. This is 18 times more than that produced from a mole of glucose under anaerobic conditions. Therefore, the ATP concentration in the cytosol is lowered and the ADP and AMP concentrations rise. At the same time, the concentration of TCA cycle intermediates falls. As described on page 13 all of this will increase the glycolytic flux. However, the Pasteur effect will not be there if the extracellular glucose concentration is above approximately 5 mM, since the Crabtree effect will then force the catabolism to be fermentative.

Many other parts of the living cell will no doubt influence the system we

[6] A typical growth curve can be found in Richard *et al.* (1993).

are looking at. But it is hard to tell exactly which things will be important and which will not, so I will now end the presentation of the biological system.

3
Complex Kinetics

From the previous chapter it is evident that biological systems are usually very complex, even when precautions have been taken to minimise the parts of the system actually under study. Contemporary biology tends to work around such problems by focusing on the molecular details of the problems. This reductionistic approach produces large amounts of high quality experimental data, but at the same time it shifts the focus away from understanding the overall behaviour of the system and towards describing the details of the system.

However, the main goal of biological research must still be to understand the behaviour of the full system. In order to do this, a firm theoretical frame is needed for describing and analysing the dynamics of such systems. If such a framework is not available, the interpretation of the behaviour of a biological system can easily become a naive and handwaving explanation focusing on only a few functional elements chosen more by taste or intuition than by deduction. Admittedly, I gave an example of this in the previous chapter, when I discussed the effects of cyanide on the thermodynamics of glycolysis and the subsequent fermentation in the yeast cells (page 22).

In this chapter I present the framework of nonlinear dynamics and discuss how this can be related to actual experiments. Nonlinear dynamics is not the usual framework for the description of metabolic systems, but since it has been very useful when applied to complex chemical and physical systems, I will try to use it for the description of metabolism as well.

In order to follow the presentation, a basic knowledge of linear algebra is required. Many books can be consulted. I learned it from Edwards and Penney (1988) which is a good place to start. For a more thorough introduction to nonlinear dynamics, Strogatz (1994) is a straightforward and readable book.

To get the “mathematical details” and in depth discussions, please consult Perko (1996).

3.1 Describing Complex Kinetics

When describing a dynamical system, we want to write down a precise descip-tion of what the system is like. Then, we want to answer the question “what is the behaviour of such a system?”

For a chemical system, it is custom to use a set of autonomous ordinary differential equations (ODEs), which describes the changes in concentration of the chemical species. In a system of n chemical species, this is written as

$$\begin{aligned}\frac{dx_1}{dt} &= f_1(x_1, \ldots, x_n)\\ &\vdots\\ \frac{dx_n}{dt} &= f_n(x_1, \ldots, x_n)\end{aligned}$$

or, in a more compact notation

$$\dot{\mathbf{x}} = \mathbf{f}(\mathbf{x}) \tag{3.1}$$

where $\mathbf{x}$ and $\mathbf{f}$ are n dimensional vectors, and the dot denotes differentiation with respect to time. The solution of the vector field defined by $\mathbf{f}$ is called the *flow* of the system; this tells us how the system evolves in time.

To visualise the behaviour of the system we look at it in *phase space* , which is an n-dimensional space with each axis corresponding to each of the variables of the system. Thus, a point in phase space corresponds to a definite state of the system, and the time-evolution of the system from such a state can be viewed as a *trajectory* in phase space. In chemical and biochemical systems, phase space is usually equivalent to concentration space.

If the differential equations are not coupled, it is quite easy to see how the system will evolve. For example, look at this simple example of an uncoupled linear system

$$\begin{aligned}\dot{x}_1 &= -x_1\\ \dot{x}_2 &= 2x_2\end{aligned} \tag{3.2}$$

with the solution

$$\begin{aligned} x_1(t) &= x_1(0)e^{-t} \\ x_2(t) &= x_2(0)e^{2t} \end{aligned} .$$

A phase portrait of this system is shown in figure 3.1. From this phase portrait

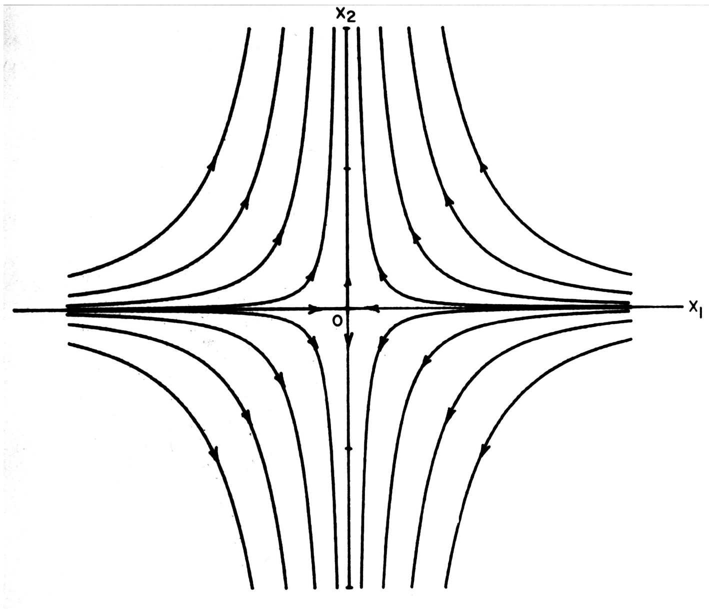

Figure 3.1: A phase portrait of the system in equation 3.2. Reproduced from Perko (1996).

we conclude that the system has two modes of motion, one along each axis. Each mode corresponds to the solution of one of the differential equations, and the flow of the system from a given starting point is given by a linear combination of the two modes. Since it is a linear system, the system in this example has one stationary point at $\mathbf{x} = \mathbf{0}$. In general, a stationary point is a point with $\dot{\mathbf{x}} = \mathbf{0}$. I will denote such a point by $\mathbf{x}^*$, and thus $\mathbf{f}(\mathbf{x}^*) \equiv \mathbf{0}$. From the solution, or from the phase portrait, it can be seen that along the x_1 axis the flow is towards the stationary point, and along the x_2 axis the motion is away from the stationary point. Thus the stationary point is stable in the x_1 direction, but unstable in the x_2 direction. Therefore, the x_1 axis is called the stable subspace E^s, and the x_2 axis is called the unstable subspace E^u. We conclude that $\lim_{t\to\infty} \mathbf{x} = \mathbf{x}^*$ for all $\mathbf{x}(0) \in E^s$. Furthermore, as time goes to infinity the state of the system goes to $(0, \infty)$ for all initial conditions chosen above the x_1 axis, and to $(0, -\infty)$ for all initial conditions chosen below.

In matrix notation the system is written as

$$\dot{\mathbf{x}} = \begin{bmatrix} -1 & 0 \\ 0 & 2 \end{bmatrix} \mathbf{x}, \tag{3.3}$$

and the solutions are given by

$$\mathbf{x}(t) = \begin{bmatrix} e^{-t} & 0 \\ 0 & e^{2t} \end{bmatrix} \mathbf{c}$$

with $\mathbf{c} = \mathbf{x}(0)$. Notice that the matrix in equation 3.3 is a diagonal matrix, because the two differential equations are uncoupled. This is what makes the axes of figure 3.1 correspond to the modes of motion in this example.

Linear Systems

The simplest general case is a two-dimensional linear system

$$\begin{aligned} \dot{x_1} &= ax_1 + bx_2 \\ \dot{x_2} &= cx_1 + dx_2 \end{aligned}$$

which we write

$$\dot{\mathbf{x}} = \mathbf{f}(\mathbf{x}) = \mathbf{A}\mathbf{x}. \tag{3.4}$$

In general, a matrix (here $\mathbf{A}$) can be diagonalized if and only if it has n lineary independent eigenvectors $\mathbf{v}_1, \ldots, \mathbf{v}_n$, each of which being a solution to the eigenvector problem $\mathbf{A}\mathbf{v}_i = \lambda_i \mathbf{v}_i$ of equation 3.4. This is usually the case in ODEs describing real systems, and this means that the n dimensional solution space is spanned by a basis of n eigenvectors, where each of these eigenvectors corresponds to an eigenmode of the system.

Suppose the two-dimensional system given by equation 3.4 has two linearly independent eigenvectors. The phase space is then spanned by the two eigenvectors $\mathbf{v}_1$ and $\mathbf{v}_2$ with eigenvalues λ_1 and λ_2, respectively. Since any motion in phase plane is given as a linear combination of an exponential motion along each of the eigenvectors

$$\mathbf{x}(t) = c_1 e^{\lambda_1 t} \mathbf{v}_1 + c_2 e^{\lambda_2 t} \mathbf{v}_2, \tag{3.5}$$

the stability of the stationary point $\mathbf{x}^* = \mathbf{0}$ is determined by the signs of the two eigenvalues. As in the example above, the phase space can be divided into E^s, spanned by the eigenvectors for which $\mathrm{Re}(\lambda) < 0$, and E^u, spanned by the eigenvectors for which $\mathrm{Re}(\lambda) > 0$, along with the center subspace E^c, which corresponds to the neutral stability of eigenvectors with $\mathrm{Re}(\lambda) = 0$. E^s, E^u, and E^c are all invariant subspaces with respect to the flow. This means that the flow of any point in the subspace will stay in the subspace for all $t \in]-\infty, \infty[$.

If the real parts of both eigenvalues are negative, then E^s is the entire phase plane, and every motion will be towards $\mathbf{x}^*$, as shown in figure 3.2 ("hyperbolic" is defined below). This is called a *sink* because all trajectories eventually end at $\mathbf{x}^*$. If both eigenvalues have positive real parts, then it's a time reversed sink, which is called a *source*. If the real part of one eigenvalue is positive, and the other one is negative, we have a *saddle* as shown in figure 3.3 (again, "hyperbolic" is defined below).

The conclusion is, that the stability of $\mathbf{x}^*$ is determined by the real parts of the eigenvalues. But what about the imaginary parts? From solving the eigenvalue problem of equation 3.4 we get

$$\lambda = \frac{(a+d) \pm \sqrt{(a+d)^2 - 4(ad-bc)}}{2}$$

from which it is evident that, at least in two dimensions, complex eigenvalues always come in complex conjugated pairs[1]. Thus $\lambda_1 = \alpha + i\beta$ and $\lambda_2 = \bar{\lambda}_1$. With the corresponding eigenvectors $\mathbf{u} \pm i\mathbf{v}$ equation 3.5 is now written

$$\begin{aligned} \mathbf{x}(t) &= c_1 e^{(\alpha+i\beta)t}(\mathbf{u}+i\mathbf{v}) + c_2 e^{(\alpha-i\beta)t}(\mathbf{u}-i\mathbf{v}) \\ &= e^{\alpha t}\left(c_1(\cos\beta t + i\sin\beta t)(\mathbf{u}+i\mathbf{v}) + c_2(\cos\beta t - i\sin\beta t)(\mathbf{u}-i\mathbf{v})\right) \end{aligned}$$

In words, this means that the motion in the phase plane is oscillatory with an amplitude[2] of $e^{\alpha t}$. So even though the imaginary parts of the eigenvalues change the motion, the stability is still determined by the real parts of the eigenvalues.

To complete the gallery of important phase portraits, a focus and a center are shown in figure 3.4 and figure 3.5, respectively. A focus is a system with complex eigenvalues which has $\mathrm{Re}(\lambda) \neq 0$, and a center is a system with complex eigenvalues and $\mathrm{Re}(\lambda) = 0$. The concepts presented above generalise to n dimensional linear systems, still with $\mathbf{R}^n = E^s \oplus E^u \oplus E^c$ and complex eigenvalues in pairs.

[1] In fact, complex eigenvalues always come in pairs.

[2] Strictly speaking, $e^{\alpha t}$ is the envelope of the amplitude.

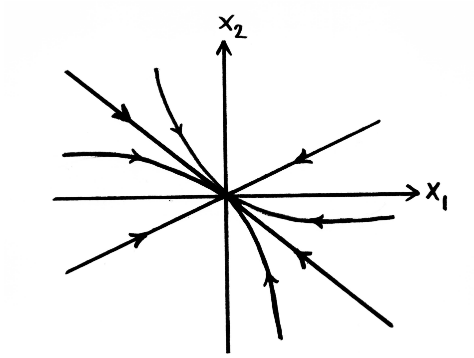

Figure 3.2: A stable node in a linear system, an example of a sink and a hyperbolic $\mathbf{x}^*$. $E^s = \mathbf{R}^2$.

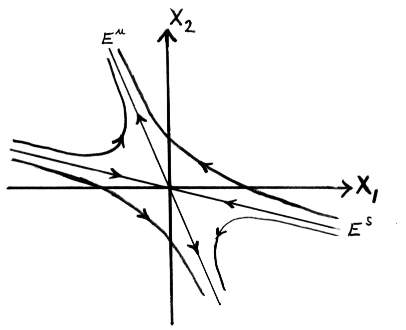

Figure 3.3: A saddle in a linear system, an example of a hyperbolic $\mathbf{x}^*$.

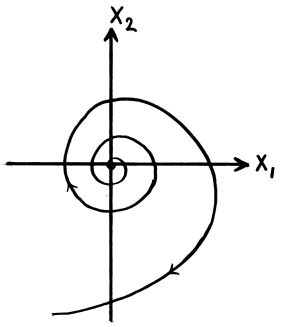

Figure 3.4: An unstable focus in a linear system, an example of a source and a hyperbolic $\mathbf{x}^*$. $E^u = \mathbf{R}^2$.

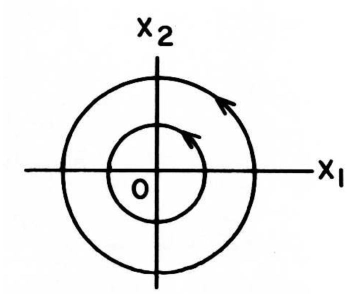

Figure 3.5: A center at the origin, an example of neutral stability and therefore a nonhyperbolic $\mathbf{x}^*$. $E^c = \mathbf{R}^2$. Reproduced from Perko (1996).

Nonlinear Systems

We want to keep this nice picture when we describe nonlinear systems, so we will find the stationary points of the system, and characterize their stability as above. Since we can now have more than one $\mathbf{x}^*$, the description will only be local, and the stability is only defined in some neighbourhood of $\mathbf{x}^*$. We might also encounter stationary points not at $\mathbf{0}$, but this is not a problem since we can always, by translation, choose a coordinate system so that $\mathbf{x}^* = \mathbf{0}$. Some phenomena need a global description to be understood, but since this is not the case for my work, I will not account for the global description of nonlinear systems.

We write $\mathbf{u} = \mathbf{x} - \mathbf{x}^*$ to obtain a coordinate system with a stationary point at the origin. We now have $\dot{\mathbf{u}} = \dot{\mathbf{x}} - \dot{\mathbf{x}}^* = \dot{\mathbf{x}} = \mathbf{f}(\mathbf{x})$. Then we do a Taylor expansion around the stationary point:

$$\begin{aligned} \dot{\mathbf{u}} &= \mathbf{f}(\mathbf{x}^*) + \mathbf{J} \cdot (\mathbf{x} - \mathbf{x}^*) + \mathbf{M}^2 \cdot (\mathbf{x} - \mathbf{x}^*)(\mathbf{x} - \mathbf{x}^*) + \dots \\ &= \mathbf{J} \cdot \mathbf{u} + O(\mathbf{u}^2) \end{aligned} \tag{3.6}$$

where

$$J_{ij} = \left. \frac{\partial f_i}{\partial x_j} \right|_{\mathbf{x}=\mathbf{x}^*}$$

and

$$M^2_{ijk} = \left. \frac{\partial^2 f_i}{\partial x_j \partial x_k} \right|_{\mathbf{x}=\mathbf{x}^*}$$

The $n \times n$ matrix $\mathbf{J}$ is known as the Jacobian matrix evaluated in $\mathbf{x} = \mathbf{x}^*$. In most cases, $\dot{\mathbf{u}} = \mathbf{J} \cdot \mathbf{u}$ gives a good description of the flow around $\mathbf{x}^*$. Therefore, we can characterize the stationary point as in the linear systems above, by solving the eigenvalue problem of the Jacobian. This immediately tells us if the description is in fact a good one in the specific case. If $\mathbf{x}^*$ is hyperbolic, that is $\mathrm{Re}(\lambda_i)|_{\mathbf{x}^*} \neq 0$ for all $i = 1, \dots, n$, then the linearization is a good approximation of the flow around $\mathbf{x}^*$, because the motion along every eigenvector of the system is well defined by the eigenvalue of the linearized system. In fact, the *Hartman-Grobman theorem* states that the flow of the full nonlinear system in the neighbourhood of a hyperbolic $\mathbf{x}^*$ is topologically equivalent to the flow of the linearized system. Thus, the qualitative behaviour of the system can be understood by looking at phase portraits like figures 3.2, 3.3 or 3.4.

If, on the other hand, the linearized system of the stationary point has $\mathrm{Re}(\lambda) = 0$ in some eigendirections, the motion along the corresponding eigenvectors will be determined by the higher order terms in equation 3.6, and the linearized system is no longer a good description of the topology.

The eigenvectors determined by $\mathbf{J}\mathbf{v}_i = \lambda_i \mathbf{v}_i$ are, of course, only approximations to the actual modes of motion of the full nonlinear system. So what do E^s, E^u, and E^c of the linearized system tell us? Another important theorem, *the stable manifold theorem*, deals with this question. It states that there exist sets of points in phase space which form generalised surfaces with properties analogous to the properties of E^s, E^u, and E^c, respectively. These surfaces are known as the stable manifold $W^s(\mathbf{x}^*)$, the unstable manifold $W^u(\mathbf{x}^*)$, and the center manifold $W^c(\mathbf{x}^*)$ of the stationary point. At the stationary point, E^s is tangent to W^s, E^u is tangent to W^u, and E^c is tangent to W^c. Furthermore, the corresponding manifold and subspace of $\mathbf{x}^*$ are of the same dimension, and W^s, W^u, and W^c are invariant with respect to the flow. This, of course, also means that W^s, W^u, and W^c have the same stability properties as E^s, E^u, and E^c of the linearized system.

3.1.1 Persistent Behaviour

From thermodynamics we know that the only persistent behaviour of a closed system is a stable stationary state, since all closed systems will eventually end up at equilibrium. Nevertheless, slow transients can display very complex dynamics in space and/or time. Examples are given by Pye (1969), Wang *et al.* (1995) and God (17,000,000,000 years BP.). When doing experiments with dynamical systems, you will normally try to avoid such transients by looking at an open system. How this can be done with a CSTR will be explained in chapter 5; for now, we just need to know that it can be done.

In unperturbed experiments you will never see the unstable states of a system, since small fluctuations will make it impossible to stay exactly in a given state. If such fluctuations displace the system from an asymptotically stable stationary state (that is, an $\mathbf{x}^*$ with $\mathrm{Re}(\lambda_i) < 0$ for all $i = 1, \ldots, n$), then the state of the system just decays exponentially back to $\mathbf{x}^*$. If, on the other hand, $\mathbf{x}^*$ is unstable then any deplacement with a component in an eigendirection with $\lambda > 0$ will grow exponentially, and the system will leave $\mathbf{x}^*$. Eventually, such a trajectory ends up on an attractor. This might be a stationary point, but it could also be a closed curve, a torus or a fractal. The only criterion is, that the final state attracts trajectories that come within a definite distance from it. The part of phase space, from which trajectories are attracted to the attractor, is called the attractor's basin of attraction. The basin of attraction might have a very complicated structure, but should always be a nonzero subset of the phase space in order to have an attractor.

We call the attractor a limit cycle if, it is a closed curve. In the typical experiment, when one component of such a system is measured as a function of time, limit-cycle oscillations are seen. The famous Sel'kov model (Sel'kov, 1968), originally proposed as a minimal model for glycolytic oscillations, illustrates this.

$$\begin{aligned} \dot{x} &= -x + ay + x^2 y \\ \dot{y} &= b - ay - x^2 y \end{aligned} \tag{3.7}$$

The system has $\mathbf{x}^* = \left(b, \frac{b}{a+b^2}\right)^{\mathrm{T}}$ (where the superscript T denotes the transpose of a vector) and the Jacobian is given by

$$\mathbf{J} = \begin{bmatrix} -1 + 2xy & a + x^2 \\ -2xy & -a - x^2 \end{bmatrix}.$$

We choose $a = 0.08$ and $b = 0.6$ and calculate the eigenvalues of the Jacobian in the stationary point: $\lambda = 0.098 \pm 0.656i$. Thus $\mathbf{x}^*$ is an unstable focus like the one shown in figure 3.4. Figure 3.6 shows what happens if the system is started with $\mathbf{x}_0 \approx \mathbf{x}^*$. Since $\mathbf{x}^*$ is an unstable focus, the state of the system spirals away from it. But as the trajectory leaves the neighbourhood of $\mathbf{x}^*$, the higher order terms of equation 3.7 becomes important and the system settles down on a limit cycle.

Since the Sel'kov oscillator is only two-dimensional, it is possible to prove the existence of the limit cycle analytically. This is done in a very pedagogically way in section 7.3 in Strogatz (1994). However, the method only works for two-dimensional systems, so I will not go into this here.

The limit-cycle is central to the work presented here, and in the experiments I have only seen two kinds of persistent behaviour, namely stationarity and limit-cycle oscillations. But to complete the picture, I will briefly mention fractal attractors and tori.

A torus could be seen as the two-dimensional analogy of a limit-cycle with trajectories moving around on a closed surface in phase space instead of on the closed curve of the limit-cycle. Such quasiperiodic behaviour has been seen experimentally, but it is quite rare in chemical systems.

A fractal attractor is also known as a "strange attractor", maybe because it is not as easy to understand as stationary points, limit-cycles or tori. Like

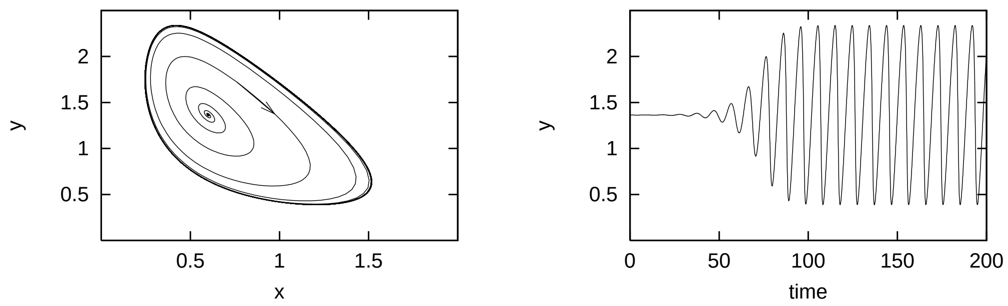

Figure 3.6: Simulation of the Sel'kov model (equation 3.7) with $a = 0.08$, $b = 0.6$ and $\mathbf{x}_0 = (0.6, 1.364)$.

the other examples of attractors, it can be thought of as a geometric object in phase space. But this object does not have integer dimension. Instead it is a fractal: The attracting states of the attractor are intertwined with the repelling states of the basin of attraction in a fractal manner. The consequence of this is that two trajectories on the attractor, arbitrarily close to each other at time t, will on average diverge from each other exponentially until they are totally uncorrelated (but, of course, both still on the attractor). This strong dependence on initial conditions and exponential divergence of neighbouring trajectories is characteristic of chaos. Since initial conditions cannot be found with arbitrary precision in the real world, chaotic systems are unpredictable on long time scales.

Even though chaos in glycolysis has never been seen in intact yeast cells, it has recently been reported in yeast extracts by Nielsen *et al.* (1997). In Nielsen *et al.* (1998) a model of this phenomenon is proposed, and I have used this model to illustrate chaos. Figure 3.7 shows two trajectories of this model which differs by a factor 1.0001 in one of the 14 initial concentrations of the model. It is evident that the two trajectories diverge. To quantify this, I have calculated the distance between the two trajecories as a function of time. The result and the technical details of this calculation can be seen in figure 3.8. The two neighbouring trajectories diverge exponentially, until they reach an upper boundary given by the size of the attractor. This is the expected behaviour of a chaotic system.

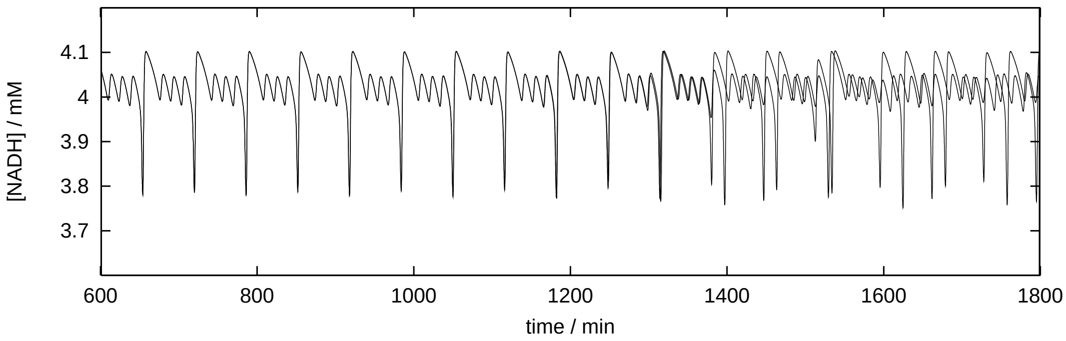

Figure 3.7: An integration of the model given in Nielsen *et al.* (1998). Parameters are chosen so that the system is in the chaotic regime. The figure shows two trajectories started on the fractal attractor at time $t = 0$. The only difference of the two trajectories is the initial concentration of NADH, which is raised by a factor of $1 + 10^{-4}$ in one of the trajectories. Parameters are as stated in the original paper, except for the corrections that the unit of time is minutes and $V_4 = 10$ mM/min instead of $V_4 = 20$ mM/min. The integration was performed with the program 'chem' (Sørensen, 1999) with a relative accuracy of 10^{-10} and an absolute accuracy of 10^{-14}.

3.1.2 Bifurcations

We have seen that the stability of a system, and thus its qualitative behaviour, is determined by the sign of the real part of its eigenvalues at least when we are sufficiently close to $\mathbf{x}^*$. Therefore, a change in the qualitative behaviour is expected when the real part of an eigenvalue changes sign. This is called a bifurcation. As it should be evident from the previous section, such a change in stability can have important consequences for the system under study, and bifurcations are therefore realizable in experiments.

We change the sign of an eigenvalue by changing some parameter of the system. In order to express this mathematically equation 3.1 is rewritten in the form

$$\dot{\mathbf{x}} = \mathbf{f}(\mathbf{x}, \mu) \tag{3.8}$$

where μ is some parameter of the system. If you like, you can think of μ as the activity of a specific enzyme, some tuneable parameter in the experimental setup, or some other effector which is not in itself a variable of the ODEs.

The simplest bifurcations are seen when a single eigenvalue changes sign. The example from the beginning of this chapter can illustrate this. We rewrite

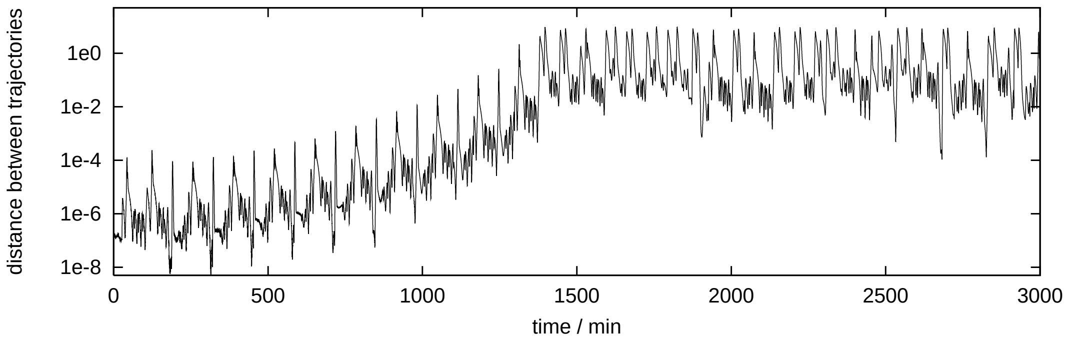

Figure 3.8: A log-plot of the distance between the two trajectories in figure 3.7. I have chosen $||\mathbf{x} - \mathbf{y}|| = \sum_{i=1}^{n}(x_i - y_i)^2$ as the measure of the distance. As long as the two trajectories are close, they diverge exponentially, but eventually they cannot diverge any more on the average, because they both stay on the attractor. In this sence, the slope of the roughly straight line that could be drawn through the points in the first half of this graph would give an estimate of the positive Lyapunov exponent of the system. Roughly speaking, positive Lyapunov exponents are a measure of the exponential divergence of two trajectories. See Ott (1993) p. 135-136 for a definition of Lyapunov exponents of a continuous time system.

equation 3.2 as

$$\begin{aligned} \dot{x}_1 &= -x_1 \\ \dot{x}_2 &= \mu x_2 \end{aligned} \tag{3.9}$$

which then has eigenvalues $\lambda_1 = -1$ and $\lambda_2 = \mu$. If we gradually decrease μ from 2 (as it was on page 28) to some negative value, we see that the system suddenly changes from a saddle (shown in figure 3.1) into a stable node (like the sketch in figure 3.2) at $\mu = \mu_c = 0$, which we therefore call the bifurcation point or the critical point. The term "critical point" is, however, problematic, since some authors use this term to denote $\mathbf{x}^*$.

Normal forms

We can think of a given system as composed of a set of modes of motion. Provided that the time scales of the different modes are widely separated, this can be used to give a low-dimensional description of the system which is (almost) quantitatively correct. A classic example is Michaelis-Menten enzyme kinetics, which is derived under the assumption that the enzyme-substrate

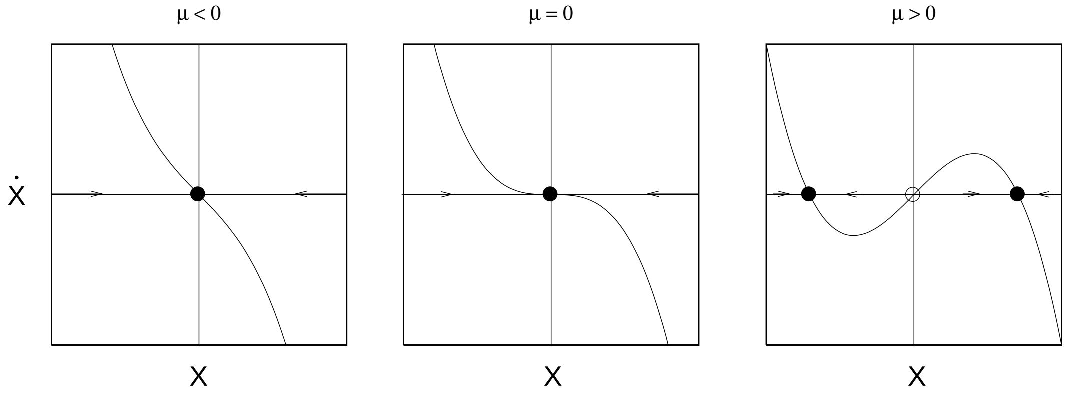

Figure 3.9: $\dot{x} = \mu x - x^3$ as a function of x for three different values of μ. By definition the stationary points are the intersections of the graph with the x-axis. The stability of a stationary point can be told from the slope of the graph: If the slope is positive then $\dot{x}$ is positive for $x = x^* + \Delta x$ and negative for $x = x^* - \Delta x$. Thus x^* is unstable (marked by a $\circ$). The reverse argument shows that x^* is stable (marked by a $\bullet$) when the slope is negative in the point of intersection.

complex reaches a steady state on a time scale much faster than the timescale of product consumption.

For complex nonlinear systems, such a reduction in dimension would be very valuable, since it would both make it easier to understand the behaviour of the system and make it computationally less demanding to simulate the system. When trying to do such a reduction, you are generally faced with the problem of deciding which modes are fast and which are slow. Usually, this problem cannot be solved, because the different time scales of the system are not separated.

At a bifurcation point the situation is different, since you now have one mode with $\mathrm{Re}(\lambda) = 0$. This mode, which corresponds to the motion on W^c, is, so to speak, infinitely slow. For parameters $\mu \approx \mu_c$ this mode still has $|\mathrm{Re}(\lambda)| \approx 0$, and we can in fact obtain a simple, but quantitatively almost correct, description by restricting the analysis to the slow manifold of the full system. This description is called the normal form description of the dynamical system at the bifurcation point. In Ipsen *et al.* (1998) it is shown how this projection of the full system onto the slow subspace – and back again – is done in a systematic form.

An illustrative example of a normal form is the pitchfork bifurcation with

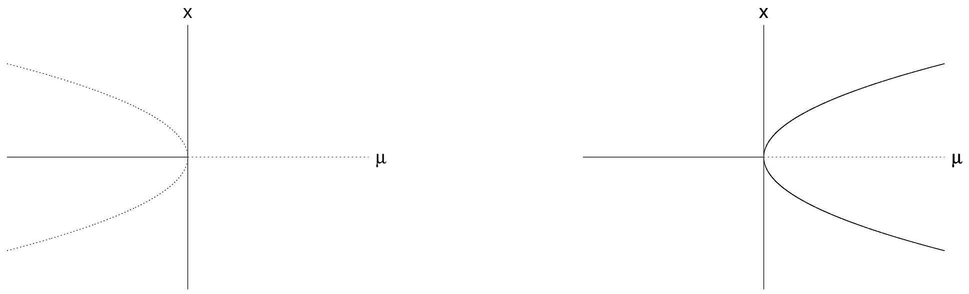

Figure 3.10: Bifurcation diagrams of a subcritical (left) and a supercritical (right) pitchfork bifurcation. Solid lines denote stable stationary states, and dotted lines denote unstable stationary states.

the normal form

$$\dot{x} = \mu x - x^3. \tag{3.10}$$

We see that there is a stationary point at $x = 0$ for all values of μ, and for $\mu > 0$ the two stationary points $x = \pm\sqrt{\mu}$ exist as well. If we plot $\dot{x}$ as a function of x, as done in figure 3.9, it is immediately seen that $x^* = 0$ is stable for $\mu \leq 0$ and unstable for $\mu > 0$, and that the two emerging stationary points $x^* = \pm\sqrt{\mu}$ are stable in their entire interval of existence.

In fact, the above normal form is only one possible normal form for the pitchfork bifurcation. The general normal form is $\dot{x} = a\mu x - bx^3$, but for simplicity the normal form parameters a and b are scaled to 1. This does not matter in this qualitative discussion, since all the normal forms are topologically equivalent[3]. If, however, you are interested in a low-dimensional quantitative description of the system close to μ_c, you should use the algorithm presented by Ipsen *et al.* (1998) to get the right normal form parameters. An example is given in Ipsen *et al.* (1997).

If we were to change the sign of the third order term in equation 3.10, so that it now reads

$$\dot{x} = \mu x + x^3, \tag{3.11}$$

[3]For this to be true, we will choose normal form parameters to be positive and real, so that the sign of the terms is a property of the normal form.

then $x^* = 0$ would still have the same stabilities as before. The other stationary points $x^* = \pm\sqrt{-\mu}$ would now only exist for $\mu < 0$, and they would always be unstable. To distinguish these two bifurcations, we say that the first one is a supercritical pitchfork bifurcation, and the second one is a subcritical pitchfork bifurcation[4].

A nice way to look at bifurcations is to make a bifurcation diagram, which is a graph showing the possible states of the system as a function of the bifurcation parameter. In figure 3.10 this is done for the two pitchfork bifurcations.

The Hopf bifurcation

The importance of bifurcation analysis in relation to my work is the onset of oscillations. The simplest, and by far most common, bifurcation leading from a stationary state to oscillations, is the Hopf bifurcation. The scenario is the following: A stable stationary point becomes unstable as a pair of complex conjugate eigenvalues crosses the imaginary axis, and a limit cycle emerges around the unstable stationary point. Thus the following conditions apply at the Hopf bifurcation:

- The Jacobian matrix of the stationary state has exactly one set of purely imaginary eigenvalues $\lambda_j = \bar{\lambda}_{j+1} = i\beta_j$. All other eigenvalues have negative real part.
- The *transversality condition* which states that the complex pair λ_j, λ_{j+1} actually crosses the imaginary axis, i.e.

$$\left.\frac{d\mathrm{Re}(\lambda_j)}{d\mu}\right|_{\mu=\mu_c} \neq 0$$

- A limit cycle with zero amplitude and frequency $\frac{\beta_j}{2\pi}$ emerges.

The general normal form of the Hopf bifurcation in a rotating coordinate system is given by the *Stuart-Landau equation* (see chapter 2 in Kuramoto (1984) for a discussion)

$$\dot{z} = \mu\lambda_1 z - gz|z|^2. \tag{3.12}$$

[4] The idea of these names is that the two new stationary points are found either above or below the critical point (i.e. bifurcation point), as seen from the stable stationary state.

(See below for notation).

However, to see that this system actually has a Hopf bifurcation when the bifurcation parameter μ is varied, I will rewrite the Stuart-Landau equation in a fixed (i.e. non-rotating) coordinate system:

$$\dot{z} = (i\omega_0 + \mu\lambda_1)z - gz|z|^2 \tag{3.13}$$

where $z = z_1 + iz_2$ and $g = g' + ig''$. Furthermore, the complex eigenvalue λ has been expanded in the parameter ϵ around the bifurcation point: $\lambda = \lambda_0 + \epsilon\lambda_1 + \dots$ with $\lambda_0 = i\omega_0$ and $\lambda_1 = \sigma_1 + i\omega_1$.

By separating the real and imaginary parts, equation 3.13 can be rewritten as:

$$\begin{aligned} \dot{z}_1 &= (\mu\sigma_1 - g'|z|^2)z_1 - (\omega_0 + \mu\omega_1 - g''|z|^2)z_2 \\ \dot{z}_2 &= (\mu\sigma_1 - g'|z|^2)z_2 + (\omega_0 + \mu\omega_1 - g''|z|^2)z_1. \end{aligned}$$

For all parameter values the system has the stationary state $z = 0$, and we write up the Jacobian matrix of the system evaluated at this state:

$$\mathbf{J}\big|_{z=0} = \begin{bmatrix} \mu\sigma_1 & -(\omega_0 + \mu\omega_1) \\ \omega_0 + \mu\omega_1 & \mu\sigma_1 \end{bmatrix}.$$

It is easy to see that the matrix has the two eigenvalues $\lambda = \mu\sigma_1 \pm i(\omega_0 + \mu\omega_1)$. Therefore, the change in stability of the stationary point $z = 0$ at $\mu = \mu_c = 0$ is evident provided that $\sigma_1 \neq 0$. At this bifurcation point $\lambda = \pm i\omega_0$. So, for $\omega_0 \neq 0$ this fulfills the first of the above conditions for a Hopf bifurcation. The transversality condition is also fulfilled since $\frac{d(\mu\sigma_1)}{d\mu}\Big|_{\mu=\mu_c} = \sigma_1$.

The emergence of the limit cycle is easiest to see when the system is rewritten once again; this time in polar coordinates $z = r(t)e^{i\theta(t)}$.

$$\dot{r} = \mu\sigma_1 r - g'r^3 \tag{3.14}$$

$$\dot{\theta} = \omega_0 + \mu\omega_1 - g''r^2 \tag{3.15}$$

For $g' > 0$ equation 3.14 is similar to equation 3.10, so by the same arguments (presented graphically in figure 3.9) we find that for $\mu\sigma_1 \leq 0$ there is only one stationary radius $r^* = 0$. This stationary state is stable[5]. For $\mu\sigma_1 > 0$ the stationary radius $r^* = \pm\sqrt{\frac{\mu\sigma_1}{g'}}$ is asymptotically stable while $r^* = 0$ is

[5]In fact it is asymptotically stable for $\mu\sigma_1 < 0$ which agrees with a sink.

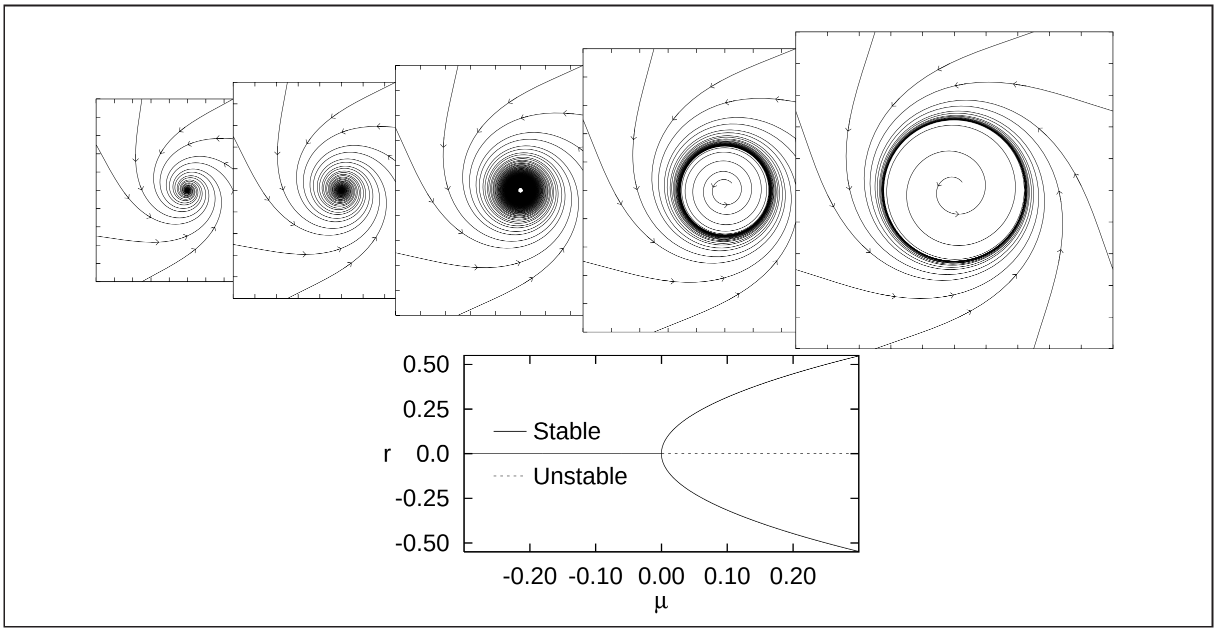

Figure 3.11: Numerically integrated phase portraits of equation 3.13 for different values of μ together with the bifurcation diagram for the supercritical Hopf bifurcation. The values of μ in the phase portraits are (from left to right): $\mu = -0.2$. $\mu = -0.1$. $\mu = 0.0$. $\mu = 0.1$. $\mu = 0.2$. The other parameters are: $g = 1$, $\lambda_1 = 1$ and $\omega_0 = 1$. This figure is kindly reproduced from Lorenzen (1996).

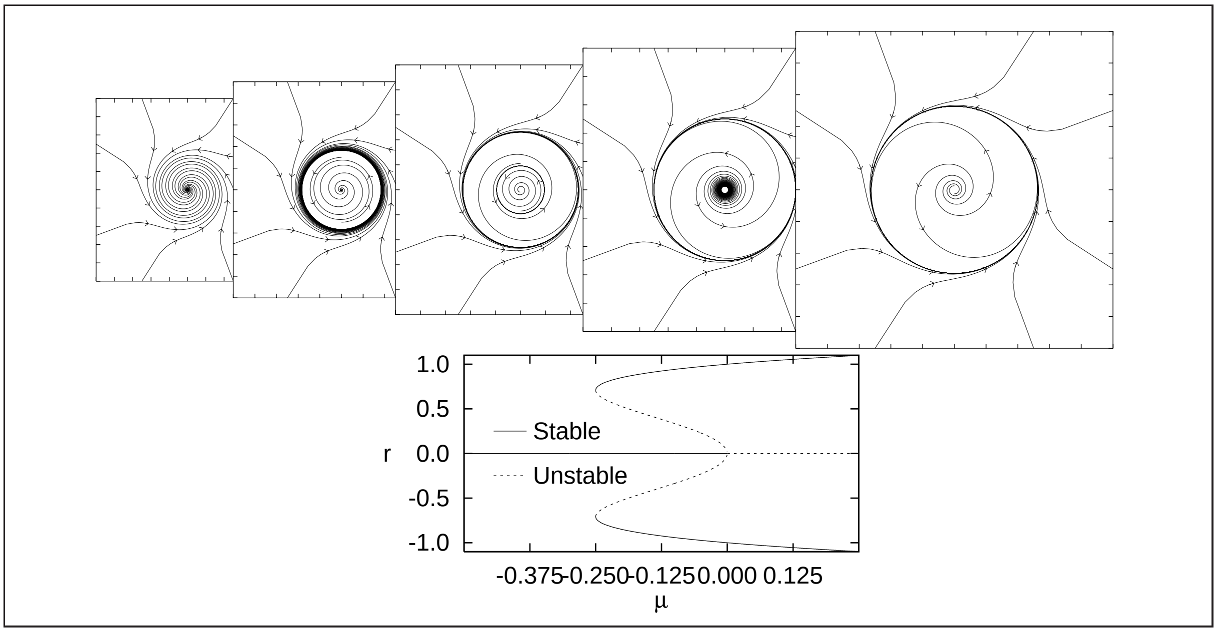

Figure 3.12: Numerically integrated phase portraits of equation 3.18 for different values of μ together with the bifurcation diagram for the subcritical Hopf bifurcation. The values of μ in the phase portraits are (from left to right): $\mu = -0.375$. $\mu = -0.250$. $\mu = -0.125$. $\mu = 0.000$. $\mu = 0.125$. This figure is also reproduced from Lorenzen (1996).

unstable. Since a negative radius $r = -\sqrt{\frac{\mu\sigma_1}{g'}}$ has no physical meaning, the conclusion is that the emerging limit cycle is stable with radius

$$r_{\text{limit cycle}} = \sqrt{\frac{\mu\sigma_1}{g'}} \tag{3.16}$$

and frequency

$$\omega_{\text{limit cycle}} = \frac{1}{2\pi}\left(\omega_0 + \mu\left(\omega_1 - \frac{g''\sigma_1}{g'}\right)\right). \tag{3.17}$$

This is called a *supercritical Hopf bifurcation*. Note that the existence of a Hopf bifurcation could also be seen directly from equation 3.14 and 3.15.

A very nice graphical presentation of a supercritical Hopf bifurcation is given in the master's thesis of Thomas Lorenzen (Lorenzen, 1996). It is reproduced in figure 3.11, and shows the bifurcation diagram and simulations of equation 3.13 for five different values of μ.

As long as we are still close to μ_c, the normal form description is a good description of the emerging limit cycle. This is because the limit cycle will have a small radius, and thus the third order terms in equation 3.13 will dominate over any higher order terms which we did not include in the normal form description.

Since two eigenvalues become positive at the Hopf bifurcation, the unstable manifold is two-dimensional at the unstable stationary point inside the limit cycle. The rest of phase space around the stationary point is spanned by the $n-2$ dimensional stable subspace. A sketch of this is shown in figure 3.13.

The Subcritical Hopf Bifurcation

If, however, we take $g' < 0$ in equation 3.14, then this equation is similar to the subcritical pitchfork bifurcation in equation 3.11, and the emerging limit cycle is unstable. This is called a *subcritical Hopf bifurcation*. To tell what the persistent behaviour of the system will be, one needs to include higher-order terms in the description, since the Stuart-Landau description has only the unstable solution $r = 0$ for $\mu\sigma_1 > 0$. A simple example of this is given by the following normal form of a subcritical Hopf bifurcation:

$$\begin{aligned} \dot{x}_1 &= \mu x_1 - x_2 + x_1^3 + x_1 x_2^2 - x_1^5 - x_1 x_2^4 - 2x_1^3 x_2^2 \\ \dot{x}_2 &= x_1 + \mu x_2 + x_2 x_1^2 + x_2^3 - x_2 x_1^4 - x_2^5 - 2x_1^2 x_2^3 \end{aligned} \tag{3.18}$$

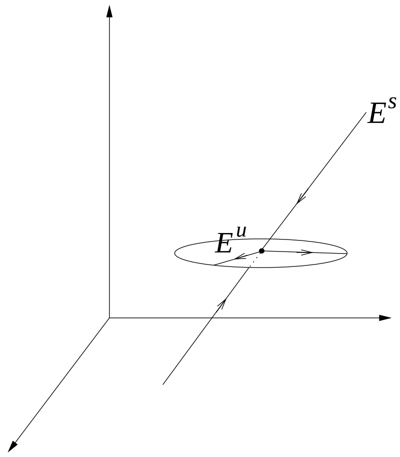

Figure 3.13: A sketch of the phase space close to a supercritical Hopf bifurcation. The limit cycle is the ellipse in the plane spanned by the unstable subspace. The unstable stationary point (marked by a •) is at the intersection of the stable and the unstable subspace.

We will not need this normal form later on, but I have included a bifurcation diagram and phase plots at different values of μ in figure 3.12 in order to show that the supercritical Hopf bifurcation is not the only bifurcation from a stable stationary state to a limit cycle.

Notice the difference between this bifurcation and its supercritical sister. The limit cycle is now born with a large amplitude, and the stable stationary point coexists with the limit cycle for some values of μ. If you pass μ_c from above, you will not reach the stationary point until the limit cycle ceases to exist. In figure 3.12 this happens at $\mu = -0.25$. On the other hand, if you pass μ_c from below, you will stay on the stationary point until it becomes unstable at $\mu = \mu_c$. We say that the system shows hysteresis at a subcritical Hopf bifurcation.

3.2 Experimental Complex Kinetics

As you have seen in the first part of this chapter, the theory of nonlinear dynamics states some general properties that a dynamical system could have, and gives a qualitative picture which is very useful when trying to understand the behaviour of a system. This qualitative picture is indeed very nice, but as chemists or biochemists we want a quantitative description of the system.

If you have a computer model of the system of interset, nonlinear dynamics is a good tool for detailed investigations of it. But, usually, such a model is exactly what is missing. In most cases, the best you can do is to build a model that works fine for some cases, but fails when different conditions are imposed. Thus, the current status is that full scale models of cellular systems have only limited biological value. In particular, it is often the case that parameters determined *in vitro*, differ from the apparent *in vivo* parameters (e.g. Babul *et al.* (1993); Benevolensky *et al.* (1994); Wright and Albe (1994); Wright *et al.* (1992)). Therefore, a way to get from the measurements of the dynamics to the actual mechanism is needed, since this would ultimately allow the components of the biological models to be determined *in vivo*.

When concerned with chemical problems, things are not as complicated since you do not have the problems of *in vivo* versus *in vitro* measurements. Furthermore, methods for deriving the reaction mechanism from the measured dynamics actually exist. One such method is that of "quenching analysis". This method was developed at our laboratory by my supervisors Preben Graae Sørensen and Finn Hynne (Hynne *et al.*, 1990). It will now be presented.

3.2.1 Quenching Analysis

The basis of the quenching experiments is the geometry of the phase space on the oscillatory side of a supercritical Hopf bifurcation (figure 3.13), so in order to do such experiments we need to be close to the bifurcation point. As described, the persistent behaviour of such a system is limit-cycle oscillations. Most perturbations will displace the state of the system from the limit cycle, but the state will soon be back on the limit cycle. If, however, you perturb the system in such a way that its state ends up very close to the unstable stationary state, the response will be quite different. The oscillations are quenched, and reappear slowly as the state of the system spirals back onto the limit cycle. You might be able to put the state of the system directly on $\mathbf{x}^*$, but placing it on the stable manifold will produce the same result, since the system will then reach $\mathbf{x}^*$ after a short transient.

In principle, the oscillations could remain quenched forever if the unstable stationary state was hit precisely. In practice this is not possible, since $\mathbf{x}^*$ will never be hit exactly. Even if it were to be an exact hit, small fluctuations would eventually drive the system off the stationary state as explained above. Thus, after the quenching the system will return to the limit cycle as shown in figure 3.6. The small fluctuations pose no problem if you want to quench the oscillations via the stable manifold; you will still be able to move along the stable manifold and reach the unstable stationary state. This is because we are close to the bifurcation point, where the motion along the stable manifold is

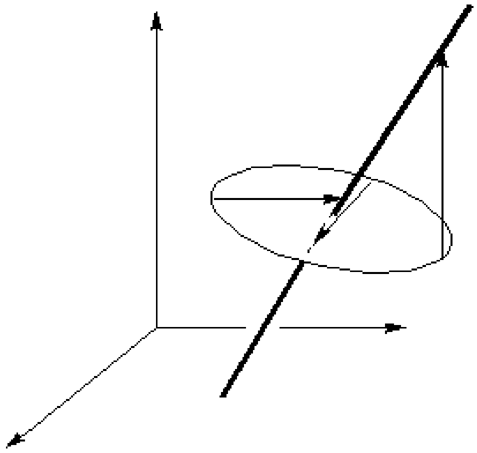

Figure 3.14: The quenching response of a perturbation with a given mixture of chemical species is unique, when we are close to a supercritical Hopf bifurcation. Here, this is exemplified by three quenchings each by addition of a pure species, which corresponds to motion in the positive direction along one of the axis in concentration space.

faster than the motion in the unstable plane of oscillations, i.e. $|\mathrm{Re}(\lambda_{\mathrm{unstable}})| < |\mathrm{Re}(\lambda_{\mathrm{stable}})|$ for $\mu \approx \mu_c$.

An early experimental realization of a quenching was reported by Winfree (1970), who was doing experiments on the influence of short pulses of intense blue light on the circadian rythm of pupal eclosion in populations of the fruit fly *Drosophila pseudoobscura*. In his experiments each perturbation was given with the same intensity of light, but at different phases relative to the daylight rythm and with different pulse durations. The surprising finding was that a unique combination of these two perturbation parameters not just shifted the phase of the circadian rythm, but seemed to leave the fruit flies with their circadian rythms completely randomised. Winfree explained this with a limit cycle scenario, where each of the fruit flies' circadian clocks had been quenched.

A few years later Winfree did another set of elegant experiments, this time on oscillating yeast cells (Winfree, 1972). Transient oscillations were induced by the transition from aerobic to anaerobic metabolism, and the pattern of phase resetting by oxygen pulses at different sizes and phases was investigated. He managed to hit the stable manifold and quench the oscillations, and concluded that a picture consisting of a limit cycle and a stable manifold [6] is qualitatively correct for the description of the yeast cells.

In Winfree's experiments, it is not possible to relate the perturbations directly to the underlying mechanisms. There is obviously no strong pulses of

[6]Winfree named this stable manifold the "isochron convergence locus" for reasons explained in the article.

light involved in the biological clock of the fruit fly, neither is there any direct quantitative way to connect O_2 to the oscillations in anaerobic yeast cells. Things are different when looking at a chemical system where perturbations are performed with chemical species actually being part of the reactions under study. If the system is perturbed with one species at a time, then this is equivalent to pushing the state of the system in the (positive) direction of the corresponding axis in phase space. Another possibility is to do a perturbation by dilution, which shifts the state of the system towards origo proportional to the concentrations of the reactants. This explicit connection between the perturbations and the geometry of the phase space makes it possible to obtain kinetic information from the perturbations. When situated on the limit cycle, and perturbing in a given direction in phase space, there is only one way to hit the stable manifold, as long as the geometry is as shown in figure 3.13. This is illustrated in figure 3.14. Thus, a small well-defined set of perturbations have a characteristic response that can be clearly distinguished experimentally.

The Theory of the Quenching Experiments

To see what can actually be calculated from quenching experiments, we write up a general quenching vector in n-dimensional phase space

$$\mathbf{q} = \mathbf{t} - \mathbf{r} \tag{3.19}$$

which describes a displacement of the state of the system, which takes it from the limit cycle to the stable manifold as shown in figure 3.15. Sufficiently close to a supercritical Hopf bifurcation, the limit cycle is described by

$$\mathbf{r}(t) = a\left(\mathbf{u}\cos(\omega t) + \mathbf{v}\sin(\omega t)\right), \tag{3.20}$$

where $\mathbf{u}$ and $\mathbf{v}$ are the real and imaginary components of the two complex conjugated eigenvectors that span the unstable subspace (as before, $\mathbf{x}^*$ has been translated to the origin). In some sense this equation states that the amplitudes and the relative phases of the oscillating concentrations are determined by theses two eigenvectors.

We will now introduce left eigenvectors $\mathbf{e}^j$ which, in principle, are solutions to the transpose of the usual eigenvalue problem:

$$\begin{bmatrix} a_{11} & \dots & a_{1n} \\ \vdots & \ddots & \vdots \\ a_{m1} & \dots & a_{mn} \end{bmatrix} \begin{bmatrix} x_1 \\ \vdots \\ x_n \end{bmatrix} = \lambda_j \begin{bmatrix} x_1 \\ \vdots \\ x_n \end{bmatrix} = \lambda_j \mathbf{e}_j$$

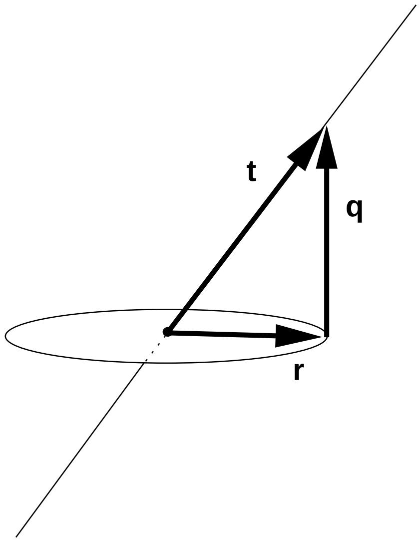

Figure 3.15: Illustration of the vectors in equation 3.19.

in analogy with

$$\begin{bmatrix} x_1 & \dots & x_n \end{bmatrix} \begin{bmatrix} a_{11} & \dots & a_{1n} \\ \vdots & \ddots & \vdots \\ a_{m1} & \dots & a_{mn} \end{bmatrix} = \lambda_j \begin{bmatrix} x_1 & \dots & x_n \end{bmatrix} = \lambda_j \mathbf{e}^j,$$

where subscripts denote right eigenvectors, i.e. the usual eigenvectors, and superscripts denote left eigenvectors. By suitable normalisation the system can be chosen biorthonormal, so that it satisfies

$$\mathbf{e}^i \cdot \mathbf{e}_j = 2\delta^i_j. \tag{3.21}$$

To see how this is accomplished, we multiply the usual eigenvalue problem $\mathbf{J} \cdot \mathbf{e}_j = \lambda_j \mathbf{e}_j$ with a left eigenvector to obtain

$$\mathbf{e}^i \cdot \mathbf{J} \cdot \mathbf{e}_j = \mathbf{e}^i \lambda_j \mathbf{e}_j. \tag{3.22}$$

Likewise,

$$\mathbf{e}^i \cdot \mathbf{J} \cdot \mathbf{e}_j = \mathbf{e}^i \lambda_i \mathbf{e}_j \tag{3.23}$$

is obtained from $\mathbf{e}^i \cdot \mathbf{J} = \mathbf{e}^i \lambda_i$ by multiplication with a right eigenvector. We subtract equation 3.23 from equation 3.22 to obtain

$$0 = (\lambda_j - \lambda_i)\mathbf{e}^i \cdot \mathbf{e}_j, \tag{3.24}$$

which shows that for $\lambda_i \neq \lambda_j$ the dot product of the two eigenvalues must be zero, which is the orthogonality we want. For $i = j$ the dot product may take any value without violating equation 3.24, so we can normalise as we wish.

The physical meaning of the left eigenvectors is somewhat unclear. Equation 3.21 states that they span a reciprocal concentration space, but what this actually means is not very clear. Nevertheless, they allow us to proceed with equation 3.19. In order to do this, we will denote the two complex left eigenvectors associated with the two complex conjugated eigenvalues of the unstable subspace by $\mathbf{e}^1$ and $\mathbf{e}^2$, and rewrite them as $\mathbf{e}^1 = \mathbf{e}^+ + i\mathbf{e}^-$ and $\mathbf{e}^2 = \mathbf{e}^+ - i\mathbf{e}^-$. This allows us to make use of the biorthonormality:

$$\mathbf{e}^1 \cdot \mathbf{e}_1 = (\mathbf{e}^+ + i\mathbf{e}^-) \cdot (\mathbf{u} - i\mathbf{v}) = 2 \tag{3.25}$$

and

$$\mathbf{e}^2 \cdot \mathbf{e}_1 = (\mathbf{e}^+ - i\mathbf{e}^-) \cdot (\mathbf{u} - i\mathbf{v}) = 0. \tag{3.26}$$

From equation 3.25 we obtain

$$\mathbf{e}^+ \cdot \mathbf{u} + \mathbf{e}^- \cdot \mathbf{v} = 2 \tag{3.27}$$

and

$$i(\mathbf{e}^- \cdot \mathbf{u} - \mathbf{e}^+ \cdot \mathbf{v}) = 0 \quad \Leftrightarrow \quad \mathbf{e}^+ \cdot \mathbf{v} = \mathbf{e}^- \cdot \mathbf{u}, \tag{3.28}$$

and from equation 3.26 we obtain

$$\mathbf{e}^+ \cdot \mathbf{u} - \mathbf{e}^- \cdot \mathbf{v} = 0 \quad \Leftrightarrow \quad \mathbf{e}^+ \cdot \mathbf{u} = \mathbf{e}^- \cdot \mathbf{v} \tag{3.29}$$

and

$$-i(\mathbf{e}^- \cdot \mathbf{u} + \mathbf{e}^+ \cdot \mathbf{v}) = 0 \quad \Leftrightarrow \quad \mathbf{e}^+ \cdot \mathbf{v} = -\mathbf{e}^- \cdot \mathbf{u}. \tag{3.30}$$

When we combine equation 3.30 with equation 3.28 and equation 3.27 with equation 3.29 we obtain

$$\begin{aligned} \mathbf{e}^+ \cdot \mathbf{u} &= 1 \\ \mathbf{e}^- \cdot \mathbf{u} &= 0 \end{aligned} \tag{3.31}$$

and

$$\begin{aligned} \mathbf{e}^{+} \cdot \mathbf{v} &= 0 \\ \mathbf{e}^{-} \cdot \mathbf{v} &= 1. \end{aligned} \tag{3.32}$$

We can now multiply equation 3.19 with $\mathbf{e}^{+}$. Since $\mathbf{t}$ is orthogonal to both $\mathbf{e}^{+}$ and $\mathbf{e}^{-}$, we can use equation 3.31 and 3.32 to obtain

$$\begin{aligned} \mathbf{e}^{+} \cdot \mathbf{q} &= \mathbf{e}^{+} \cdot \mathbf{t} - \mathbf{e}^{+} \cdot \mathbf{r} \\ &= -\mathbf{e}^{+} \cdot a\,(\mathbf{u}\cos(\omega t) + \mathbf{v}\sin(\omega t)) \\ &= -a\cos(\phi), \end{aligned} \tag{3.33}$$

and likewise with $\mathbf{e}^{-}$

$$\mathbf{e}^{-} \cdot \mathbf{q} = -a\sin(\phi). \tag{3.34}$$

The angle ϕ denotes the place on the limit cycle from which $\mathbf{q}$ originates.

Now, if a quenching is obtained by addition of a single chemical species, then $\mathbf{q}$ has only one non-zero component. By scaling the concentration space so that the amplitude a of the oscillations is one, equation 3.33 and 3.34 give

$$q_j e_j^{+} = -\cos(\phi_j), \qquad q_j e_j^{-} = -\sin(\phi_j) \tag{3.35}$$

for the j'th species. This shows that $\mathbf{e}^{+}$ and $\mathbf{e}^{-}$ can be determined from n such quenchings.

According to equation 3.21, the vectors that span the stable subspace must all be orthogonal to $\mathbf{e}^{1}$ and $\mathbf{e}^{2}$. Thus, when $\mathbf{e}^{+}$ and $\mathbf{e}^{-}$ are known, we also know a basis of the stable subspace. Equation 3.31 and 3.32 give us two sets of each two equations, which can be solved if each set has no more than two unknowns. If we know $\mathbf{e}^{+}$ and $\mathbf{e}^{-}$ from n linearly independent quenchings, two components of $\mathbf{u}$ and $\mathbf{v}$, i.e. the oscillations of two species, can be determined. The last $n-2$ components of $\mathbf{u}$ and $\mathbf{v}$ must be determined by direct measurements of the oscillations of the corresponding species. Alternatively, equation 3.31 and 3.32 can be solved with $n-1$ quenchings, if $n-1$ species have been monitored.

The conclusion is that, in principle, it is possible to obtain a detailed description of the motion in the unstable subspace around $\mathbf{x}^{*}$. Since this is the slow subspace of the system, this is the essential part of the dynamics (cf. page 39). Furthermore, the stable and the unstable subspace can be positioned in phase space.

Quenchings can be hard to obtain experimentally, and often only one or a few of the species can be monitored during the oscillations. So in practice you will usually end up with a low-dimensional description of the system. But this description could, nevertheless, still be a quite good one, especially if some of the species only show oscillations with a small amplitude. For a more detailed discussion of the validity of such a description see Sørensen *et al.* (1990).

For the j'th species, equation 3.35 describes a circle in the complex plane (see figure 3.16). Therefore, the phase and amount needed to quench the system with this species can be calculated from

$$\phi_j = \arg\left(-e_j^+ - ie_j^-\right) \quad (3.36)$$

$$q_j = \frac{1}{\sqrt{\left(e_j^+\right)^2 + \left(e_j^-\right)^2}}. \quad (3.37)$$

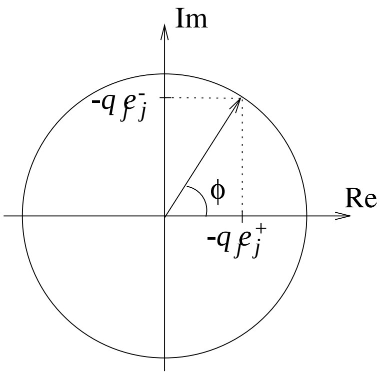

Figure 3.16: Equation 3.35 describes a circle in the complex plane.

Using this equation, quenching parameters for a given species can be calculated from a set of ODEs, and compared to experimental quenching parameters. This way, quenching data can be used to validate models of the system under study (Hynne *et al.*, 1993a; Vukojević *et al.*, 1996).

When working with intact yeast cells, this is probably the best one can hope for, since most of the glycolytic intermediates cannot pass the cell membrane, and thus cannot be used to quench the oscillations. Also, quenching by dilution is not possible. Most cells could in principle have their cytoplasm diluted by osmotic shock, but this cannot be done with yeast cells, since their rigid cell wall preserves their shape and volume.

Alternative Methods

Other methods for experimental determination of reaction mechanisms are avaliable, but most of them suffer from the drawback that all species of interest should be measured continuously. For an overview, see Stemwedel *et al.* (1995). This is difficult and very laborious, especially when working with intact cells. Therefore, these methods are not suited for *in vivo* investigations.

Recently, a new method for the experimental determination of the Jacobian matrix has been developed. The method is derived from control analysis, and has the advantage that only one species needs to be measured while the system is being perturbed with different species. Furthermore, the method is – unlike quenching analysis – not restricted to a special state of the system, but can be used on any steady state in an open system. However, this method has not yet proven successful experimentally, because the demands to the signal-to-noise ratio of the measurements, and the stability and reproducibility of the steady state, are very high (Skødt, 1999; Mihaliuk *et al.*, 1999).

4
Glycolytic Oscillations

In 1957 Duysens and Amesz measured the fluorescence of intracellular NADH in yeast cells (*Saccharomyces carlsbergensis*), and found the first indication that glycolysis can show oscillations in living cells. But the study of these oscillations did not take form until the work of Ghosh, Chance and Estabrook was published in 1964 (Chance *et al.* (1964); Ghosh and Chance (1964); see figure 4.1). For the next 15 years, a substantial amount of work was done in this field. The motivation then was the same as it is for me today: The glycolytic oscillations represent a striking and intriguing example of complex dynamics in an enzyme system which is fundamental to almost all living cells. At the same time, the phenomenon involves cell communication – A topic which is turning out to be of great importance, as we learn more and more about the molecular machinery of the individual cells.

The investigations came to a dead stop in the 1980s; maybe the reason was the success of the first fifteen years of work. The nature of the glycolytic oscillator had been established, and detailed knowledge of the factors which might effect the oscillations, had been gathered. Furthermore, the glycolytic oscillations had been established in other cell types than yeast, and these systems were studied instead. The idea that the glycolytic oscillations could function as a biological clock had also been abolished by this time.

By the start of the 1990s, a group of biochemists in Amsterdam resumed the investigations focusing on the cell communication which was still a mystery. At the same time, the strain of yeast cells commonly used for the experiments was changed from *Saccharomyces carlsbergensis* to *Saccharomyces cerevisiae*. Today, almost ten years later, we know that an intriguing concept of cell communication is involved. This concept is quite unlike what is normally seen, but

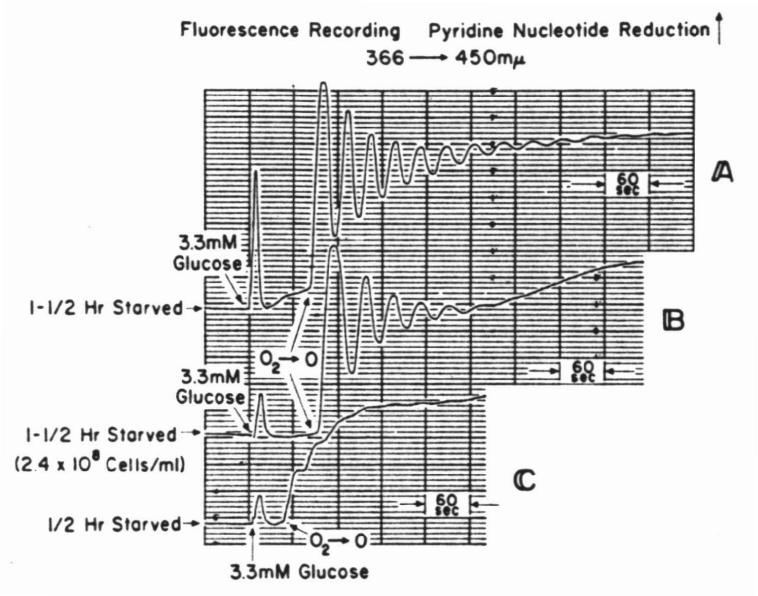

Figure 4.1: Glycolytic oscillations as reported by Chance *et al.* (1964). The originat figure legend reads:"Forms of RPN oscillatio in *S. carlsbergensis* recorded by the fluorescence method. (*A*) A recording of the oscillations initiated by aerobic-anaerobic transition (oxygen $\to$ 0) under optimal conditions (7/2/63). (*B*) Oscillations in a yeast cell suspension aerated for $1\frac{1}{2}$ hr (7/2/63). (*C*) Oscillations aerated for $\frac{1}{2}$ hr pror to the addition of glucose; 2% yeast 25° (7/2/63)". RPN: Reduced Pyridine Nucleotide, now called NADH.

it is still not widely appreciated.

4.1 Glycolytic Oscillations

Glycolytic oscillations in yeast cells can be induced in several ways, but the oscillations are all related to anaerobic metabolism where the mitochondria are not active. In many of the early experiments, the anaerobic conditions where caused by the yeast cells themselves, who used up all the oxygen in a reaction chamber while a pulse of glucose was being metabolised. Oxygen was kept away from the cells either by excluding oxygen from the reaction chamber, or simply by avoiding stirring. This way, the Pasteur effect induces damped oscillations in the yeast cells. Later on, chemical inhibitors of respiration was used to simulate anaerobiosis for reasons described in section 4.2.

Since the experiments are carried out in closed systems, the observed oscillations are all transient. Nevertheless, the yeast cells function in a way so that they can put up their own open flow-system for quite a long time. This is done by transporting the glucose into the cells at a slow, steady rate, hereby creating a long-lasting transient towards the depletion of glucose. On this transient, limit-cycle oscillations are sometimes found, but the oscillations usually reported correspond to a system spiralling towards the stable stationary state of a focus.

The Glycolytic Oscillator

From the early investigations it became clear that PFK is an enzyme of great importance for the dynamics of glycolysis. In particular, the positive feedback loop created by the product activation by ADP, FBP and indirectly by AMP (as described in chapter 2) is often used to explain how the glycolytic oscillations can arise.

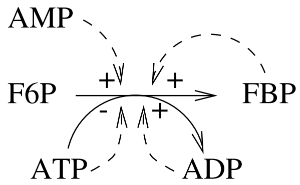

When PFK is active, activators are produced and make PFK even more active. However, this autocatalytic cycle cannot go on forever, since the substrate for PFK will be used up. Simultaneously, the lower part of glycolysis converts FBP into Pyr, and thereby ATP is produced from ADP (because of the AK reaction, this consumes the AMP as well). Consequently, PFK slows down. This piles up F6P, and at some point PFK will again become active. This brings us back to the beginning of the cycle, which will then repeat itself.

This is the standard explanation of the glycolytic oscillations as it can be found (with various variations) in several papers and textbooks, e.g. Ghosh and Chance (1964); Boiteux and Hess (1973); Mathews and van Holde (1990) and the Sel'kov model mentioned on page 35 (see inset). Often AMP is pointed out as the most important of the activating products (Sel'kov and Betz, 1973; Betz, 1973).

Several experimental facts seem to comply with this picture. Eschrich *et al.* (1983) showed that a reconstituted enzyme system consisting of PFK, PK, G6P and AK is not capable of producing oscillations, but oscillations can be seen when fructose 1,6-bisphosphatase is included. Thus, an *in vitro* system which is almost as simple as the picture given above, can in fact produce oscillations.

A consequense of the simple picture is that F6P will pile up when FBP is being consumed and vice versa. When the metabolites are measured, this is seen as a 180° phase difference between these two metabolites. Ghosh and Chance (1964) take this phase difference as evidence that the product activation of PFK is the basic oscillator mechanism of glycolysis. This way of reasoning is known as the *cross-over theorem*[1]. When yeast extract is used, this argument identifies both PFK, PK and GAPDH as control points, but PFK is still pointed out as the most important of these (Boiteux and Hess, 1973).

Boiteux and Hess (1973) also report that F6P is a minimal substrate for the glycolytic oscillations. This means that oscillations can be seen when Glc, G6P or F6P is supplied to an extract, but not when metabolites from FBP and down are supplied. This is taken as further evidence that PFK is the origin of the oscillations; the so-called "oscillophore".

The Sel'kov model formulated as chemical kinetics:

$$\begin{array}{llll} & \longrightarrow & \mathrm{Y} & v = b \\ \mathrm{Y} & \longrightarrow & \mathrm{X} & v = \mathrm{y}(a+\mathrm{x}^2) \\ \mathrm{X} & \longrightarrow & & v = \mathrm{x} \end{array}$$

As we know from the previous chapter, oscillations are a property of the entire dynamical system more than a property of a single reaction. Therefore, the picture presented above is too simple, even though there is no doubt that PFK is an important part of the dynamics of the system. This notion is also in compliance with the results of metabolic control analysis, which I presented on page 11. I will go along with Winfree (1980), and site *The Steppenwolf Treatise* by Hermann Hesse: "Things are not so simple in life as in our thoughts, nor so rough and ready as in our poor idiotic language".

In fact it is obvious, that the simple picture cannot be the whole truth: The oscillations are measured as NADH oscillations, so we should at least explain how they arise. One could imagine the NAD^+/NADH system as a "slave" of the PFK/adenosine nucleotide system: It oscillates when the glycolytic flux oscillates, but the state of the NAD^+/NADH system has no effect on the PFK/adenosine nucleotide system. This is, however, not the case.

As shown by Pye (1969) and Nielsen *et al.* (1998), yeast extracts respond to perturbations with components of the PFK/adenosine nucleotide system. But they respond to perturbations of the NAD^+/NADH system just as well. In particular, additions of ACA, Pyr or acetate will influence the oscillations (Pye, 1973; Betz and Chance, 1965a). This is also seen when intact cells are used (Betz and Becker, 1975; Richter *et al.*, 1975; Winfree, 1980; Bakker, 1993;

[1]See Fell (1997) for a discussion of the cross-over theorem.

Richard *et al.*, 1996a). Therefore, we conclude that the NAD^+/NADH system is not merely a slave of the PFK/adenosine nucleotide system.

Moreover, the measurements of the phase differences of the different metabolites – which were used together with the cross-over theorem to point out PFK as the oscillophore – cannot be explained on the basis of the simple PFK/adenosine nucleotide picture, which was presented above (Betz and Chance, 1965b).

Thus, it seems that the PFK/adenosine nucleotide system and the NAD^+/NADH system are intimately connected; probably through the joint action of GAPDH and PGK (Betz and Chance, 1965b; Pye, 1973; Richard *et al.*, 1996b).

Since most of the work on the nature of the glycolytic oscillations was done before it was realised that F2,6BP is a potent activator of PFK, this metabolite was not included in the experiments. However, Richard *et al.* (1996b) have measured an almost constant level of F2,6BP in oscillating yeast cells, and Yuan *et al.* (1990) report that the metabolite is not an essential part of the oscillations, since the F2,6BP concentration in oscillating extracts is too low to have any significant effect. Also, they report that oscillations can be seen in mutants with no detectable F2,6BP. On the other hand, this does not mean that F2,6BP has no effect on the oscillations, since yeast extracts show strong responses to perturbations with this metabolite (Yuan *et al.*, 1990).

Growth Dependence

The above discussion of the glycolytic oscillator was given in the context of changing metabolite concentrations, but with enzyme concentrations fixed. However, the enzyme activity is also of great importance for the appearance of glycolytic oscillations. This is realised experimentally by noting the importance of the time of harvesting of the yeast. As described on page 25, the yeast is usually grown in an aerobic batch, where the composition of the growth medium is constantly changing as a result of the growth. Under these growth conditions, yeast cells that are harvested at the diauxic shift, show oscillations that are significantly less damped (quantified simply by counting the number of cycles) than oscillations induced in cells harvested at other times of the growth (Hess and Boiteux, 1968; Pye, 1969; Kreuzberg and Betz, 1979; Richard *et al.*, 1993). As noted, this difference is ascribed to differences in the enzymatic composition of the yeast cells harvested at different times, but it is not well understood how the dynamics of glycolysis is affected by these changes.

However, the microcalorimetry measurements by Teusink *et al.* (1996b)

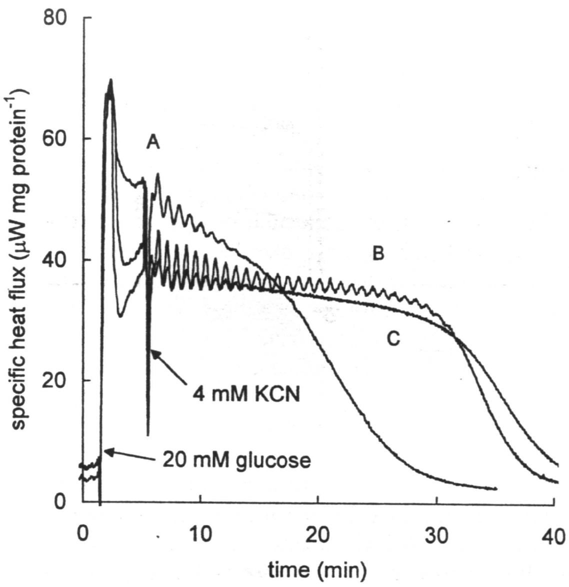

Figure 4.2: Growth-phase dependence of the specific heat flux under oscillating conditions. Cells were harvested at mid-exponential phase (A), transition phase (B), or respiratory phase (C), starved for 2 h, and oscillations induced by glucose ($t = 0$ min) and KCN ($t = 4$ min). Reproduced from Teusink *et al.* (1996b).

(see figure 4.2) have given some insights into this. They show that the time-evolution of the glycolytic flux – following a glucose and a cyanide pulse – depends strongly on the time of harvesting. Cells harvested in the mid-exponential phase show a steadily decreasing flux, while cells harvested at the diauxic shift, or when growing on ethanol, show an almost constant flux that goes abruptly to zero when the glucose is depleted. Thus, it seems like cells harvested at the glucose depletion or later do in fact set up their own steady flow system, while the cells harvested in the first exponential growth phase do not. Teusink *et al.* suggest the changing glucose affinity of the glucose transporter (cf. page 25) as a mechanism for this: When the glucose transporter has a high affinity for glucose, it is saturated almost until the glucose is completely depleted. But when the transporter has a low affinity component, the glycolytic flux decreases when the extracellular glucose concentration is decreased. Note, however, that the cells harvested later than the diauxic shift do not show bulk oscillations even though the overall time-evolution of the flux is similar to that of the cells harvested at the shift.

Unfortunately, many of the early experiments are carried out with yeast cells harvested according to time of growth, instead of some direct measure of the growth phase. Since there will unavoidably be variations in the duration of the initial growth phase, this means that the yeast is not well defined. Therefore, it is difficult to compare or reproduce these experiments.

Hess and Boiteux (1968) report that yeast cells grown anaerobically show pronounced oscillations as well, but this is even less understood than the differences between the yeast cells grown aerobically.

Models of Glycolytic Oscillations

Based on the detailed knowledge of glycolytic oscillations presented in chapter 2 and in this chapter, glycolytic oscillations in extracts have been modeled extensively. In broad terms, the models are either simple models focusing on the dynamics of PFK (e.g. Sel'kov (1968), Goldbeter (1996) and Baier *et al.* (1999)) or elaborated models which encompass most of the glycolytic reactions (Richter *et al.*, 1975; Termonia and Ross, 1981; Hocker *et al.*, 1994; Nielsen *et al.*, 1998). The PFK models are made in order to do qualitative investigations of the dynamics, while the aim of the comprehensive models is to explain and predict the behaviours of the experimental systems at the biochemical level.

It should come as no surprise to the reader that the comprehensive models are, in principle, the most interesting ones in my mind. But there is a serious problem with such models: They all contain a lot of parameters that must somehow be determined. This is a very difficult task, because the experimental estimation of the parameters is uncertain. Therefore, the formulation of such models involves a fair deal of guessing. Nevertheless, the stable oscillating states of the models show good agreement with experimental values of concentration ranges and phase differences of the metabolites. Furthermore, the models presented by Richter *et al.* (1975) and Nielsen *et al.* (1998) have shown successful when compared with experimental perturbations. Thus, there is an indication that the dynamics of these two models are good descriptions of the dynamics of the oscillating extracts.

With this in mind, it is striking how little the real biological system, i.e. the glycolytic oscillations in intact yeast cells, has been modelled. One reason for this might be the difficulties of using parameters obtained from *in vitro* studies for modelling the *in vivo* system as already mentioned on page 46. To be more specific, it is often the case that the V_{max} values of the enzymes seem to be much higher *in vivo* than when they are measured *in vitro* (e.g. Babul *et al.* (1993) and Benevolensky *et al.* (1994)). Several explanations have been offered for such phenomena (for a review see Aragón and Sols (1991)). This includes the concept of substrate channeling where different enzymes form complexes that should prevent diffusion of the intermediate metabolite by directly transferring it between the active sites of the interacting enzymes. It is also reported that some enzymes increase their activity by aggregating (with themselves) as the enzyme concentration is increased. In our context PFK and PK are important examples of this.

These problems have been circumvented in the study by Theobald *et al.* (1997); Rizzi *et al.* (1997). In this study, a culture of *Saccharomyces cerevisiae* is perturbed with a pulse of glucose while it is growing aerobically under glucose limitation. (The yeast cells do not oscillate under these conditions). The resulting transient is traced by rapid sampling and extensive enzymatic measurements of the metabolites. These data are then used to fit the kinetic parameters of a comprehensive model which incorporates both glycolysis, fermentation, oxidative phosphorylation and drains for biosynthesis. In this way, a model is obtained which fit the transients of most of the metabolites quite well. However, the fit is not perfect, and some of the parameters resulting from the fit seem unrealistic. The biggest problem is the pyruvate concentration, but the concentrations of the adenosine nucleotides and of $NAD^+/NADH$ do not fit well either. This model does of course not show glycolytic oscillations, but nevertheless it is a serious attempt to model the *in vivo* dynamics of *Saccharomyces cerevisiae*.

Modelling of glycolytic oscillations with explicit reference to intact yeast cells has been done by Aon *et al.* (1991) and Bier *et al.* (1996), using 4 and 6 coupled differential equations, respectively. These models are centered around the stoichiometric positive feedback of ATP, and disregards the regulation of PFK. It is interesting – from a biological point of view – that the complex kinetics of PFK are not needed to explain the oscillations. However, this should come as no surprise (see, e.g., the Oregonator model by Field and Noyes (1972)).

When seeking a realistic model, I see no sound reason to disregard PFK, which is a well established parts of the real-world system. Thus, we must conclude that – despite three decades of experiments and extensive modelling of yeast extracts – a comprehensive model of glycolytic oscillations in yeast cells does not exist.

4.2 Cell Synchronization

The glycolytic oscillations are measured as an average over many million cells. When such macroscopic oscillations are seen, the yeast cells must be at least partly synchronized; if they were not, the macroscopic sum that we measure in the experiments would not oscillate.

A suspension of yeast cells is generally a heterogenic collection of cells which differ in size, age and probably many other properties. Therefore, if no active synchronization takes place, differences in the intrinsic frequencies of the cellular oscillators will make them run out of phase with each other. The bulk oscillations will then die out, even though there might be oscillations on the level of the single cells.

One of the most fascinating aspects of the glycolytic oscillations in yeast cells is the fact that the individual cells actually do synchronize their oscillations with each other. This capability was demonstrated unambiguously in an elegant experiment: If equal amounts of two suspensions oscillating 180° out of phase are mixed, the bulk oscillations of NADH disappear immediately after the mixing, but reappear spontaneously after some time (Pye, 1969; Ghosh *et al.*, 1971; Richard *et al.*, 1996a). According to Ghosh and coworkers, yeast cells at the minimum of the NADH oscillations are likely to synchronize the other yeast cells to their own phase of oscillation, but otherwise no firm conclusions have been made in terms of predicting the phase of the reappearing oscillations. However, a systematic presentation of the data, which might be of some predictive value, is given by Winfree (1980).

The Mechanism of Cell Synchronization

The strength of this synchronization differs with different experimental parameters. As mentioned, the time of harvesting is important, but it seems that an extracellular ACA drain is important as well. The cyanide, which was originally used because of its ability to block the respiratory chain, happens to provide just this.

Cyanide is a nucleophilic reagent in its deprotonated form, and as such it reacts with ACA to form lactonitril:

$$\mathrm{CH_3CHO} + {}^{-}\mathrm{CN} + \mathrm{H^+} \quad \longrightarrow \quad \mathrm{CH_3CH(OH)CN}$$

As one could expect, this reaction has bimolecular reaction kinetics (Svirbely and Roth, 1953), and since CN^- is one of the reactive species, the rate constant increases with pH. At pH = 6.8, Richard *et al.* (1996a) report a rate constant of 1.5 M^{-1} s^{-1}. According to Svirbely and Roth (1953), this reaction is in practice irreversible. Following an indication by Betz and Chance (1965a) (see

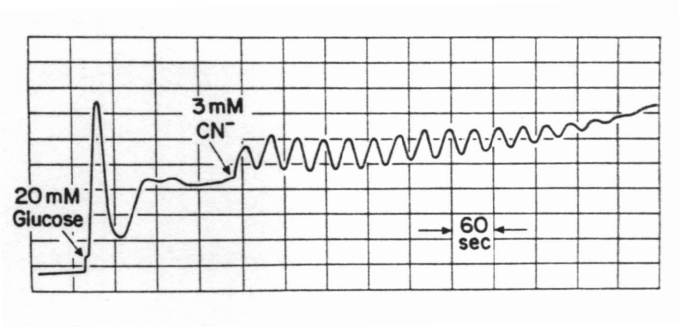

Figure 4.3: Cyanide-induced oscillations as reported by Betz and Chance (1965a). See the original paper for details.

figure 4.3), the first investigations of this was carried out by Ghosh *et al.* (1971), who found that a pulse of KCN induces much longer trains of oscillations than the depletion of oxygen does. When other respiratory inhibitors are used[2], the oscillations are more damped. But when an extracellular ACA trap, in the form of ADH and NADH, is added to the suspension, the long-lasting oscillations are seen again. A similar pyruvate trap, in the form of lactate dehydrogenase and NADH, has no effect. When the experiment with KCN-induced oscillations is repeated at a low pH, the oscillations are damped again. – If CN^- shall act as a ACA trap in order to maintain the oscillations, then this observation is in accordance with the expected reaction kinetics of the trapping reaction.

Richard *et al.* (1994) elaborated on this work and found that there is both a lower (3 mM) and an upper (8 mM) threshold for the cyanide concentration, if long-lasting oscillations are to appear. From this, and the fact that > 95% of the respiration is inhibited at $[CN^-]$ = 3 mM, they concluded that cyanide plays a dual role in the system: It serves both to inhibit cytochrome C oxidase and to react with ACA. They also measured a steadily increasing concentration of "total acetaldehyde" (which includes both ACA and lactonitril), and established that the glycerol production increases with increasing cyanide concentrations. This is probably due to the increased drainage of ACA as already

[2]Sodium azide was used, and since N_3^- is also a nucleophile reagent the argument might not hold (Bakker, 1993).

discussed (cf. page 20). Further studies by the Amsterdam group revealed

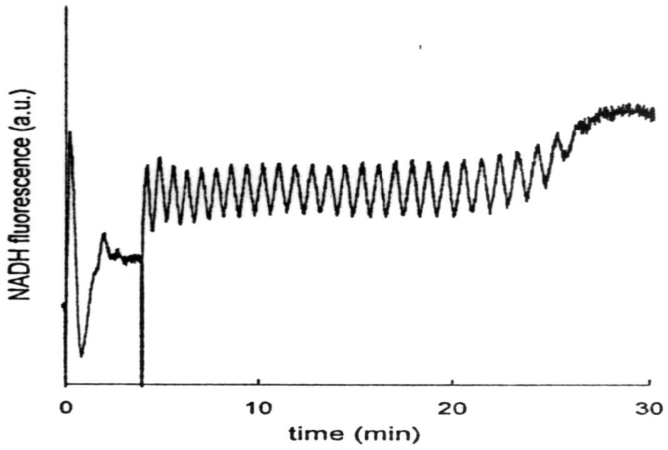

Figure 4.4: A typical example of the glycolytic oscillations, as reported by the Amsterdam group. *Saccharomyces cerevisiae* is harvested at the point of glucose depletion, and then starved for two hours. The oscillations are induced by adding a 20 mM glucose pulse at $t = 0$, followed by a 4 mM cyanide pulse at $t = 4$ min. This figure is reproduced from Bier *et al.* (1996); see Richard *et al.* (1993) for details.

that the concentration of free extracellular ACA is oscillating around a rather stable mean value (Richard *et al.*, 1996a). Under these conditions, the oscillations persist until the depletion of glucose, and they can then be restarted by adding another pulse of glucose. This can be done a couple of times, but at some point additional glucose pulses do not cause another train of oscillations. If, however, an additional cyanide pulse is given along with the third glucose pulse, this limitation is circumvented (Teusink *et al.*, 1996b). This strongly suggests that the cyanide in the cell suspension is actually being consumed.

In summary, it seems that the yeast cells synchronize their glycolytic oscillations by means of the ACA which diffuses between the cytoplasm of the oscillating yeast cells and the extracellular medium. In order for this synchronization to work, the extracellular ACA concentration shall remain within a certain range; the ACA drain should neither be too slow nor too fast. We know that this mechanism can in fact synchronize the yeast cells, since ACA can phase shift the oscillators when added in pulses comparable in size to the extracellular ACA oscillations (Betz and Becker, 1975; Richard *et al.*, 1996a);

Winfree (1980)[3] even reports a quenching of damped oscillations with ACA. Also, the notion of ACA as a mediator of the synchronization fits the data from the mixing experiment of Ghosh *et al.* (1971): The cells with the "winning phase" are the cells with NADH at its minimum; at this point the ACA concentration is at its maximum.

The proposed synchronization mechanism might also explain why yeast cells harvested after the diauxic shift do not show bulk oscillations, even though their glycolytic flux is comparable to that of the cells harvested at the shift (cf. page 60). Presumably, the yeast cells growing on EtOH have a higher ADH activity than the yeast cells harvested at the diauxic shift, as discussed on page 25. Therefore, their intracellular ACA concentration is lower, and the amount of ACA which diffuses out of the cells, will be quite low as well. This weakens the synchronization.

Notice how this explanation can also account for the extremely low lactate dehydrogenase activity which is seen in β-cells, provided that they rely on a synchronization mechanism similar to the one described in this chapter (cf. page 4).

The Effect of Cell Density

If this is actually the synchronization mechanism, then the strength of the synchronization must depend on the thickness of the suspension, since the ACA which diffuses out of the cells, will be less diluted the thicker the cell suspensions are. At some point, the synchronizing signal will be so weak that it cannot synchronize the yeast cells. In this sense, the cell density is a direct measure of the coupling strength of the glycolytic oscillators. This is illustrated by the results of Aon *et al.* (1992). Oscillations are induced by addition of a glucose pulse and a cyanide pulse, and the amplitude is graphed as a function of time. For low cell densities, the amplitude of the oscillations decays exponentially as the independent oscillators run out of phase. At high cell densities the amplitude remains roughly constant – thereby indicating synchronization – until it suddenly decreases[4].

Experiments by Bakker (1993) point to stronger synchronization at high cell densities as well. She counted the number of cycles following a glucose and

[3] Winfree cites a thesis by L. D. Greller, but I have not had the opportunity to see this thesis.

[4] The yeast cells used in this experiment were harvested while they were still growing on glucose, so this decrease is probably due to the falling glucose concentration (cf. page 60).

a cyanide pulse. It is seen that denser cell suspensions oscillate for a longer time. At very high densities the duration of the oscillations falls again. The reason for this is probably very simple: More cells consume the glucose faster. To avoid such effects Aldridge and Pye (1976) quantified the strength of the synchronization by measuring the amplitude of the second peak. They found that both too low and too high cell densities will diminish this amplitude. In my mind, it is difficult to judge whether this is an effect of cell synchronization. If this is really the case, I know no explanation for it.

4.2.1 The Appearance of Macroscopic Oscillations

If the oscillating yeast cells are all coupled, then the macroscopic measurements will reflect the oscillation of the individual cells. However, if the cells are not strongly coupled then the averaged measurements might not reflect the oscillations of the single cells. In particular, the sinusoidal oscillations usually seen in suspensions of oscillating yeast cells, might result from individual cells with non-sinusoidal oscillations. Also, transient macroscopic oscillations might arise from oscillating cells running out of phase as already described.

Such phenomena were investigated by Chance *et al.* (1973) in an impressive experiment. They worked with damped oscillations induced by the transition from aerobic to anaerobic metabolism, and characterised these oscillations by a damping factor describing an exponentially decaying envelope of the oscillations. By combining fluorescence microscopy with normal fluorescence measurements they showed that the macroscopic oscillations are more damped than the oscillations of the individual cells, and thus the macroscopic oscillations disappear partly as a result of desynchronization. Apart from the damping factor, the fluorescence trace of a single cell is similar to the macroscopic trace.

A similar result (but not as convincing) was reported by Aon *et al.* (1992), who worked on damped, cyanide induced oscillations in yeast cells, harvested during the first exponential growth phase.

Theoretical Studies

But the dynamics of the yeast cell suspension could be much richer than this. This is known from theoretical and numerical studies of globally coupled oscillators. The basis of these investigations is the Stuart-Landau equation (equation 3.12 on page 41), which is used to model each of the oscillators. Like the yeast cells, these oscillators are not all alike, since the intrinsic frequency of each of the oscillators is picked randomly from a frequency distribution. The N oscillators interact with each other with a linear, all-to-all coupling, and thus the equation describing the j'th oscillator reads

$$\frac{dz_j}{dt} = (i\omega_j + \sigma_j)z_j - g_j z_j |z_j|^2 + d\frac{1}{N}\sum_{i=1}^{N}(z_i - z_j) \tag{4.1}$$

where $g_j = g'_j + g''_j i$ and the coupling constant d is given by $d = d' + d''i$. Once again, the pioneering work was done by Winfree (1967). His work concerns only weak coupling in the particular sence that the mutual interactions among the oscillators are weak, relative to the attractiveness of the limit cycles of the individual oscillators. Then the dominant effect of the coupling is to influence the phase of the oscillations rather than the amplitude. Thus, in the limit of weak coupling, the only effect is that of phase variations; the amplitude $r_j(t)$ is fixed at $r_j = r_{\text{limit cycle}} = \sqrt{\frac{\sigma_j}{g'_j}}$. Kuramoto (1975) formulated this scenario in a clear mathematical sense by writing equation 4.1 with the following simplifications:

- $\sigma, g' \to \infty$ but $\frac{\sigma}{g'}$ is finite (the limit cycle is infinitely stiff)
- $N \to \infty$ (infinitely many oscillators)
- the frequency distribution is symmetric
- $\sigma_j = \sigma$ and $g_j = g$ (the oscillators only differ in ω_j)
- $d'' = 0$ (simple coupling)

When written in polar coordinates $z_j = r_j e^{i\theta_j}$ the simplified equation reads:

$$\dot{\theta}_j = \omega_j + \frac{d'}{N}\sum_{i=1}^{N}(\sin\theta_i - \sin\theta_j)\,. \tag{4.2}$$

This huge simplification comes about because one only has to consider the phase of the oscillators, because all the oscillators have the same constant amplitude. The above assumptions are not very realistic, but on the other hand they make the problem tractable since it is possible to do a mathematical analysis of equation 4.2. This analysis is presented in a clear and logical way by Strogatz (1993). The result is that basically two types of collective behaviour can be seen: (1) Incoherence – all the oscillators oscillate with their own frequency without synchronizing. This happens, of course, when the coupling is weak relative to the spread of the intrinsic frequencies. (2) Locking – all the oscillators oscillate with the same frequency and phase. This is seen when the coupling is strong. For intermediate coupling strengths, partial locking is seen; the oscillators with their intrinsic frequency closest to the mean frequency are locked, but the fast and the slow ones drift at different frequencies. This gives a frequency distribution with a sharp peak in the middle and broad tails at the extreme frequencies. From the onset of partial locking at $d = d_c$, the amplitude of the bulk oscillations r grows as $r \propto \sqrt{d - d_c}$.

This result is important, since it tells us that if a bifurcation parameter is varied in the experiments, and we see the amplitude of the bulk oscillations increasing with a square-root dependence on this parameter, then we would not be able to tell whether this is caused by a synchronization phenomenon or by simultaneous supercritical Hopf bifurcations in each of the strongly coupled oscillators[5], as discussed in the previous chapter.

However, we cannot expect the yeast cells to have infinitely stiff limit cycles. Therefore, it would be more interesting to look at equation 4.1 without the above simplifications. A thorough investigation of such a system has been done by Matthews *et al.* (1991). Along with a detailed bifurcation analysis, they present numerical integrations of the system with the following parameters:

- N is typically round 1000 individual oscillators
- $\sigma_j = 1$ and $g_j = 1$; the oscillators only differ in ω, and the frequency of the oscillators does not depend on their amplitude
- $d'' = 0$ (simple coupling)
- different frequency distributions are tested
- the observed variable is the "order parameter" r defined by $re^{i\theta} = \sum_{j=1}^{N} r_j e^{i\theta_j}$, which is a measure of the mean amplitude in a rotating coordinate system

The richness of the dynamics in this system is impressing: For some coupling strengths the behaviour is similar to what is seen in the work of Winfree and Kuramoto, but for other parameters the average of the oscillators shows

[5]To be precise, each of these many Hopf bifurcations would be Hopf bifurcations in a system consisting of a single yeast cell *and* the extracellular medium.

complex oscillations, period-doubled oscillations[6], quasiperiodic behaviour or chaos. However, nothing like this has ever been reported in experiments with intact yeast cells.

Coupling of limit-cycle oscillators, with explicit reference to glycolytic oscillations in yeast cells, have been studied in a collection of identical Sel'kov oscillators (cf. page 35) coupling through either the product or the substrate of the autocatalytic reaction (Wolf and Heinrich, 1997). This model of coupling shows some interesting dynamical phenomena. However, these phenonena arise because a single substance is the mediator of the synchronization. Since my experiments indicate that *both* glucose and acetaldehyde can synchronize the oscillations, I will not go into details about this modelling.

4.2.2 Some Concluding Remarks

The concept of cell communication which I have presented in this chapter, is different from what is usually seen: It does not rely on specific receptors and specialised signalling molecules. On the contrary, it is mediated by common metabolites which are – at the same time – central to the energy metabolism of the cell.

Ironically, the conclusion drawn by Ghosh, Chance and Pye from their pioneering work (Ghosh *et al.*, 1971) was that ACA is a "desyncronizer" of the oscillations. This stresses once more the importance of a proper conceptual framework when trying to understand dynamical systems: The dynamics is a property of the system as a whole; not a property of single reactions or substances.

This notion might also explain why this remarkable concept of cell communication is not widely appreciated. When the cell communicaton is so intimately related to the processes taking place inside the cell, you cannot characterise it by inhibiting its components or by constructing mutants, since this would affect the entire cell and not just the cell communication. In other words: You cannot see the wood for the trees.

[6]See Strogatz (1994) or Ott (1993) for an explanation of this phenomenon.

5
Experiments

The overall idea of my experiments is simple: Take the oscillating yeast cells and put them in an open system in order to get sustained oscillations indefinitely. This allows, among other things, for quenching experiments and bifurcation analysis.

In this chapter, I will describe how this is actually done, and present the results from the experiments. To avoid too many technical details in the text, all instruments and materials used are listed with full details in appendix B on page 141. Please consult this appendix, if you do not find the details in the text.

A proven way of making an open system is to use a Continuous–flow Stirred Tank Reactor, known as a CSTR. This means that reactants are flowed into a thermostated, stirred reactor, and the volume of this reactor is kept constant by outflow of surplus liquid. In my setup, starved yeast cells are kept in a cold stock which is stirred to avoid sedimentation. From here, they are continuously flowed into the cuvette along with cyanide and glucose solutions. The reactor is a 1×1 cm cuvette. A sketch of the setup is shown in figure 5.1.

When I started doing my experiments with glycolytic oscillations in yeast cells, there was no one at our laboratory who knew how to do such experiments. And, even worse, we had no equipment for the growth of the yeast. I have worked hard to get it all working anyway, but my efforts would no doubt have been fruitless, had it not been for the kind and encouraging help of many people. Above all, I am in debt to Bas Teusink at the E. C. Slater Institute, University of Amsterdam, who showed me how to grow and handle the yeast in his laboratory. I have also received much help from other people, but since they cannot all be mentioned here, I have put their names in the preface.

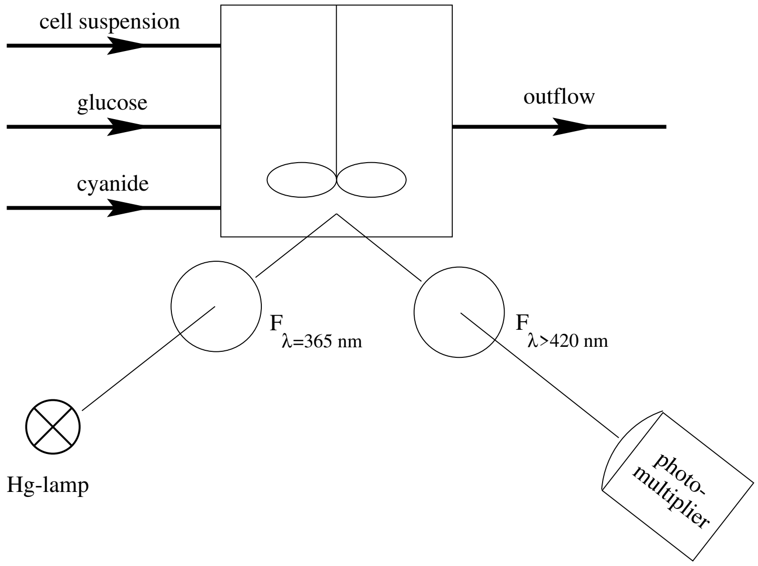

Figure 5.1: The experimental setup. The reactor is a stirred 1×1 cm cuvette thermostated at 25°C. The cell suspension is kept in a cold reservoir (2°C). From here, it is flowed into the reactor by a peristaltic pump with a constant rate of 80.2 μL/min. Two additional small and adjustable flows of glucose and cyanide solutions are provided by stepper motor driven piston burettes. The volume is kept constant at 1.89 ± 0.11 ml, and the mean residence time is 23.6 min. Fluorescence of NADH is brought about by excitation with the 365 nm Hg-line, and is measured as the emission of light in the interval 420–660 nm with a photomultiplier.

5.1 Growth of the Yeast

Yeast is considered to be an organism which is easily handled. This is important, since the aim of my work was to do nonlinear dynamics and not microbiology. By the same reasoning, it is a good idea to start out with a system which is already known to oscillate. Therefore the growth conditions are as close as possible to those used by the Amsterdam group (described by Richard *et al.* (1996b) and Richard *et al.* (1993)).

In short, the yeast is grown in a batch culture until glucose is deplete. Then further growth is avoided by removing the yeast from the growth medium, and the yeast cells are starved.

When growing the yeast for the experiments, the aim is to get large amounts of yeast in a well defined form. To reach this goal one has to consider several things.

First of all the life cycle of the yeast should be considered (figure 2.1 on page 6). Normally, yeast has both sexual and asexual reproduction. The asexual reproduction is by far the most common way of reproduction in *Saccharomyces cerevisiae* . Here new diploid cells are made by mitosis and subsequent budding. But wild-type *Saccharomyces cerevisiae* can also perform meiosis to produce haploid cells, which later conjugate with other haploid cells to make a diploid yeast cell. Having different kinds of yeast cells, could very well complicate the control and interpretation of the experiments. Therefore, a strain without sexual reproduction is used. Apart from this, the strain used (*Saccharomyces cerevisiae* x-2180a) is a standard wild-type strain. These things, along with the fact that other groups have used the same strain, makes *Saccharomyces cerevisiae* x-2180a a good choice for the experiments. The strain was obtained from the Department of Genetics, University of Copenhagen.

Further more, the growth conditions should be right and well controlled. Sufficient aeration is needed for the yeast to grow properly. This is the main problem when scaling up the amount of yeast grown. To overcome this problem the yeast is grown in an Erlenmeyer flask in a rotary incubator. The flask is filled with one fifth of the nominal volume, and scaling is done by using bigger bottles. The biggest bottle, which fit into our rotary incubator, is 6000 ml, and this is the bottle normally used for the main culture. The incubator is running at 180 rpm, which is almost the maximum speed avaliable in our lab. This is also the speed used in the experiments performed by the Amsterdam group, but it is somewhat slower than the 300 rpm which is normally used when growing yeast (Ausubel *et al.*, 1996). I have tried to grow the yeast at 300 rpm in another lab. This seems to produce the same yeast, at least when judged by the measurements of NADH oscillations. The growth temperature is 30°C, which is the standard choice of temperature for the growth of yeast (Ausubel *et al.*, 1996). A storage of the yeast strain is maintained on agar plates at 4°C. Standard sterile techniques are applied when growing and harvesting the yeast. The growth medium is composed as described in appendix B.

Determining the Harvesting Time

Since the yeast is growing in a batch culture, the environment is constantly changing while the yeast is growing. Furthermore, the yeast is adapting to these changes, so the make-up of the yeast is constantly changing. More specificly, the enzyme activities change as response to the available nutrients as described on page 25. Therefore it is very important to harvest the yeast in a well defined state of the growth. This is done by measuring the glucose concentration while the yeast is growing, and harvesting the yeast when the glucose is depleted. If the glucose concentration is measured at least once every 30 minutes, it is possible to obtain the same, well defined yeast suspension from every batch growth. A quick, cheap and easy way of measuring the glucose concentration is to use glucose sticks originally designed for glucose determination in urine.

To ease the timing of the growth and harvesting, the main culture is inoculated with a preculture. Approximately 0.5% vol. of outgrown preculture is needed to have the main culture ready for harvesting overnight. This way the long and ill-defined lag phase, which normally precedes the exponential growth, is avoided in the main culture.

Harvesting the Yeast

Harvesting the yeast means removing the yeast from the growth medium, and placing it in phosphate buffer. This stops the growth, since there are no nutrients in the phosphate buffer. The harvesting is done by centrifugation and resuspension of the yeast in cold phosphate buffer for washing. The yeast is then centrifuged again, and resuspended in phosphate buffer once more. The yeast suspension is now free of nutrients, but there might be some internal energy stores left, e.g. glycogen. This is removed by starving the yeast cells for two to three hours in the rotary incubator (See Kreuzberg and Betz (1979) for a thorough investigation of the effects of starvation). The yeast is then centrifuged once more and suspended (10% wet weight) in phosphate buffer. Afterwards, a more precise measure of the thickness of the suspension is obtained by measuring its OD (light scattering; "Optical Density"). The OD measurements have been calibrated to the number of cells in the suspension by counting the cells in a suspension of a known OD.

By following this procedure, it it possible to obtain approximately 70 ml of thick yeast cell suspension from each batch growth. Furthermore, the method produces the same yeast cells from different batches – as judged by the glycolytic oscillations – as long as care is taken to harvest exactly at the time of glucose depletion.

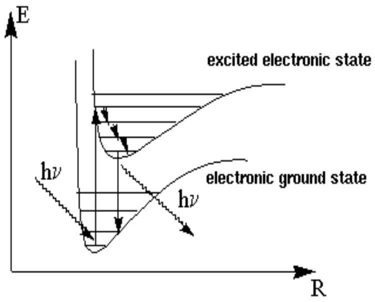

Figure 5.2: Flourescence. A sketch to illustrate the principles of fluorescence in a diatomic molecule. E is energy, and R is interatomic distance. The excitation light excites the electronic state of the fluorophore from the vibrational ground state of the electronic ground state to a higher orbital. Since the electronic transition is much faster than the atomic movements, this transition leads to a vibrationally excited state. However, the decay to the vibrational ground state is fast relative to the lifetime of the excited state, and therefore the electronic decay back to the ground state takes place from a state of lower energy. Consequently, the emitted light has a longer wavelength than the excitation light.

5.2 Setting up the CSTR Experiment

With the yeast cells on hand, it is now time to design the experimental setup. This involves basically two things: Performing online measurements and setting up an open system.

Measuring Fluorescence of NADH

The glycolytic oscillations are followed by measuring the fluorescence of NADH. From previous studies (Richard *et al.*, 1993), it is known that the oscillations in autofluorescence of the yeast cells corresponds to NADH oscillations inside the cells, even though other metabolites might also contribute to the fluorescence (e.g. NADPH). These NADH oscillations have a maximum around 400 μM and a minimum around 200 μM.

As shown in figure 5.2, fluorescence is the re-emittance of light at a longer wavelength than that of the excitation. The exact difference of the excitation and emission wavelengths depends on the chemical mircoenvironment of the fluorophore, and since NADH is found both free in the cytosol and associated with various proteins, the emission peak of NADH in the yeast cells is very broad ($>$ 40 nm, centered at 460 nm. Data not shown). The fluorescence of NADH is brought about by excitation with the 365 nm Hg-line, and because of the broad emission peak, I measure it as emitted light in the interval 420–660 nm with a photomultiplier. Due to the opacity of the cell suspension, the fluorescence originates from a thin layer at the surface of the cuvette.

To compensate for variations of the output from the mercury lamp, the intensity is measured by a photo-detector at 365 nm and used to correct the photomultiplier signal. For this correction, which is done by the program

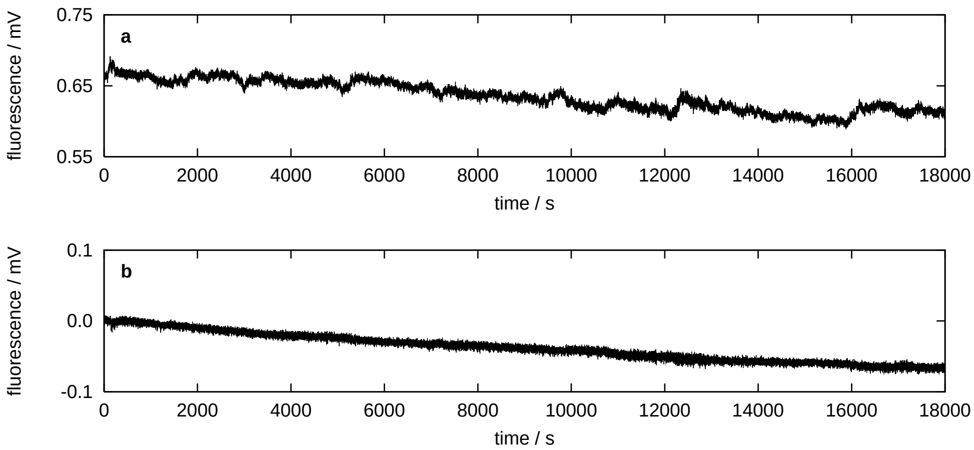

Figure 5.3: Compensation for variations in lamp output. To test the stability of the lamp, the fluorescence of a tiny piece of paper was monitored for five hours. **a** The uncorrected fluorescence trace. **b** The same fluorescence trace, corrected for lamp output variations according to equation 5.2. (The reference measurements are not shown).

`yeast`, a simple linear dependence of the signal from the photomultiplier F and the reference signal R is assumed

$$F = \alpha R + \beta, \tag{5.1}$$

where the constant term is included to allow for the dark current of the photomultiplier. The coefficients α and β are found before each series of measurements by calibration of the mercury-lamp output with a variable power supply. The corrected signal S is then calculated from

$$S = F - (\alpha R + \beta). \tag{5.2}$$

As shown in figure 5.3, this is a cheap and efficient way to remove the noise caused by lamp fluctuations.

I have found no easy way of calibrating the fluorescence measurements to the absolute intracellular NADH concentration. The calibration is made more difficult by the fact that the fluorescence originates from a thin layer of the cell suspension, since the thickness of this layer, as well as the fraction of emitted light scattered by the cells, depends on the thickness of the cell suspension.

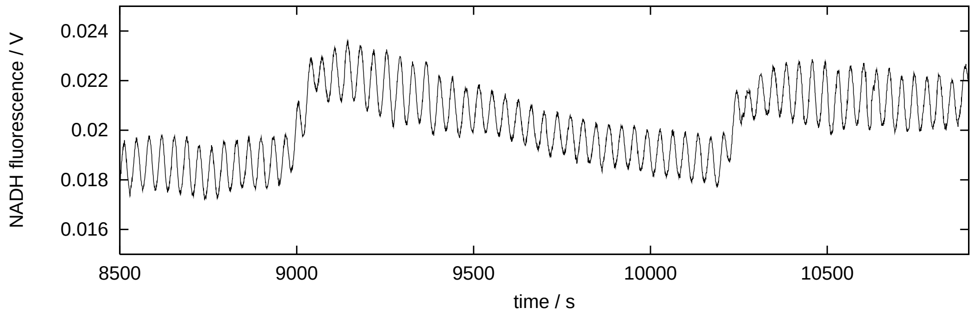

Figure 5.4: Early experiments showing "jumps", caused by an uneven flow of the yeast cell suspension.

Pumps and Burettes

In order to run a CSTR properly, you need stable flows. The yeast cell suspension makes up the main part of the flow. It is flowed into the cuvette by a peristaltic pump, which also drives the outflow. It turned out that the yeast cells are sedimented inside the tube which leads to the cuvette. This makes the tube more and more narrow, until – at some point – the sedimented yeast cells are washed out of the tube and into the cuvette. This uneven flow causes the fluorescence trace to "jump" now and then, as shown in figure 5.4. This problem was solved by constant, rapid injection of small bubbles of air into the tube with the cell suspension. Each bubble fills out the entire tube, and thereby it pushes the sedimented yeast cells through the tube.

The glucose and the cyanide flows are smaller than the flow of suspension. Therefore, a peristaltic pump is not well suited for these flows. Instead the two solutions are flowed into the cuvette by stepper-motor driven piston burettes. These burettes are fitted with valves and work in pairs, so that one burette can maintain the flow while the other is being refilled. The valves and stepper-motors are controlled by a computer, which also records the fluorescence trace. This allows for automatic adjustments of the flow rates, which is useful when doing experiments with flow rates as bifurcation parameters.

Additions to the cuvette can be made from two additional burettes. These perturbations can be pre-programmed with respect to runtime or with respect to both the phase of the oscillations and runtime (see details on page 84).

The program `yeast`, which controls the experimental setup, can be found at my website[1].

5.3 Experimental Results

With the setup described above, it is possible to run a CSTR with living yeast cells. The duration is, of course, limited by the amount of yeast cell suspension avaliable from the batch growth. – Still, stable oscillations can be observed for a prolonged period of time. The system turns out to be very stable. This can be seen in figure 5.5, where an unperturbed part of a run is shown. If desirable, even longer periods of stable oscillations can be observed, since one batch growth produces cell suspension for more than 14 hours of experiments.

When doing such experiments, it is important to demonstrate that the observed oscillations are in fact produced by the internal dynamics of the biological system, and not by some periodic forcing due to the setup.

5.3.1 Simple Experiments

One way to ascertain that the oscillations are in fact glycolytic is to reproduce the oscillations reported by the Amsterdam group (see Richard *et al.* (1996a); Bier *et al.* (1996); Teusink *et al.* (1996b); Bakker (1993); Teusink (1993) and figure 4.4). This is a good test, since these experiments are done in a closed system, where the risk of technical artifacts is not as big as in the complete flow system. Figure 5.6 shows such an experiment, and confirms that the nature of the oscillations in my experiments is the same as in those reported earlier. As also reported by Richard *et al.* (1993) and Teusink *et al.* (1996b), the oscillations persist until the glucose is used up, and the duration of the oscillations is roughly proportional to the amount of glucose added (data not shown). Notice that the period of the oscillations increases as the glucose concentration decreases, and that the final state of the yeast cells – as indicated by the level of NADH – is different from the initial state.

The glucose transient seen at the start of a CSTR experiment is similar to that seen in a closed system (compare figures 5.6 and 5.7). This is worth noticing, since the initial glucose concentration in the flow experiment is much lower than in the experiments in the closed system. With cyanide, the response in the flow system is more like one would expect; i.e. it is gradual in accordance with the slow build-up of the the cyanide concentration. Due to the blocking

[1] `http://theochem.ki.ku.dk/~sdd/`

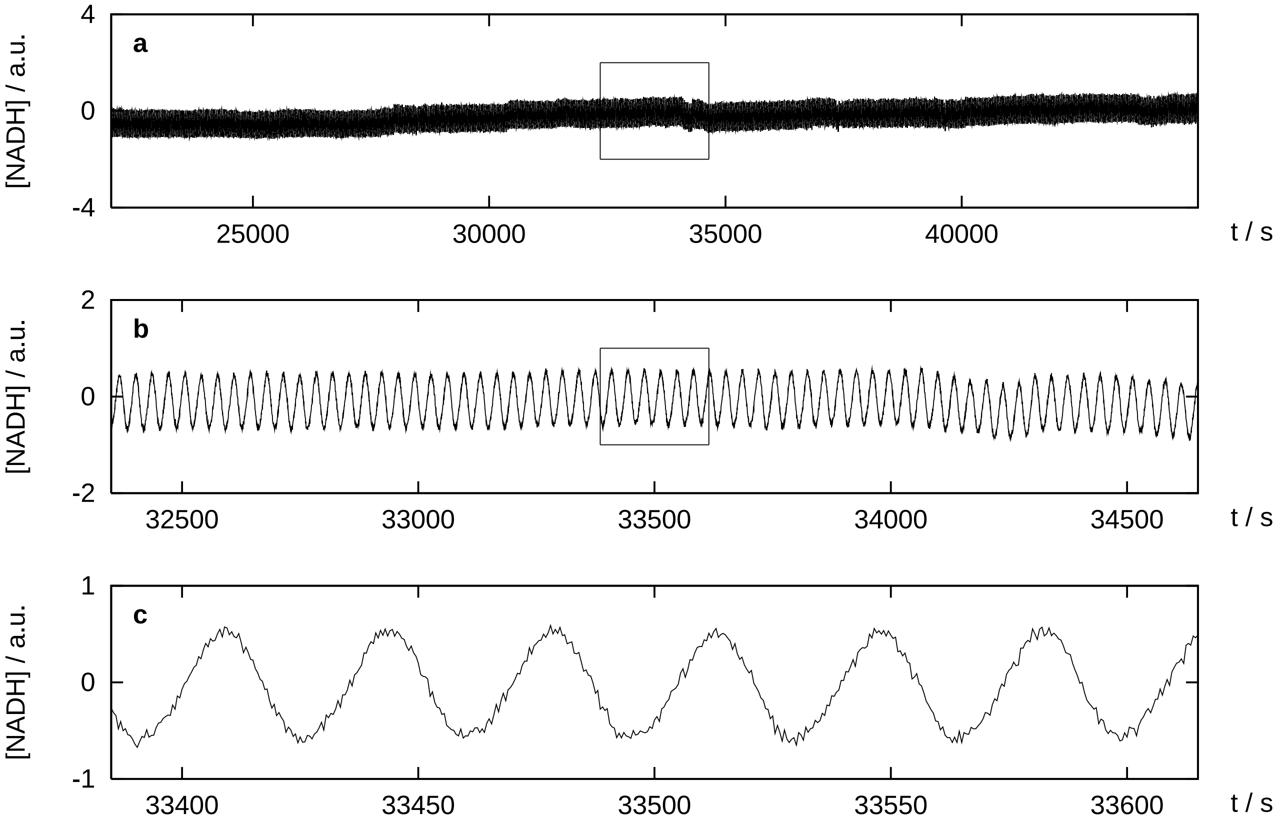

Figure 5.5: Sustained oscillations in *Saccharomyces cerevisiae*. **a** An unperturbed part of a CSTR experiment. The period of the oscillations is 34.8 s ± 0.20 s, and the amplitude is constant with a relative standard deviation of 2.8 %. These calculations are explained in the text on page 81. **b** An expansion of the box in the top panel. **c** A similar expansion of the box in the middle panel. Since new cells are constantly flowed into the cuvette, these stable oscillations provide another proof of the active cell synchronization. The cell density is $1.61 \cdot 10^9$ cells/ml and the specific flow rate is $50.6{\cdot}10^{-3}$ min^{-1}. The mixed flow concentrations of glucose and cyanide are 35.0 mM and 5.38 mM, respectively, and t is the time since the start of the experiment.

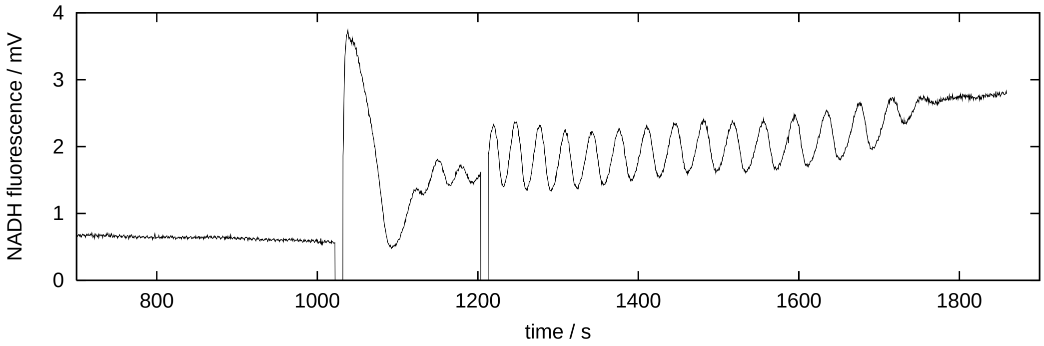

Figure 5.6: Glycolytic oscillations in a closed system. The same experiment as reported in Richard *et al.* (1996a); Teusink *et al.* (1996b); Bakker (1993); Teusink (1993). At $t = 1030$ s glucose was added to a final concentration of 20 mM, and at $t = 1210$ s cyanide was added to a final concentration of 3 mM.

of the respiratory chain, the NADH level rises shortly after the flow has been turned on. Then, the amplitude of the oscillations builds up slowly.

The dramatic response to very small amounts of glucose might explain the appearance of the strange-looking oscillations reported by von Klitzing and Betz (1970) in an often cited article. They carried out experiments with *Saccharomyces carlsbergensis* in a semi-open reactor with an inflow of glucose, but no outflow. A "lid" of N_2 was put above the stirred suspension to keep it anaerobic. The oscillations (reported to persist for some 40 h) look very different from other glycolytic oscillations in intact yeast cells (see figure 5.8), and have some strange properties: The amplitude is almost constant for different glucose flow rates, while the frequency increases proportionally to flow rate. Furthermore, von Klitzing and Betz report that "a sudden rise in free glucose is observed shortly before NADH rises", and that "we must assume that in this short interval excess glucose is set free" by the yeast cells!

A possible explanation of these peculiarities is that each "oscillation" originates from a small pulse of glucose injected into the suspension. Indeed, when this is tried in my setup, "saw tooth oscillations" – just like the ones reported – appears (compare figures 5.8 and 5.9). Thus, it seems that the oscillations reported by von Klitzing and Betz are caused by an uneven glucose flow, and not by the dynamics of the yeast cells.

My reason for pointing this out is to emphasise the importance of a proper experimental setup; not to criticize the work of other people. This is especially

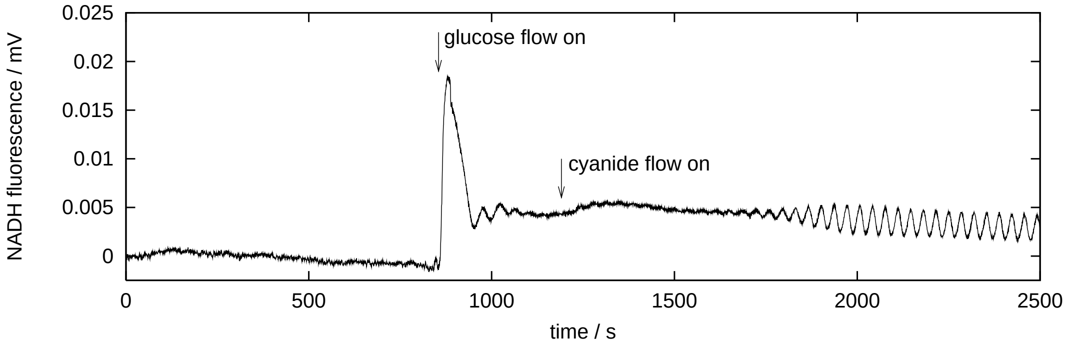

Figure 5.7: Transients at the start of a CSTR experiment. At time $t = 0$, only the flow of cell suspension is on. The glucose flow and the cyanide flow are then turned on as indicated by the arrows. See text for comments. Cell density is $1.61 \cdot 10^9$ cells/ml. When all three flows are on, the specific flow rate is $50.6 \cdot 10^{-3}$ min^{-1} and the mixed flow concentrations of glucose and cyanide are 35.1 mM and 5.38 mM, respectively.

important when operating setups like a CSTR, since failure to do so can lead to false conclusions about the nature of the biological system.

As I will now show, the oscillations in my experiments can be manipulated in the CSTR by changing the flow rates or by additions of extracellular metabolites. This is further evidence that the oscillations are in fact a result of the metabolic dynamics of the yeast cells.

5.3.2 Birfurcation Analysis

To get firm data on the dependence of the oscillations on the experimental parameters, a set of experiments with varying flow rates of either glucose or cyanide were carried out. Starting in the oscillating regime, the flow rate is adjusted slightly every 5000 s, and the amplitude of the resulting oscillations, if any, is determined at the end of the period.

Data Analysis

To perform this bifurcation analysis, an acurate description of the oscillations is needed for the amplitude calculations. Initially, I used Fourier analysis for this task (FFT module of `Mathematica`, Wolfram Research, Inc.). Figure 5.10 shows a typical Fourier spectrum of the oscillations. This particular spectrum

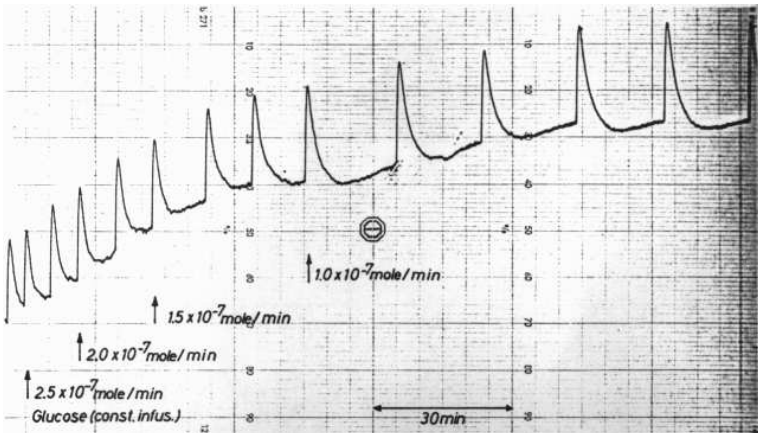

Figure 5.8: Oscillations in a semi-open system as reported by von Klitzing and Betz. To show how the frequency depends on it, the infusion rate is changed as indicated by the arrows. Reproduced from von Klitzing and Betz (1970).

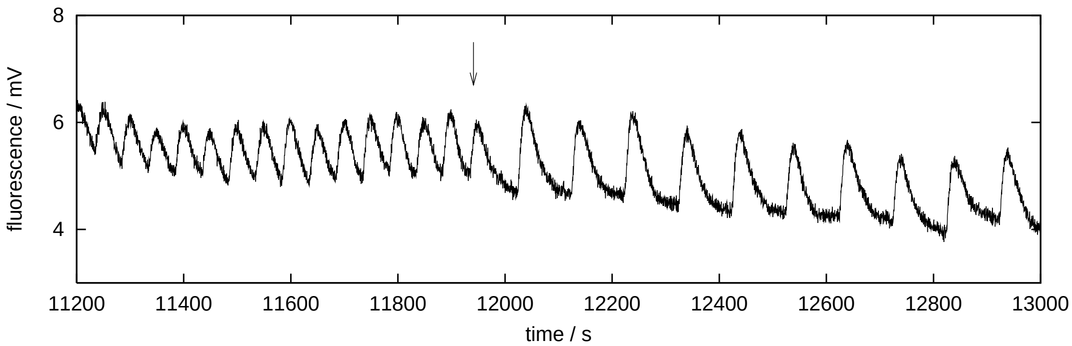

Figure 5.9: "Oscillations" caused by pulsed glucose inflow. A CSTR experiment with no cyanide flow and very low glucose flow rate (round 5% of the flow rates normally used). Each of the rising "saw tooths" correlates with a step by the stepper-motor which drives the glucose burette. The glucose flow rate is doubled at $t = 11940$ s (indicated by $\downarrow$). The specific flow rate is $43 \cdot 10^{-3}$ min^{-1}.

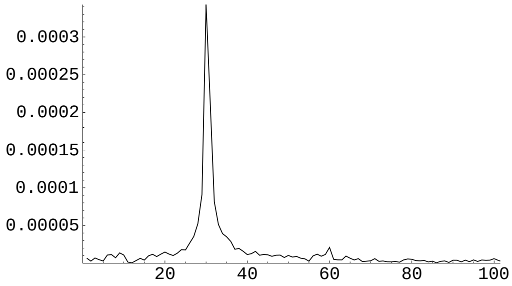

Figure 5.10: The Fourier spectrum of the oscillations shown in figure 5.11 (2048 data points). Ordinate is amplitude, abscissa is frequency. The main peak at "29" corresponds to a period of 35.3 s. (The low-frequency part of the spectrum has been left out for display purposes).

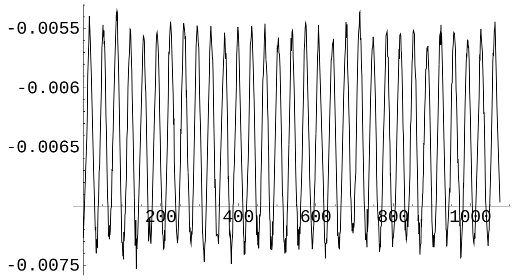

Figure 5.11: The data used to obtain the Fourier spectrum on the left. The x-axis is time in seconds, and the y-axis is fluorescense in volts.

is obtained from the data shown in figure 5.11. It is clear that, for any practical purpose, the oscillations are sinusoidal. Remarkably, this is true for the whole range of experimental parameters investigated (mixed flow glucose concentrations ranging from 0 mM to 85 mM, and mixed flow cyanide concentrations covering the entire interval of oscillations).

It turns out that the discretisation of the frequency, which is introduced as a consequence of the finite number of data points, makes FFT a bad tool for acurate amplitude determination. When the period is incorrect, the maxima of the measured trace and the fitted function do not coincide throughout the fitted interval. As a consequence, the determined amplitude is lower than the actual amplitude. An example of this is shown in figure 5.12. The significance of such an error varies from data set to data set, because the frequency of the oscillations in some data sets fits the discretised frequencies better than others. The only way to avoid this problem with FFT is to collect more data points, thereby obtaining a finer determination of the phase within the same window of observation.

Since the computer in the laboratory is too slow for this, and the data files are already rather big, some other approach must be taken. From the Fourier spectrums we know that the oscillations are – to a very good approximation – sinusoidal. Thus we just need to do a curve fit to a sine function

$$S = a \sin(\omega t + \varphi) + m. \tag{5.3}$$

Several different algorithms for nonlinear curve-fitting were tried, but they all failed because they treat a, ω, φ and m as independent parameters. However, to obtain a good fit, φ and ω need to be varied in accordance with each other. If we write

$$\mathbf{c} = \begin{pmatrix} a\cos\varphi \\ a\sin\varphi \\ m \end{pmatrix}, \quad \mathbf{f} = \begin{pmatrix} \sin(\omega t) \\ \cos(\omega t) \\ 1 \end{pmatrix},$$

then equation 5.3 can be rewritten as

$$\begin{aligned} S &= a\left(\cos\varphi\sin\omega t + \sin\varphi\cos\omega t\right) + m \\ &= c_1 f_1 + c_2 f_2 + c_3 f_3 \\ &= \mathbf{c}\cdot\mathbf{f} \\ &= \textstyle\sum_i c_i f_i(t). \end{aligned}$$

Since $S = \mathbf{c}\cdot\mathbf{f}$ is linear, then, for any given value of ω, $\mathbf{c}$ can be determined by a least square fit of the system

$$\begin{bmatrix} S_1 \\ S_2 \\ \vdots \\ S_N \end{bmatrix} = \begin{bmatrix} f_1(\omega, t_1) & f_2(\omega, t_1) & f_3(\omega, t_1) \\ f_1(\omega, t_2) & f_2(\omega, t_2) & f_3(\omega, t_2) \\ \vdots & \vdots & \vdots \\ f_1(\omega, t_N) & f_2(\omega, t_N) & f_3(\omega, t_N) \end{bmatrix} \begin{bmatrix} c_1 \\ c_2 \\ c_3 \end{bmatrix}, \tag{5.4}$$

where N is the number of data points. This is just what we need, since φ is now always in accordance with ω.

The actual fitting is now done by minimising

$$\chi^2 = \sum_{n=1}^{N} \left(S_n - \sum_i c_i f_i(\omega, t_n) \right)^2$$

by bisection with different values of ω.

The programs `fit.f` and `slidefit.f` (which can be found at my website) are implementations of this method. When I chose the size of the moving window (N in equation 5.4), I wanted to have it as small as possible in order to catch all the variations of the measurements. On the other hand, the window should not be too small, since it would then fit the noise in the data instead of the actual oscillations. By trial and error, I have found that a window size of 200 datapoints (i.e. approximately three cycles of oscillations), is a good compromise. Consequently, this size has been used throughout the data analysis.

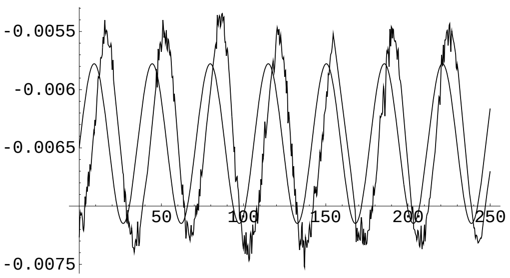

Figure 5.12: The left-most part of the fit obtained from the Fourier analysis shown in figure 5.10. The fitted period is too long (35.3 s instead of 34.8 s), and this results in a too low value of the fitted amplitude. The x-axis is time in seconds, and the y-axis is fluorescense in volts. Compare with figure 5.13.

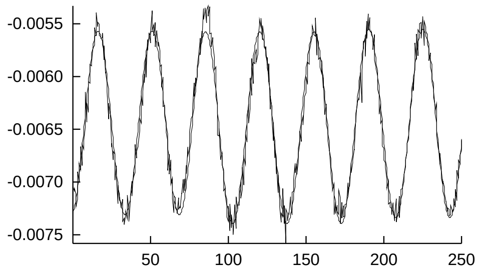

Figure 5.13: A fit of the same data as in figure 5.12, but now fitted with `fit.f` as described in the text. The period is 34.8 s and the amplitude is 0.87 mV. This is round 25% more than the amplitude obtained from the Fourier analysis. The x-axis is time in seconds, and the y-axis is fluorescense in volts.

Results of the Bifurcation Analysis

The exact location of the bifurcation points varies among different experiments. This is probably due to variations in the thickness of the cell suspensions or in the time of harvesting. However, the overall picture is clear: A tongue-shaped region with sinusoidal oscillations, which is situated within a region with a stable stationary state, is found. At low glucose flow rates, no oscillations are seen; above a certain threshold oscillations can be found, provided the flow rate of cyanide is set properly (figure 5.14). The cyanide flow rate has both an upper and a lower bifurcation; between those, sinusoidal oscillations are found (figures 5.16 and 5.18).

From the amplitude determinations, a square-root dependence of the amplitude on the flow rate can be established close to the borders of the regions. The dependence is clear at low flow rates of both glucose and cyanide (figures 5.14 and 5.16, respectively), and somewhat unclear at high flow rates of cyanide (figure 5.18). Due to the variations mentioned above, each of these graphs represents only one CSTR experiment.

The dependence of the frequency on the bifurcation parameter in the same three experiments is shown in figures 5.15, 5.17 and 5.19. The frequency is roughly constant when cyanide is the bifurcation parameter. I have no explanation of the difference between the frequencies in figures 5.17 and 5.19, except that it might be caused by bad timing of the harvesting in the later experi-

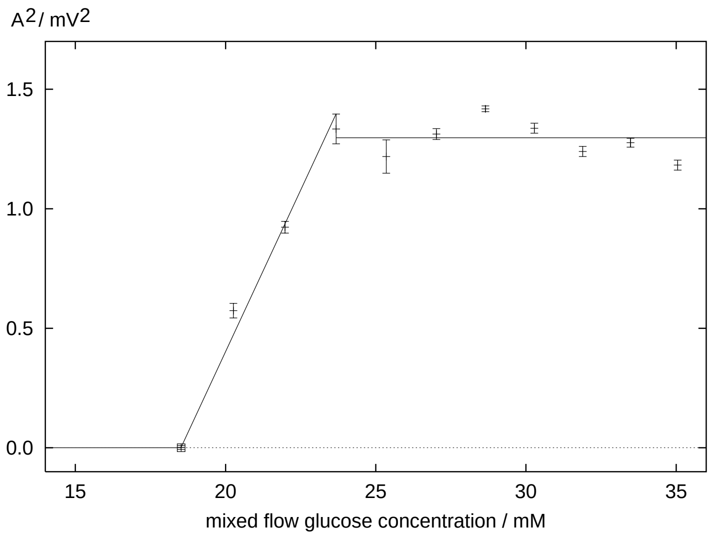

Figure 5.14: Plot of the square of the amplitude A as a function of the mixed flow glucose concentration. Straight lines are drawn to indicate the square-root dependence of A on the mixed flow glucose concentration and the stabilisation of the amplitude, which seems to persist throughout the entire range of glucose concentrations tried (up to a mixed flow glucose concentration of 85 mM). The amplitude is determined with `slidefit.f` (see text) using 400 overlapping windows in a time interval of 300 s. The standard deviation is indicated by the errorbars. Cell density, mixed flow cyanide concentration, and specific flow rate were fixed at $1.61 \cdot 10^9$ cells/ml, 5.6 mM, and $49 \cdot 10^{-3}$ min^{-1}, respectively.

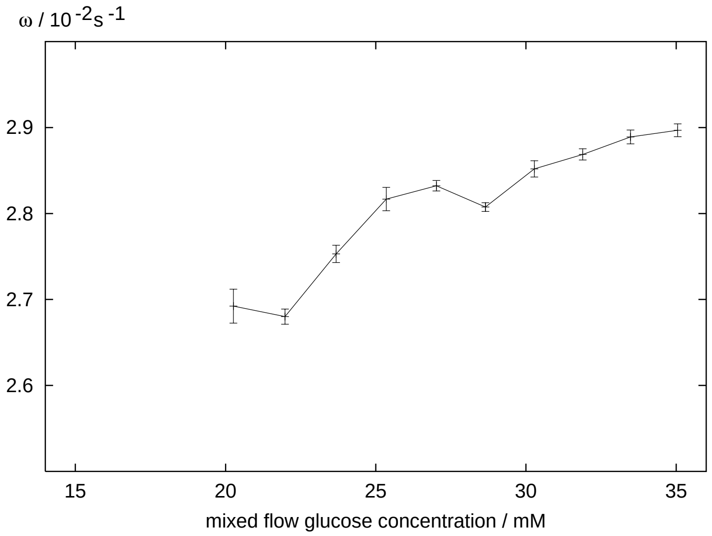

Figure 5.15: Plot of the frequency of the oscillations T as a function of the mixed flow glucose concentration. The frequency is determined with `slidefit.f` (see text) using 400 overlapping windows in a time interval of 300 s. The standard deviation is indicated by the errorbars. Experimental conditions are as described in figure 5.14 (above).

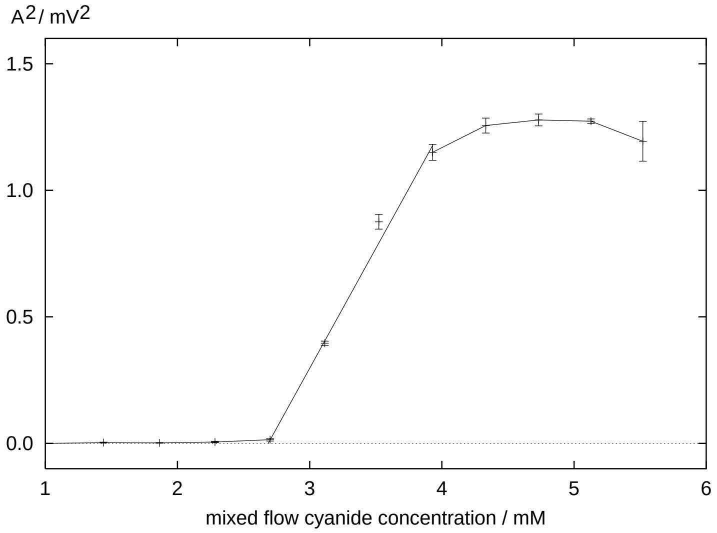

Figure 5.16: Plot of A^2 (the square of the amplitude) as a function of mixed flow cyanide concentration. To illustrate the square-root dependence of A on the mixed flow concentration, a straight line has been drawn through the data points close to the bifurcation point. The amplitude is determined with `slidefit.f` (see text) using 400 overlapping windows in a time interval of 300 s. The standard deviation is indicated by the errorbars. Cell density, mixed flow glucose concentration, and specific flow rate were fixed at $1.64 \cdot 10^9$ cells/ml, 28 mM, and $48 \cdot 10^{-3}$ min^{-1}, respectively.

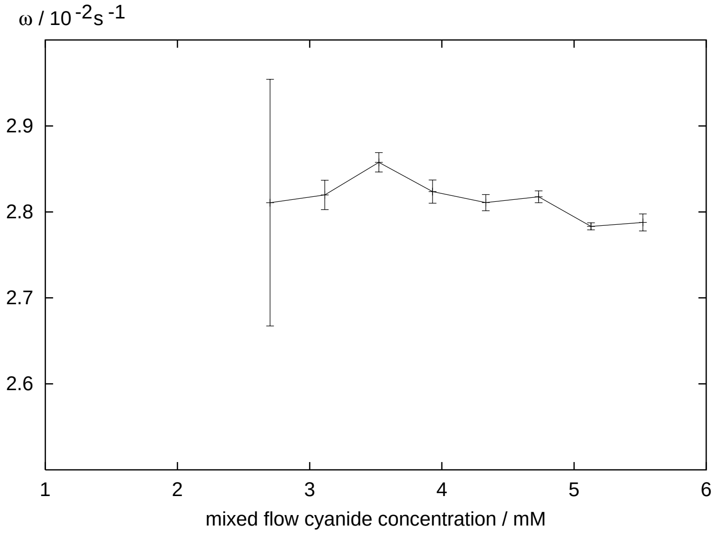

Figure 5.17: Plot of the frequency of the oscillations T as a function of the mixed flow cyanide concentration. The frequency is determined with `slidefit.f` (see text) using 400 overlapping windows in a time interval of 300 s. The standard deviation is indicated by the errorbars. Experimental conditions are as described in figure 5.16 (above).

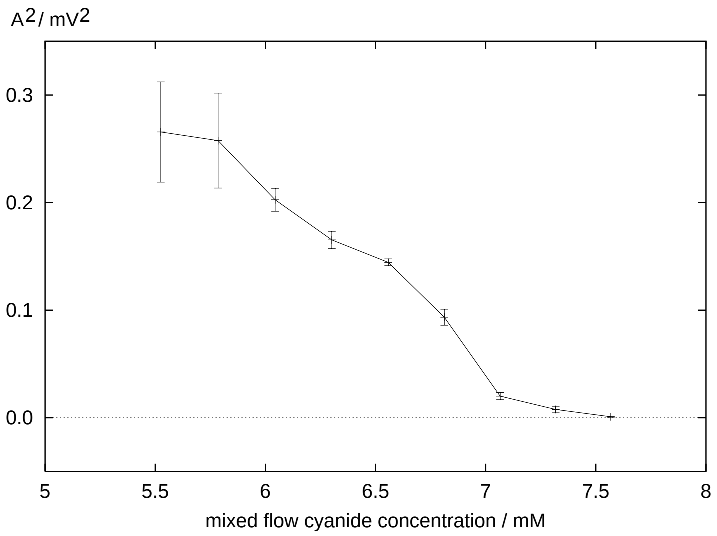

Figure 5.18: Plot of the square of the amplitude A as a function of the mixed flow cyanide concentration. The amplitude is determined with `slidefit.f` (see text) using 400 overlapping windows in a time interval of 300 s. The standard deviation is indicated by the errorbars. Cell density, mixed flow glucose concentration, and specific flow rate were fixed at $1.61 \cdot 10^9$ cells/ml, 27 mM, and $50 \cdot 10^{-3}$ min^{-1}, respectively.

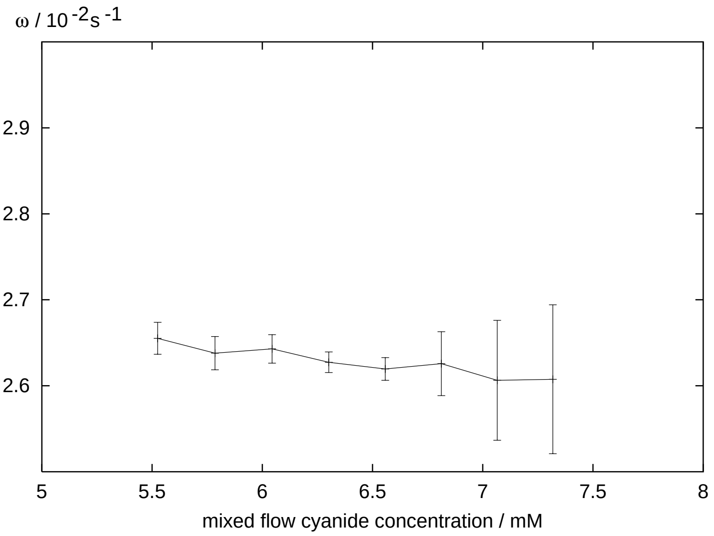

Figure 5.19: Plot of the frequency of the oscillations T as a function of cyanide flow rate. The frequency is determined with `slidefit.f` (see text) using 400 overlapping windows in a time interval of 300 s. The standard deviation is indicated by the errorbars. Experimental conditions are as described in figure 5.18 (above).

ment. When mixed flow glucose concentration is the bifurcation parameter, an increase of the frequency is seen as a result of increasing glucose concentration. This is a phenomenon which is well known from experiments with intact yeast cells in closed systems (see Kreuzberg and Betz (1979) and figure 5.6), but it is just the opposite of what is usually seen at supercritical Hopf bifurcations in inorganic chemical reaction systems like the Belousov-Zhabotinsky. However, the linear dependence of the frequency on the bifurcation parameter close to the bifurcation point, which was predicted by equation 3.17 on page 44, is not obvious.

The occurrence of both an upper and a lower bifurcation with cyanide concentration as the bifurcation parameter is in agreement with Richard *et al.* (1994), who reported that neither too low nor too high cyanide concentrations will induce long-lasting glycolytic oscillations in closed systems. My experiments with glucose as the bifurcation parameter agree with the findings of Kreuzberg and Betz (1979), who report increasing amplitude with increasing glucose pulses for low glucose concentrations, and a constant amplitude for high glucose concentrations.

As described in chapter 3, the square-root dependence of the amplitude on the bifurcation parameter, which I have demonstrated, is the expected behaviour of a system at a supercritical Hopf bifurcation. However, it might also be a synchronization phenomenon as discussed in chapter 4.

5.3.3 Quenching Experiments

The stable oscillations shown in figure 5.5 are ideal for quenching experiments, first of all because we know the approximate location of what could be a supercritical Hopf bifurcation. Furthermore, the oscillations are sinusoidal as expected near such a bifurcation.

Real-Time Phase Determination

In order to do this quenching analysis in a practical way, the perturbation experiments are automated so that both the approximate time and the exact phase of the addition can be pre-programmed. The real-time determination of the phase of the oscillations, which makes this possible, is done by the procedure `findperiod` in the program `yeast`.

I will now describe how this procedure, which was originally designed by my supervisor Preben Graae Sørensen, works. The maximum and minimum

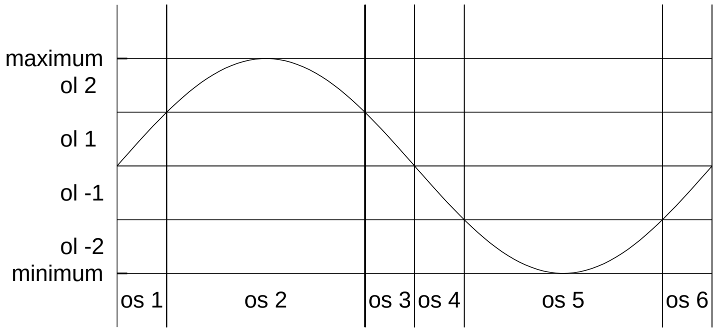

Figure 5.20: The principle of the real-time phase determination. See text for explanations.

values of the measurements are continuously updated. Using these values, the newly measured signal is placed into one of four intervals (ol -2, ol -1, ol 1 or ol 2 in figure 5.20). From the beginning, a phase category is assigned (os 1, os 2, os 3, os 4, os 5 or os 6 as indicated in figure 5.20). Once the phase is placed in one of these categories, it will stay there until the newly measured signal falls into the interval which fits the next phase category. This can be illustrated with an example: If the phase category is os 2, it will change into os 3 provided that the measurement falls into ol 1. Otherwise it stays in os 2.

This procedure is carried out with every measurement, and the number of measurements used to complete one full cycle in the phase categories is counted. From this number, the period is calculated to within the sampling interval of 0.5 s. The instantaneous phase is calculated from each measurement using the previously obtained period, and the number of measurements in the present cycle of phase categories.

Results of the Quenching Experiments

I have tried to quench the oscillations with glucose, cyanide, acetaldehyde, ethanol, pyruvate and pyruvate ethyl ester. Successful quenchings can be obtained with glucose (figure 5.21a) and with acetaldehyde (figure 5.21b). In accordance with figure 3.14 on page 47, the quenching response is sensible to both size and phase of the perturbation. Examples of this is shown in figures 5.22 and 5.23. This geometry of phase space is what one expects of a system close to a supercritical Hopf bifurcation. When taken together with the result of the bifurcation analysis, this indicates that the onset of the glycolytic oscillations corresponds to a supercritical Hopf bifurcation.

Figure 5.21b reveals more about the phase-space geometry than the quenching in itself. The quenching takes place via the stable manifold; this is seen as an immediate downward deflection of the NADH concentration out of its range of oscillations. The motion along the stable manifold back to the plane of oscillations is quite slow, so we can conclude that the unstable modes are not the only slow modes of the system. In other words: The two complex conjugated eigenvalues of the Jacobian matrix, which are associated with the unstable subspace, are not the only eigenvalues with $\mathrm{Re}(\lambda)$ close to 0. This additional slow mode must be internal to the yeast cell – as opposed to a transport phenomenon – since the deflection is seen immediately. This result is not new; the same argument can be found in Winfree (1980), who comments on ACA quenchings of the spiralling motion towards a stable focus. It also follows from the observation of chaos in glycolysis reported by Nielsen *et al.* (1998), since a phase space of at least three dimensions is needed for the description of chaos.

Quenching with acetaldehyde is possible in a wide range of flow rates, but quenching with glucose is only possible for low glucose flow rates. The upper limit of glucose flows, for which quenching with glucose is possible, coincides with the sudden stabilisation of the amplitude at higher flow rates, which is evident from figure 5.14.

Attempts to quench with cyanide, ethanol or pyruvate were unsuccessful. Pyruvate induces a rather slow, phase-independent decrease of the NADH level (data not shown). At first sight, this seems to be in disagreement with Betz and Becker (1975), who report phase shifts with both acetaldehyde and pyruvate in a closed system at pH = 4.6. However, as I discussed on page 22, the reason for this might be that pyruvate is slow at entering the cells at the pH used in my experiments (pH = 6.8). Since fluorescent dyes can be loaded into yeast cells quite easily (Haworth *et al.*, 1991; Aon and Cortassa, 1997), an unspecific esterase is present in the yeast cells. I tried to use this to do indirect quenchings with pyruvate by perturbing with the ethyl ester of pyruvate, which will pass the cell membrane much faster than pyruvate itself. The esterase should then degrade it into ethanol and pyruvate which could quench the oscillations. However, the response is still slow and phase-independent.

Many or large perturbations with pyruvate or acetaldehyde affect the oscillations in such a way that the amplitude is decreased and the baseline starts to fluctuate (data not shown). This phenomenon is not seen otherwise. However, it has not been systematically investigated.

Ethanol produces no response at all, for the perturbation sizes I have tried (up to 45 mM final concentration, data not shown).

Cyanide perturbations increase the NADH level, and can diminish the amplitude of the oscillations significantly. The initial response is phase-dependent, as can be seen by comparing figures 5.24a and 5.24b. However, all perturbations induce a damping, because the system is taken closer to the upper cyanide bifurcation point described in the previous section (compare the cyanide concentrations in figure 5.24 with figure 5.18). This damping is phase-independent. If the perturbation is smaller, a similar response is seen, but the oscillations are not so damped (compare figures 5.24b and 5.24c). The oscillations only disappear completely when the cyanide concentration exceeds the upper bifurcation point.

5.4 A Closing Remark

In this chapter I have presented the results of my experiments, and I have stated some remarks and conclusions which are directly related to the different experiments in themselves. This is done in order to allow the reader to follow the general idea of performing the different experiments, and to illustrate how they relate to each other. However, the last two chapters both refer to the experiments presented above. In the following chapter, I will outline how the above experiments can be combined with the experiments of the Amsterdam group to obtain a model of glycolysis, which is comprehensive both with respect to its level of detail and to its experimental validation. In the last chapter I will draw further conclusions and present the ideas of some ongoing experiments, which I have not had the time to complete. So, rather than marking the end of the experimental part of this thesis, this sentence merely marks a change of perspective.

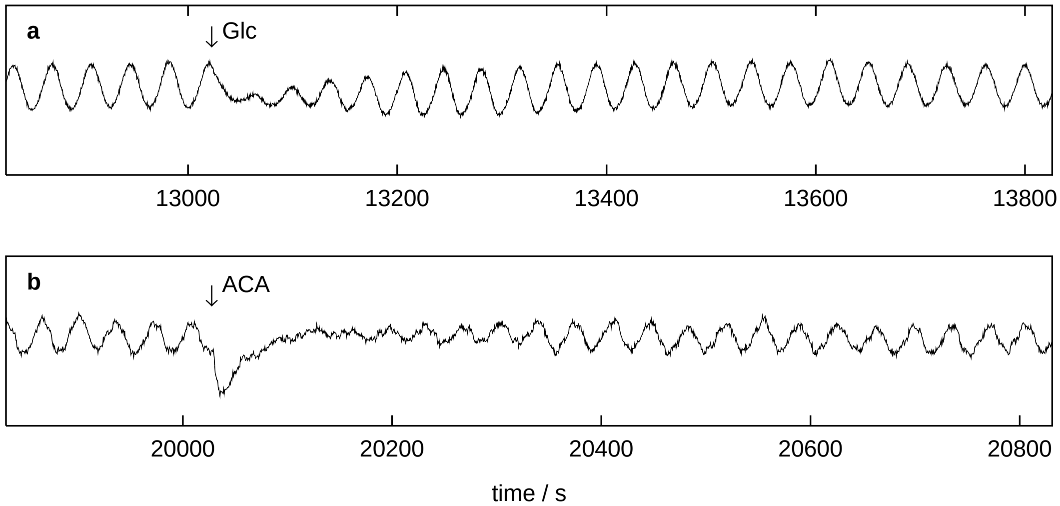

Figure 5.21: Quenching of the oscillations by extracellular perturbations (indicated by an arrow). **a** Quenching of the oscillations by addition of glucose. The extracellular concentration is changed by 1.11 mM at a phase of 4°. The cell density is $1.62 \cdot 10^9$ cells/ml and mixed flow concentrations of glucose and cyanide are 23.1 mM and 4.26 mM, respectively. The specific flow rate is $50.6{\cdot}10^{-3}$ min^{-1}. **b** Quenching of the oscillations by addition of acetaldehyde. The extracellular concentration is changed by 98 μM at a phase of 172°. The cell density is $1.66 \cdot 10^9$ cells/ml and the mixed flow concentrations of glucose and cyanide are 35.0 mM and 5.37 mM, respectively. The specific flow rate is $47.9{\cdot}10^{-3}$ min^{-1}. In both experiments "time" is time elapsed since the start of the experiment.

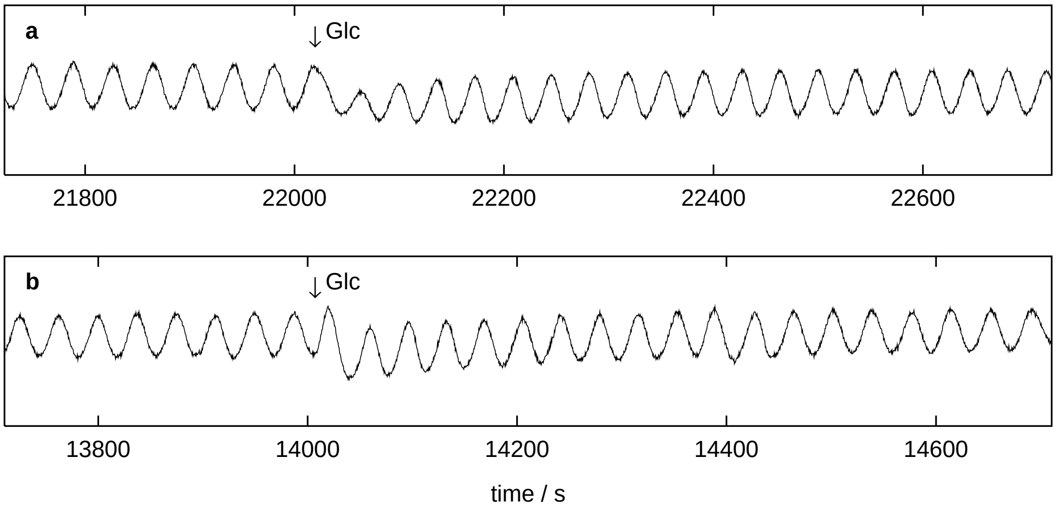

Figure 5.22: Fluorescence traces showing the response to extracellular perturbations with glucose (indicated by an arrow). **a** Sensitivity towards the size of the perturbation. The experiment in figure 5.21a is repeated except that the perturbation increases the glucose concentration by 1.33 mM instead of 1.11 mM. The addition is made at a phase of 0° which is close to the 4° in figure 5.21a. **b** Perturbation in a phase opposite to the quenching phase. The same amount of glucose as in figure 5.21a is added at a phase of 180°, which is approximately the opposite of the quenching phase. This results in a momentary increase of the amplitude, as the system is displaced from the limit cycle. In both panels, the experimental conditions are as described in figure 5.21a.

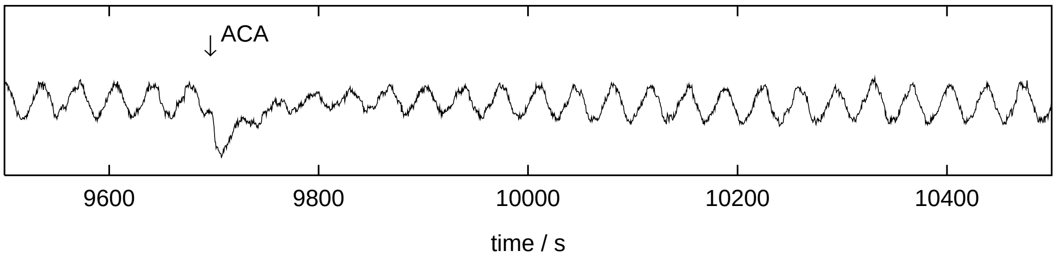

Figure 5.23: Sensitivity towards the phase of perturbation. The experiment in figure 5.21b is repeated exactly, except that the addition of ACA (indicated by the arrow) is made at a phase of 180° instead of 172°, the amplitude of the oscillations is diminished, but the oscillations do not stop completely. Experimental conditions are as described in figure 5.21b.

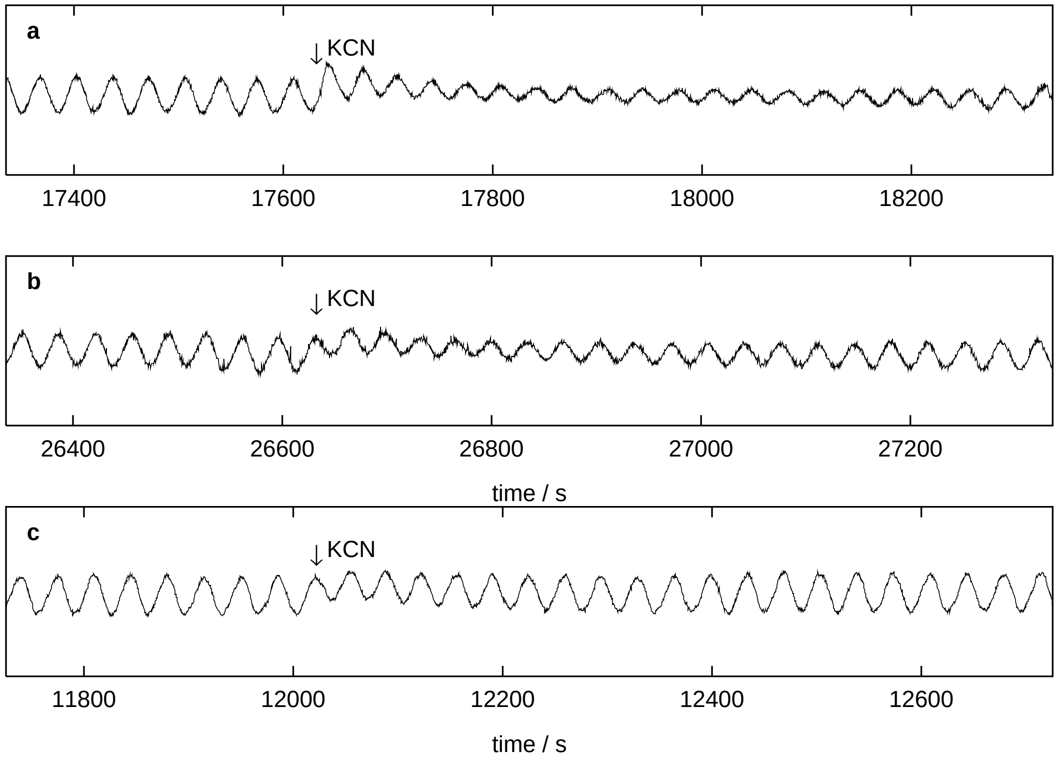

Figure 5.24: Perturbations with cyanide. **a** The extracellular cyanide concentration is changed by 2.2 mM at a phase of 228° (indicated by ↓). **b** The extracellular cyanide concentration is changed by 2.2 mM at a phase of 1°. In both **a** and **b** the cell density is $1.64 \cdot 10^9$ cells/ml and the mixed flow concentrations of glucose and cyanide are 35.0 mM and 5.37 mM respectively. The specific flow rate is $50.6 \cdot 10^{-3}$ min^{-1}. **c** The extracellular cyanide concentration is changed by 1.7 mM at a phase of 3° (indicated by ↓). The cell density is $1.61 \cdot 10^9$ cells/ml and the mixed flow concentrations of glucose and cyanide are 35.0 mM and 5.38 mM respectively. The specific flow rate is $50.6 \cdot 10^{-3}$ min^{-1}. "Time" is time elapsed since the start of the experiment.

6
Modelling Glycolysis

Even though the two successful quenchings are far from enough to do a complete quenching analysis, they are still very useful for validating comprehensive models of glycolytic oscillations in yeast extracts. But, as discussed in chapter 4, such models do not exist. Therefore, my supervisor Finn Hynne and I are presently building such one. The strategy which we apply relies heavily on the presence of a Hopf bifurcation. As you will see below this has several advantages; among other things it allows us to utilise most of the Amsterdam group's measurements of oscillating metabolites in *Saccharomyces cerevisiae* for further validation of the model.

The strategy is to start out with a "skeleton" of equations and a set of parameters which are approximately right. This is obtained from the models of glycolytic oscillations in yeast extracts, which already exist. The idea is to vary the parameters of this model in order to find a set of parameters that fit the experimental results well. The fundamental problem of this approach is that the parameter space is of a very high dimension, and since we do not have access to a Turing machine it is impossible to cover all of this space with just a moderate resolution. Therefore, we need to make some kind of compromise between the level of detail we want in the model, and the quality of the fit which we will obtain with the model.

We choose to get a very detailed model with the trade-off that we will probably not be able to find *the* optimal parameter set for this model. Thus, the aim is to obtain a detailed model and a set of parameters that are in reasonable agreement with the experiments. In fact, the optimization scheme presented below will test millions of parameter sets, so even though we cannot find the optimal parameter set, we will no doubt find sets of parameters which are much better than what one could get from just playing around with the parameters and integrating the model.

6.1 The Model

The starting point of this modelling is the enzyme kinetics already known and the dynamics we see in the experiments. To merge these things into a detailed model, we need to start out with the assumption that the yeast cells are strongly coupled, so that the bulk oscillations reflect similar oscillations at the level of the individual cells. We have no definitive proof of this but – as you will see in the next chapter – this is a fair assumption.

In order to reduce the number of parameters in the optimization, the model is constructed in two stages. First we work on a model which includes only intracellular substances (see tables 6.1 and 6.2). As described below, this core model includes all the complicated rate expressions. We use this simpler submodel to find suitable kinetic parameters for these expressions. Then, when we arrive at a handful of suitable parameter sets, we extend the model to include extracellular substances, membrane transport and the extracellular reaction of ACA and cyanide as well (see tables 6.3 and 6.4). This full model is then optimized once more, preferably by adjusting the newly introduced parameters.

This reflects the view that the intact cells are basically small portions of yeast extracts with a cell membrane around them. This might not be true, but it is a practical working hypothesis.

6.1.1 The Core Model

The basis of the core model is the yeast-extract model by Nielsen *et al.* (1998). As mentioned in chapter 4, this model describes the dynamics of the extracts quite well: It predicts the same series of bifurcations as is seen in a CSTR with yeast extract, when the specific flow rate is used as bifurcation parameter, and it gives a quite good description of the response to perturbations (Nielsen *et al.*, 1998). The results obtained when other parameters are adjusted in this model also fit nicely with the experiments (Hoffmann, 1999).

To obtain a model of intact yeast cells, some changes and extensions of the extract model is needed. For obvious reasons, the membrane transport must be such an extension. We have adopted the rate equation of the glucose transporter from Rizzi *et al.* (1996) who obtained this rate expression by fitting

r	Reaction			Reference
1:		$\rightleftharpoons$	Glc	Rizzi *et al.* (1996)
2:	Glc + ATP	$\rightarrow$	G6P + ADP	Viola *et al.* (1982)†
3:	G6P	$\rightleftharpoons$	F6P	Richter *et al.* (1975)
4:	F6P + ATP	$\rightarrow$	FBP + ADP	Termonia and Ross (1981)†
5:	FBP	$\rightleftharpoons$	GAP + DHAP	Richter *et al.* (1975)
6:	GAP + NAD^+	$\rightleftharpoons$	DPG + NADH	–
7:	DPG + ADP	$\rightleftharpoons$	PEP + ATP	Nielsen *et al.* (1998)
8:	PEP + ADP	$\rightarrow$	Pyr + ATP	Boiteux *et al.* (1983)†
9:	Pyr	$\rightarrow$	ACA	Nielsen *et al.* (1998)
10:	ACA + NADH	$\rightarrow$	EtOH + NAD^+	–
11:	AMP + ATP	$\rightleftharpoons$	2 ADP	Nielsen *et al.* (1998)
12:	ACA	$\rightarrow$		–
13:	EtOH	$\rightarrow$		–
14:	DHAP	$\rightleftharpoons$	GAP	Richter *et al.* (1975)
15:	DHAP + NADH	$\rightarrow$	glycerol + NAD^+	Cai *et al.* (1996)
16:	glycerol	$\rightarrow$		–
17:	ATP	$\rightarrow$	ADP	–

$$[\mathrm{NAD}^+] + [\mathrm{NADH}] = \text{constant}$$
$$[\mathrm{ATP}] + [\mathrm{ADP}] + [\mathrm{AMP}] = \text{constant}$$

Table 6.1: The reactions of the core model. †: Parameters are from Nielsen *et al.* (1998). See text for details.

kinetic parameters to Glc and G6P transients, caused by addition of a glucose pulse to a growing culture of glucose limited *Saccharomyces cerevisiae*. Since the glucose transporter is inhibited by G6P, this metabolite must be explicitly included in our model. This is done by modelling the PGI reaction as in Richter *et al.* (1975); the K_m values of the HK reaction are kept unchanged. Three simple transport processes are included as well: Diffusion of glycerol, ACA and EtOH from the cytosol to the extracellular medium.

Another feature, which might be important in a model of intact yeast cells, is the glycerol production. As described on page 20, the glycerol is produced by two successive reactions. But we assume the dephosphorylation of glycerol 3-P to be fast, so the two reactions are lumped into reaction 15 in table 6.1 and described by a rate equation for the DHAP reductase reaction. In order to include the glycerol formation, DHAP needs to be in the model as well; this is obtained by including the ALD reaction and the reaction catalyzed by TIM (both of these rate equations are taken from Richter *et al.* (1975)).

Compared to the extract model of Nielsen *et al.* (1998), we have simplified the core model by having only one "inflow" (of Glc via the glucose transporter) and only "outflow" of EtOH, ACA and glycerol. In the CSTR experiments with the intact cells this would be equivalent to keeping the same cells in the cuvette all the time instead of having an inflow of cells. Some numbers can illustrate the significance of this assumption: If a metabolite has an intracellular concentration of 10 mM then the drain caused by outflow of cells is approximately 0.4 mM/min, because the residence time of the CSTR is round 25 min. This is low compared to the intracellular glycolytic flux of almost 30 mM/min (see below). Since all the intracellular metabolite concentrations are below 10 mM, this approximation should not introduce any significant errors. Furthermore, the metabolite measurements of the Amsterdam group – which we use for the optimization – are made in closed systems, where there is obviously not any flow of cells. Nevertheless, the approximation simplifies the optimization of the model because it results in the two stoichiometric constraints shown in table 6.1. It also reduces the number of extreme currents in the core model; the meaning of this statement will become clear below.

From the ΔG calculations in table 2.3 it is seen that the GAPDH reaction is close to equilibrium; therefore, this reaction is modelled as a reversible bimolecular reaction instead of an irreversible reaction with a Michaelis-Menten like rate expression. From the same calculations it is seen that the ADH reaction is not at equilibrium, and therefore we prefer to model it as an irreversible reaction with Michaelis-Menten kinetics instead of a reversible bimolecular reaction[1]. This simplification of the model is also justified by my experimental finding, that the yeast cells are insensitive to EtOH perturbations. Finally, a first-order ATP consumption is included. One can think of this ATP hydrolysis as driving the glycogen production mentioned on page 21 as well as some basic cellular demands like the maintenance of membrane potentials.

The above changes and additions to the model by Nielsen *et al.* (1998) result in the core model which is presented in tables 6.1 and 6.2. Note that the extracellular glucose concentration is constant in the core model.

Reaction (r)	Rate Equation (v_r)
1:	$v_{\rightarrow} = \dfrac{V_{1mf}\frac{[\mathrm{Glc}_{ex}]}{K_{1\mathrm{Glc}}}}{1+\frac{[\mathrm{Glc}_{ex}]}{K_{1\mathrm{Glc}}}+\frac{P_1\frac{[\mathrm{Glc}_{ex}]}{K_{1\mathrm{Glc}}}+1}{P_1\frac{[\mathrm{Glc}]}{K_{1\mathrm{Glc}}}+1}\left(1+\frac{[\mathrm{Glc}]}{K_{1\mathrm{Glc}}}+\frac{[\mathrm{G6P}]}{K_{1\mathrm{IG6P}}}+\frac{[\mathrm{Glc}][\mathrm{G6P}]}{K_{1\mathrm{Glc}}K_{1\mathrm{IIG6P}}}\right)}$ $v_{\leftarrow} = \dfrac{V_{1mr}\frac{[\mathrm{Glc}]}{K_{1\mathrm{Glc}}}}{1+\frac{[\mathrm{Glc}]}{K_{1\mathrm{Glc}}}+\frac{P_1\frac{[\mathrm{Glc}]}{K_{1\mathrm{Glc}}}+1}{P_1\frac{[\mathrm{Glc}_{ex}]}{K_{1\mathrm{Glc}}}+1}\left(1+\frac{[\mathrm{Glc}_{ex}]}{K_{1\mathrm{Glc}}}+\frac{[\mathrm{G6P}]}{K_{1\mathrm{IG6P}}}+\frac{[\mathrm{Glc}][\mathrm{G6P}]}{K_{1\mathrm{Glc}}K_{1\mathrm{IIG6P}}}\right)}$
2:	$v_{\rightarrow} = \dfrac{V_{2m}[\mathrm{ATP}][\mathrm{Glc}]}{K_{2\mathrm{DGlc}}K_{2\mathrm{ATP}}+K_{2\mathrm{Glc}}[\mathrm{ATP}]+K_{2\mathrm{ATP}}[\mathrm{Glc}]+[\mathrm{Glc}][\mathrm{ATP}]}$
3:	$v_{\rightarrow} = \dfrac{V_{3m}[\mathrm{G6P}]}{K_{3\mathrm{G6P}}\left(1+\frac{[\mathrm{F6P}]}{K_{3\mathrm{F6P}}}\right)+[\mathrm{G6P}]}$ $v_{\leftarrow} = \dfrac{V_{3m}\frac{[\mathrm{F6P}]}{K_{3\mathrm{eq}}}}{K_{3\mathrm{G6P}}\left(1+\frac{[\mathrm{F6P}]}{K_{3\mathrm{F6P}}}\right)+[\mathrm{G6P}]}$
4:	$v_{\rightarrow} = \dfrac{V_{4m}[\mathrm{F6P}]^2[\mathrm{ATP}]}{\left(K_4\left(1+\kappa_4\frac{[\mathrm{ATP}]^2}{[\mathrm{AMP}]^2}\right)+[\mathrm{F6P}]^2\right)(K_{4\mathrm{mATP}}+[\mathrm{ATP}])}$
5:	$v_{\rightarrow} = \dfrac{V_{5f}[\mathrm{FBP}]}{K_{5\mathrm{FBP}}+[\mathrm{FBP}]+\frac{[\mathrm{GAP}]K_{5\mathrm{DHAP}}V_{5f}}{K_{5eq}V_{5r}}+\frac{[\mathrm{DHAP}]K_{5\mathrm{GAP}}V_{5f}}{K_{5eq}V_{5r}}+\frac{[\mathrm{FBP}][\mathrm{GAP}]}{K_{5\mathrm{IGAP}}}+\frac{[\mathrm{GAP}][\mathrm{DHAP}]V_{5f}}{K_{5eq}V_{5r}}}$ $v_{\leftarrow} = \dfrac{V_{5f}\frac{[\mathrm{GAP}][\mathrm{DHAP}]}{K_{5eq}}}{K_{5\mathrm{FBP}}+[\mathrm{FBP}]+\frac{[\mathrm{GAP}]K_{5\mathrm{DHAP}}V_{5f}}{K_{5eq}V_{5r}}+\frac{[\mathrm{DHAP}]K_{5\mathrm{GAP}}V_{5f}}{K_{5eq}V_{5r}}+\frac{[\mathrm{FBP}][\mathrm{GAP}]}{K_{5\mathrm{IGAP}}}+\frac{[\mathrm{GAP}][\mathrm{DHAP}]V_{5f}}{K_{5eq}V_{5r}}}$

Table 6.2: The rate equations of the core model. Note that $[\mathrm{Glc}_{ex}]$ is treated as a constant.

[1]Similar arguments have been used by other authors, when the irreversibilities of the HK, PFK and PK reactions were introduced.

Reaction (r)	Rate Equation (v_r)
6:	$v_{\rightarrow} = k_{6f}[\mathrm{GAP}][\mathrm{NAD}^{+}]$ $v_{\leftarrow} = k_{6r}[\mathrm{DPG}][\mathrm{NADH}]$
7:	$v_{\rightarrow} = k_{7f}[\mathrm{DPG}][\mathrm{ADP}]$ $v_{\leftarrow} = k_{7r}[\mathrm{PEP}][\mathrm{ATP}]$
8:	$v_{\rightarrow} = \frac{V_{8m}[\mathrm{ADP}][\mathrm{PEP}]}{(K_{8\mathrm{PEP}}+[\mathrm{PEP}])(K_{8\mathrm{ADP}}+[\mathrm{ADP}])}$
9:	$v_{\rightarrow} = \frac{V_{9m}[\mathrm{Pyr}]}{K_9+[\mathrm{Pyr}]}$
10:	$v_{\rightarrow} = \frac{V_{10m}[\mathrm{ACA}][\mathrm{NADH}]}{(K_{10\mathrm{NADH}}+[\mathrm{NADH}])(K_{10\mathrm{ACA}}+[\mathrm{ACA}])}$
11:	$v_{\rightarrow} = k_{11f}[\mathrm{AMP}][\mathrm{ATP}]$ $v_{\leftarrow} = k_{11r}[\mathrm{ADP}][\mathrm{ADP}]$
12:	$v_{\rightarrow} = k_{12}[\mathrm{ACA}]$
13:	$v_{\rightarrow} = k_{13}[\mathrm{EtOH}]$
14:	$v_{\rightarrow} = \frac{V_{14m}[\mathrm{DHAP}]}{K_{14\mathrm{DHAP}}+[\mathrm{DHAP}]+\frac{K_{14\mathrm{DHAP}}}{K_{14\mathrm{GAP}}}[\mathrm{GAP}]}$ $v_{\leftarrow} = \frac{V_{14m}\frac{[\mathrm{GAP}]}{K_{14eq}}}{K_{14\mathrm{DHAP}}+[\mathrm{DHAP}]+\frac{K_{14\mathrm{DHAP}}}{K_{14\mathrm{GAP}}}[\mathrm{GAP}]}$
15:	$v_{\rightarrow} = \frac{V_{15m}[\mathrm{DHAP}]}{K_{15\mathrm{DHAP}}\left(1+\frac{K_{15\mathrm{INADH}}}{[\mathrm{NADH}]}\right)\left(1+\frac{[\mathrm{NAD+}]}{K_{15\mathrm{INAD}}}\right)+[\mathrm{DHAP}]\left(1+\frac{K_{15\mathrm{NADH}}}{[\mathrm{NADH}]}\right)\left(1+\frac{[\mathrm{NAD+}]}{K_{15\mathrm{INAD}}}\right)}$
16:	$v_{\rightarrow} = k_{16}[\mathrm{glycerol}]$
17:	$v_{\rightarrow} = k_{17}[\mathrm{ATP}]$

Table 6.2: The rate equations of the core model. Note that $[\mathrm{Glc}_{ex}]$ is treated as a constant.

6.1.2 The Extended Model

The extension of the core model involves the introduction of five additional dynamical variables, namely extracellular EtOH, extracellular ACA, extracellular glycerol, extracellular Glc and extracellular cyanide. The reason for including ACA_{ex} and Glc_{ex} is obvious; we know that these species can quench the oscillations, and we want to exploit this fact when we optimize the model. CN^-_{ex} is included because we want to be able to investigate its proposed role in the cell synchronization. $EtOH_{ex}$ and $glycerol_{ex}$ are included because they are important for some possible applications of the model; they will not influence the dynamics of the rest of the model since the ADH reaction and the glycerol formation are modelled irreversible, and neither glycerol nor EtOH is part of any other rate expressions than their own diffusion through the cell membrane.

We will stick to the picture where the cells remain in the cuvette, but in order to obtain stationarity we do need an outflow of the extracellular species just like in a CSTR. This gives reactions 19–23 in table 6.3. The inflows of Glc and cyanide are also given in reactions 19 and 20. Reactions 1, 12, 13 and 16 are changed so that they now describe the exchange of the metabolites between the extracellular medium and the cell. Since we use concentrations for all the calculations, we need to compensate for the fact that the extracellular volume is V_{ratio} times larger than that of the cytoplasm. This is done by introducing V_{ratio} as a "stoichiometric factor" in these reactions.

Two genuine chemical reactions have been added as well. One of these (reaction 24) is the reaction between ACA and cyanide which was discussed on page 64. The other one is reaction 18 which is a schematic representation of the glycogen production, discussed on page 21.

Table 6.3 lists the reactions of the full-size model, and table 6.4 lists the rate expressions of the full-size model.

6.2 Optimization of the Model

The method used for the optimization is described in detail in Hynne *et al.* (1993b). It works by looking at different stationary states of the model. At first sight it might seem strange to look at stationary states when modelling oscillations. However, this approach gives us several advantages: First of all, it allows us to include dynamic properties in the optimization by evaluating the Jacobian matrix. By demanding stationary states, we also put some constraints on the model which helps us to fit some of the parameters. And since we have

r	Reaction			Reference
1:*	Glc_{ex}	$\rightleftharpoons$	V_{ratio} Glc	Rizzi *et al.* (1996)
2:	Glc + ATP	$\rightarrow$	G6P + ADP	Viola *et al.* (1982)†
3:	G6P	$\rightleftharpoons$	F6P	Richter *et al.* (1975)
4:	F6P + ATP	$\rightarrow$	FBP + ADP	Termonia and Ross (1981)†
5:	FBP	$\rightleftharpoons$	GAP + DHAP	Richter *et al.* (1975)
6:	GAP + NAD^+	$\rightleftharpoons$	DPG + NADH	–
7:	DPG + ADP	$\rightleftharpoons$	PEP + ATP	Nielsen *et al.* (1998)
8:	PEP + ADP	$\rightarrow$	Pyr + ATP	Boiteux *et al.* (1983)†
9:	Pyr	$\rightarrow$	ACA	Nielsen *et al.* (1998)
10:	ACA + NADH	$\rightarrow$	EtOH + NAD^+	–
11:	AMP + ATP	$\rightleftharpoons$	2 ADP	Nielsen *et al.* (1998)
12:*	V_{ratio} ACA	$\rightleftharpoons$	ACA_{ex}	–
13:*	V_{ratio} EtOH	$\rightleftharpoons$	$EtOH_{ex}$	–
14:	DHAP	$\rightleftharpoons$	GAP	Richter *et al.* (1975)
15:	DHAP + NADH	$\rightarrow$	glycerol + NAD^+	Cai *et al.* (1996)
16:*	V_{ratio} glycerol	$\rightleftharpoons$	$glycerol_{ex}$	–
17:	ATP	$\rightarrow$	ADP	–
18:‡	ATP + G6P	$\rightarrow$	ADP	–
19:‡		$\rightleftharpoons$	Glc_{ex}	–
20:‡		$\rightleftharpoons$	CN^-_{ex}	–
21:‡	$glycerol_{ex}$	$\rightarrow$		–
22:‡	ACA_{ex}	$\rightarrow$		–
23:‡	$EtOH_{ex}$	$\rightarrow$		–
24:‡	ACA_{ex} + CN^-_{ex}	$\rightarrow$		Richard *et al.* (1996a)

$$[NAD^+] + [NADH] = \text{constant}$$
$$[ATP] + [ADP] + [AMP] = \text{constant}$$

Table 6.3: The reactions of the extended model. *: Reaction changed from that in the core model. †: Parameters are from Nielsen *et al.* (1998). ‡: Reaction not in the core model. See text for details.

r	Rate Equation (v_r)	r	Rate Equation (v_r)
12:	$v_{\rightarrow} = k_{12f}[\mathrm{ACA}]$ $v_{\leftarrow} = k_{12r}[\mathrm{ACA}_{ex}]$	20:	$v_{\rightarrow} = j_{\mathrm{total}}[\mathrm{CN}^-]_{\mathrm{m.f.}}$ $v_{\leftarrow} = j_{\mathrm{total}}[\mathrm{CN}^-_{ex}]$
13:	$v_{\rightarrow} = k_{13f}[\mathrm{EtOH}]$ $v_{\leftarrow} = k_{13r}[\mathrm{EtOH}_{ex}]$	21:	$v_{\rightarrow} = j_{\mathrm{total}}[\mathrm{glycerol}_{ex}]$
		22:	$v_{\rightarrow} = j_{\mathrm{total}}[\mathrm{ACA}_{ex}]$
16:	$v_{\rightarrow} = k_{16f}[\mathrm{glycerol}]$ $v_{\leftarrow} = k_{16r}[\mathrm{glycerol}_{ex}]$	23:	$v_{\rightarrow} = j_{\mathrm{total}}[\mathrm{EtOH}_{ex}]$
18:	$v_{\rightarrow} = k_{18}[\mathrm{ATP}][\mathrm{G6P}]$	24:	$v_{\rightarrow} = k_{24}[\mathrm{ACA}_{ex}][\mathrm{CN}^-_{ex}]$
19:	$v_{\rightarrow} = j_{\mathrm{total}}[\mathrm{Glc}]_{\mathrm{m.f.}}$ $v_{\leftarrow} = j_{\mathrm{total}}[\mathrm{Glc}_{ex}]$		

Table 6.4: The rate equations of the extended model. The rate expressions for reaction numbers 1–11, 14, 15 and 17 are unchanged; see table 6.2 for these rate expressions. m.f.: mixed flow. $j_{\mathrm{total}} = j_{\mathrm{Glc}} + j_{\mathrm{CN}^-} + j_{\mathrm{suspension}}$ is the specific flow rate of the CSTR.

a strong experimental indication of a supercritical Hopf bifurcation, we have a perfectly valid connection from the stationary states to the oscillations.

6.2.1 Optimizing the Core Model

In order to use this approach, we want to be able to scan all the possible stationary states of the system in a systematic way. In the core model each molecule of glucose will either end up as two molecules of EtOH, or as one molecule of ACA and one molecule of glycerol. These extreme possibilities for the net flux distribution are called the extreme currents[2] $\mathbf{E}_1$ and $\mathbf{E}_2$ of the core model (see table 6.5). They are useful for the parameterisation of the flux, since all possible stationary net reaction velocity vectors $\mathbf{v}$ (known as a "currents") for a given total flux v_0 are given by

$$\frac{\mathbf{v}}{v_0} = j_1 \cdot \mathbf{E}_1 + j_2 \cdot \mathbf{E}_2 \tag{6.1}$$

with $j_1 + j_2 = 1$ and $j_1, j_2 \geq 0$ (see Hynne *et al.* (1993b) for details). As already mentioned, this simple description, which involves only two extreme currents, is a result of the approximation that the yeast cells themselves do not flow in or out of the cuvette.

We will use the parameterisation in equation 6.1 to scan a system consisting of m (net) chemical reactions labeled by r. Each of these reactions have a reaction velocity v_r which is given by the rate expressions in table 6.2. (We need to use $v_r = v_{r,\text{net}} = v_{r,\rightarrow} - v_{r,\leftarrow}$ for the reversible reactions; see below).

By choosing a stationary velocity vector $\mathbf{v}$ we can calculate each of its components from equation 6.1 by specifying the j's and v_0. Thus, we obtain m equations from which we can determine m parameters or stationary concentrations provided that we supply the remaining ones. When modelling enzyme kinetics v_r is often a complicated expression, but it can generally be split into two factors

$$v_r = V_r \cdot G_r(\mathbf{c},\boldsymbol{\mu}). \tag{6.2}$$

[2]In fact they are the "non-trivial" extreme currents. A pair of opposite reactions always gives rise to a "trivial" extreme current with equal velocities of these two reactions and zero velocity of all other reactions. For the sake of simplicity we will only treat non-trivial extreme currents; reversible reactions are treated separately, as described below.

r	$\mathbf{E}_1$	$\mathbf{E}_2$
1	1	1
2	1	1
3	1	1
4	1	1
5	1	1
6	2	1
7	2	1
8	2	1
9	2	1
10	2	0
11	0	0
12	0	1
13	2	0
14	1	0
15	0	1
16	0	1
17	2	0

Table 6.5: The extreme currents of the core model. The numbers in the first column refer to the numbering of the reactions in table 6.1.

For the Michaelis-Menten like rate expressions[3] we have $V = V_{\max}$, and for rate expressions formulated as elementary reactions[4] we have $V = k$. We use these m equations to fit the k and $V_{\max}$ values, since these are the ones that are inherently difficult to obtain from *in vitro* measurements (cf. page 62). Furthermore, by calculating the V's we avoid the difficulties of estimating the actual enzyme concentrations inside the cell.

Reversible Reactions

The calculations described in equation 6.2 apply to the actual rates of the reactions, but $\mathbf{v}$ contains the net reaction rates. This raises the question of how to handle reversible reactions which have $v_{\text{net}} = v_{\rightarrow} - v_{\leftarrow}$. If the rate expressions of a reversible reaction are formulated as elementary reactions[5] then the forward and the reverse reactions do not have any common elements, and we need to calculate a value for both $k_{\rightarrow}$ and $k_{\leftarrow}$. This is done by introducing the ratio of the two reaction rates $v_{\rightarrow}/v_{\leftarrow}$ as a variable parameter, which is then varied as described below.

This approach cannot be taken with reactions 3, 5 and 14 of the core model, since $V_{\max}$ is the same for both the forward and the reverse reaction. Since the rate expressions for the forward and the reverse reactions have common denominators in these particular cases, we can easily calculate $V_{\max}$ from the two rate expressions and v_{net}:

$$\begin{aligned} V_{3\max} &= \frac{v_{3\text{net}}}{[\text{G6P}] - \frac{[\text{F6P}]}{K_{3eq}}} \\ V_{5\max} &= \frac{v_{5\text{net}}}{[\text{FBP}] - \frac{[\text{GAP}][\text{DHAP}]}{K_{5eq}}} \\ V_{14\max} &= \frac{v_{14\text{net}}}{[\text{DHAP}] - \frac{[\text{GAP}]}{K_{14eq}}}. \end{aligned}$$

We allow the forward and the reverse reactions of the glucose transporter (reaction 1 of the core model) to have different values of $V_{\max}$. This is handled by introducing $v_{1\rightarrow}/v_{1\leftarrow}$ as a variable parameter as described above.

Scanning the Parameter Space

In order to evaluate equation 6.2 we need to know $\mathbf{c}$ and $\boldsymbol{\mu}$. Some of the components of $\boldsymbol{\mu}$ are fixed parameters because we have judged them to be well

[3]Reaction numbers 1, 2, 3, 4, 5, 8, 9, 10, 14 and 15 of the core model.
[4]Reaction numbers 6, 7, 11, 12, 13, 16 and 17 of the core model
[5]Reaction numbers 6, 7 and 11 of the core model.

Fixed Parameter		Reference
P_1	1.8	Azam and Kotyk (1969)
$K_{2\mathrm{ATP}}$	0.063 mM	Nielsen *et al.* (1998)
$K_{2\mathrm{Glc}}$	0.1 mM	Nielsen *et al.* (1998)
$K_{2\mathrm{DGlc}}$	0.1 mM	Nielsen *et al.* (1998)
$K_{3\mathrm{G6P}}$	0.03 mM	Richter *et al.* (1975)
$K_{3\mathrm{F6P}}$	0.01 mM	Richter *et al.* (1975)
$K_{3\mathrm{eq}}$	0.298	Richter *et al.* (1975)
K_4	0.0016 mM^2	Nielsen *et al.* (1998)
κ_4	0.017	Nielsen *et al.* (1998)
$K_{4\mathrm{mATP}}$	0.01 mM	Nielsen *et al.* (1998)
V_{5r}	$5{\cdot}V_{5f}$	Richter *et al.* (1975)
K_{5eq}	0.081 mM	Richter *et al.* (1975)
$K_{5\mathrm{FBP}}$	0.3 mM	Richter *et al.* (1975)
$K_{5\mathrm{GAP}}$	2.0 mM	Richter *et al.* (1975)
$K_{5\mathrm{DHAP}}$	2.0 mM	Richter *et al.* (1975)
$K_{8\mathrm{ADP}}$	0.3 mM	Nielsen *et al.* (1998)
$K_{8\mathrm{PEP}}$	0.2 mM	Nielsen *et al.* (1998)
$K_{14\mathrm{DHAP}}$	0.4 mM	Richter *et al.* (1975)
K_{14eq}	0.05	†
$K_{15\mathrm{NADH}}$	0.13 mM	Cai *et al.* (1996)
$K_{15\mathrm{DHAP}}$	1.6 mM	Cai *et al.* (1996)
$K_{15\mathrm{INADH}}$	0.034 mM	Cai *et al.* (1996)
$K_{15\mathrm{INAD}}$	0.13 mM	Cai *et al.* (1996)

Table 6.6: Fixed parameters of the core model. These parameters are not varied during the optimization; they are fixed at the value given in the reference. †: Changed from 0.0455 to 0.05 in order to allow for the concentrations measured by Richard *et al.* (1996b).

determined (table 6.6), and the stationary concentrations of ATP, ADP, AMP, NAD^+, NADH, G6P, F6P, FBP, GAP, DHAP, DPG, PEP, and Pyr (listed in table 2.1) are known from the work of Richard *et al.* (1996b).

These intracellular concentrations are measured in a closed system, but we can use them for the optimization anyhow. The reason for this is that the cells harvested at the diauxic shift presumably set up their own open system as discussed on page 57. Thus, the cells are more or less in a steady state with regard to the intracellular metabolites. This is in contrast to the extracellular ethanol and glycerol concentrations which are increasing steadily, and the extracellular glucose and cyanide concentrations, which are decreasing. We can take the average concentrations of the different oscillating metabolites as their stationary concentrations, since we know from my experiments that we are close to a supercritical Hopf bifurcation.

Still, we are far from knowing all the elements of $\mathbf{c}$ and $\boldsymbol{\mu}$; finding proper values for these unknown concentrations and parameters is the purpose of the optimization. This is done in a straight forward way: We vary the parameters and concentrations and use a validation scheme to decide which values to keep. We want to make this scan of the parameter space as simple as possible, so I will present some considerations on the different unknown parameters before presenting the validation scheme.

The concentrations of Glc and DPG are unknown; the DPG concentration is too low to be determined, and no Glc measurements were made because its concentration is believed to be low. – So the only thing we know about these concentrations is that they should be low. The intracellular concentrations of ACA, EtOH and glycerol are also unknown, but their extracellular concentrations are known (taken from Richard *et al.* (1994) and Richard *et al.* (1996a); listed in table 2.2). Consequently, the intracellular concentrations of these metabolites should be at least as high as their extracellular concentrations.

For reasons given in table 6.7, the kinetic parameters in this list are also varied.

Apart from these unknown concentrations and parameters, we need to find values for v_0, j_1 and j_2 in order to use equation 6.1. The glycerol production was estimated to approximately 17% on page 21; this gives $j_1 = 0.83$ and $j_2 = 0.17$. This estimate is obtained from an experiment with higher cyanide concentration than that used by Richard *et al.* (1996b). Therefore, this estimate of the glycerol production is probably somewhat high.

The glycolytic flux is estimated to approximately 0.6 mM/min when measured as extracellular glucose consumption. This estimate is made in the following way: From table 2.2 we have an extracellular glucose consumption of $\frac{1}{2}\cdot 18\ \mu$M/s + 1.9 μM/s = 0.654 mM/min at a cell density of 6.6 (g protein)/l; this leaves us with 0.6 mM/min at the cell density of 6 (g protein)/l reported by Richard *et al.* (1996b). Still referring to Richard *et al.* (1996b), we have the ratio of the extracellular volume to the volume of the cytoplasm $V_{\text{ratio}} = \frac{V_{\text{extracellular}}}{V_{\text{cytoplasm}}} = 45$. Therefore, v_0 (the glycolytic flux as measured in the cytosol) is estimated to 27 (mM Glc)/min.

When the extracellular glucose consumption is measured directly, it amounts to approximately 1 mM/min. (This can be seen from various data presented in Teusink (1993)). As mentioned on page 21 this is explained with large amounts of glucose being built into glycogen. In fact Betz and Hinrichs (1968) report that 50% of the glucose taken up by the starved cells is converted to ethanol. This agrees with our estimation of v_0.

Validating the Parameter Sets

All of these more or less unknown concentrations and parameters are varied, and for each of these sets of parameters we calculate the eigenvalues and eigenvectors of the Jacobian matrix at the particular stationary state[6] of the core model.

This allows us to pick out parameter sets which have a supercritical Hopf bifurcation. The Hopf bifurcation is seen directly from the complex conjugated eigenvalues $\lambda_\pm = \alpha \pm i\omega$ (if any); as explained in chapter 3 the bifurcation occurs when these eigenvalues are purely imaginary. The discrimination between supercritical and subcritical Hopf bifurcations is made by demanding $g' > 0$ (cf. equation 3.14 on page 42).

Subsequently, we discard parameter sets that do not have frequencies close to the experimental value of $\omega = 9.12$ rad/min reported by Richard *et al.* (1996b).

This analysis will discriminate good sets of parameters from bad ones, so we should obtain some likely sets of parameters for the core model.

As a preliminary result I have listed a set of parameters for the core model. Table 6.10 shows the eigenvalues of the Jacobian matrix, the calculated parameters are listed in table 6.9, and the fitted parameters are found in table 6.8. Given these parameters, the model possesses a supercritical Hopf bifurcation,

[6] Since the eigenvalues can be calculated much faster than the eigenvectors, we start by calculating the eigenvalues. The eigenvectors are only calculated for the points of the parameter space that are of special interest.

Parameter	Original Value	Comment
$v_{1\rightarrow}/v_{1\leftarrow}$	–	no estimate
$K_{1\mathrm{Glc}}$	1.1 mM	the orig. value is not measured directly
$K_{1\mathrm{IG6P}}$	1.2 mM	the orig. value is not measured directly
$K_{1\mathrm{IIG6P}}$	7.2 mM	the orig. value is not measured directly
$K_{5\mathrm{IGAP}}$	10 mM	the orig. value is just a guess
$v_{6\rightarrow}/v_{6\leftarrow}$	–	no estimate
$v_{7\rightarrow}/v_{7\leftarrow}$	–	no estimate
K_9	0.3 mM	the orig. value is just a guess
$K_{10\mathrm{NADH}}$	0.01 mM†	varied around this estimate
$K_{10\mathrm{ACA}}$	0.78 mM†	varied around this estimate
$v_{11\rightarrow}/v_{11\leftarrow}$	–	no estimate
$K_{14\mathrm{GAP}}$	0.4 mM	the orig. value is just a guess
j_1, j_2	$j_2 = 0.17$	varied around this estimate
v_0	27 mM/min	varied around this estimate
[Glc]	–	varied between 1 μM and 0.4 mM
[DPG]	–	varied between 1 μM and 0.2 mM
[EtOH]	7.1 mM	$\geq$ this extracellular concentration
[ACA]	0.07 mM	$\geq$ this extracellular concentration
[glycerol]	1.3 mM	$\geq$ this extracellular concentration

Table 6.7: The variable parameters of the core model. †: Enzyme Handbook (1969), Springer-Verlag.

oscillates with the right frequency, and has the concentrations of intracellular metabolites reported by the Amsterdam group. It even shows (two) moderately slow eigenvalues associated with the stable manifold, as we expect from the transient seen when the oscillations are quenched with ACA (cf. page 91).

The values of the adjustable parameters v_0, j_2, $K_{1\mathrm{Glc}}$, $K_{1\mathrm{IG6P}}$, and $K_{1\mathrm{IIG6P}}$ are close to their original values; this is accomplished because we allow the Glc concentration to be rather high. If the Glc concentration shall be lower, then the values of $K_{1\mathrm{Glc}}$, $K_{1\mathrm{IG6P}}$, and $K_{1\mathrm{IIG6P}}$ must be changed significantly. This result is consistent with the modelling done by Rizzi *et al.* (1997). [DPG], $K_{10\mathrm{NADH}}$ and $K_{10\mathrm{ACA}}$ do not have large influences on the eigenvalues, so most of the fitting has been done by adjusting the remaining variable parameters. (The values of [EtOH], [ACA] and [glycerol] have not been varied).

The conclusion drawn from this preliminary result is that the core model can behave like the experiment without any drastic changes of its parameters; this is promising for the optimization of the full-size model.

6.2.2 Optimizing the Extended Model

The most promising parameter sets obtained from the core model are used to optimize the full-size model by varying the newly introduced parameters (see tables 6.4 and 6.12). This optimization is extended, so that we now use the quenching data and the phases of the oscillating metabolites – along with the other validation criteria – to validate the model.

We need to handle the newly introduced reversible reactions (reactions 12, 13, 16, 19 and 20). As discussed on page 23 we can estimate the relative rate constants of the three membrane diffusion processes. Thus, we write

$$\begin{aligned} k_{12f} &= k_{12r} = k_d \cdot d_{\mathrm{ACA}} \\ k_{13f} &= k_{13r} = k_d \cdot d_{\mathrm{EtOH}} \\ k_{16f} &= k_{16r} = k_d \cdot d_{\mathrm{glycerol}} \end{aligned}$$

with $d_{\mathrm{ACA}} : d_{\mathrm{EtOH}} : d_{\mathrm{glycerol}} = 13 : 8.8 : 1$. If we specify the value of one of those (for example by specifying $k_d{\cdot}d_{\mathrm{ACA}}$) then we know both $k_{12f}, k_{12r}, k_{13f}, k_{13r}, k_{16f}$ and k_{16r}. This allows us to calculate the intracellular concentrations of ACA, EtOH and glycerol from $v_{12\mathrm{net}}, v_{13\mathrm{net}}$ and $v_{16\mathrm{net}}$, because we already know the extracellular values from the Amsterdam group's measurements. Be aware that the extracellular glycerol and EtOH concentrations are definitely not at a steady state in the closed system, so the corresponding calculated intracellular concentrations are not relevant in themselves. However, the extracellular

Parameter	Original Value	Fitted Value
$v_{1\rightarrow}/v_{1\leftarrow}$	–	1000
$K_{1\mathrm{Glc}}$	1.1 mM	1.1 mM
$K_{1\mathrm{IG6P}}$	1.2 mM	1.2 mM
$K_{1\mathrm{IIG6P}}$	7.2 mM	7.2 mM
$K_{5\mathrm{IGAP}}$	10 mM	1 mM
$v_{6\rightarrow}/v_{6\leftarrow}$	–	2
$v_{7\rightarrow}/v_{7\leftarrow}$	–	2
K_9	0.3 mM	0.9 mM
$K_{10\mathrm{NADH}}$	0.01 mM	0.01 mM
$K_{10\mathrm{ACA}}$	0.78 mM	0.78 mM
$v_{11\rightarrow}/v_{11\leftarrow}$	–	1
$K_{14\mathrm{GAP}}$	0.4 mM	0.1 mM
j_1, j_2	$j_2 = 0.17$	$j_2 = 0.14$
v_0	27 mM/min	32.4 mM/min
[Glc]	–	0.353 mM
[DPG]	–	0.001 mM
[EtOH]	7.1 mM	7.1 mM
[ACA]	0.07 mM	0.07 mM
[glycerol]	1.3 mM	1.3 mM

Table 6.8: A preliminary result of the optimization of the core model: The fitted parameters. See table 6.9 for the calculated parameters, and table 6.6 for the fixed parameters.

Reaction (r)	Calculated Parameters (mM/min)	
1	$V_{1mf} = 223.0$	$V_{1mr} = 0.2470$
2	$V_{2m} = 42.39$	
3	$V_{3m} = 74.56$	
4	$V_{4m} = 32.58$	
5	$V_{5mf} = 452.3$	$V_{5mr} = 2262$
6	$k_{6f} = 1530^{\dagger}$	$k_{6r} = 180792^{\dagger}$
7	$k_{7f} = 79549^{\dagger}$	$k_{7r} = 710.3^{\dagger}$
8	$V_{8m} = 429.6$	
9	$V_{9m} = 61.72$	
10	$V_{10m} = 690.2$	
11	$k_{11f} = 1.443^{\dagger}$	$k_{11r} = 0.4444^{\dagger}$
12	$k_{12} = 64.15^{\ddagger}$	
13	$k_{13} = 7.771^{\ddagger}$	
14	$V_{14m} = 932.4$	
15	$V_{15m} = 19.76$	
16	$k_{16} = 3.454^{\ddagger}$	
17	$k_{17} = 26.27^{\ddagger}$	

Table 6.9: A preliminary result of the optimization of the core model: The calculated parameters. See table 6.8 for the fitted parameters, and table 6.6 for the fixed parameters. †: In units of mM^{-1} min^{-1}. ‡: In units of min^{-1}.

Re(λ)	Im(λ)	Re(λ)	Im(λ)
-180522.	0	0.00000	-9.20635
-7189.58	0	0.00000	9.20635
-1726.45	0	-3.82078	0
-792.72	0	-3.45434	0
-245.467	0	-0.275249	0
-141.726	0	-0.193772	0
-70.1578	0	-7.77052	0
-24.536	0		

Table 6.10: A preliminary result of the optimization of the core model: The eigenvalues of the Jacobian matrix evaluated at the stationary point.

r	$\mathbf{E}_1$	$\mathbf{E}_2$	$\mathbf{E}_3$	$\mathbf{E}_4$
1	$\frac{1}{V_{\mathrm{ratio}}}$	$\frac{1}{V_{\mathrm{ratio}}}$	$\frac{2}{V_{\mathrm{ratio}}}$	$\frac{1}{V_{\mathrm{ratio}}}$
2	1	1	2	1
3	1	1	1	1
4	1	1	1	1
5	1	1	1	1
6	2	1	2	1
7	2	1	2	1
8	2	1	2	1
9	2	1	2	1
10	2	0	2	0
11	0	0	0	0
12	0	$\frac{1}{V_{\mathrm{ratio}}}$	0	$\frac{1}{V_{\mathrm{ratio}}}$
13	$\frac{2}{V_{\mathrm{ratio}}}$	0	$\frac{2}{V_{\mathrm{ratio}}}$	0
14	1	0	1	0
15	0	1	0	1
16	0	$\frac{1}{V_{\mathrm{ratio}}}$	0	$\frac{1}{V_{\mathrm{ratio}}}$
17	2	0	0	0
18	0	0	1	0
19	$\frac{1}{V_{\mathrm{ratio}}}$	$\frac{1}{V_{\mathrm{ratio}}}$	$\frac{2}{V_{\mathrm{ratio}}}$	$\frac{1}{V_{\mathrm{ratio}}}$
20	0	0	0	$\frac{1}{V_{\mathrm{ratio}}}$
21	0	$\frac{1}{V_{\mathrm{ratio}}}$	0	$\frac{1}{V_{\mathrm{ratio}}}$
22	0	$\frac{1}{V_{\mathrm{ratio}}}$	0	0
23	$\frac{2}{V_{\mathrm{ratio}}}$	0	$\frac{2}{V_{\mathrm{ratio}}}$	0
24	0	0	0	$\frac{1}{V_{\mathrm{ratio}}}$

Table 6.11: The extreme currents of the extended model. The numbers in the first column refer to the numbering of the reactions in table 6.3. $\mathbf{E}_1$: Glycolysis and fermentation. $\mathbf{E}_2$: Glycerol production. $\mathbf{E}_3$: Glycolysis, fermentation and glycogen production. $\mathbf{E}_4$: Glycerol production and formation of lactonitril. $V_{\mathrm{ratio}} = \frac{V_{\mathrm{extracellular}}}{V_{\mathrm{cytoplasm}}}$.

and intracellular concentrations relative to each other should be about right. The extracellular ACA measurements are made over a two-minutes time span; within this period of time the concentration seems to oscillate around a stable mean value. Thus, it might be justified to use this mean value as a stationary ACA_{ex} concentration provided that the results are interpreted with caution.

The values of the specific flow rate j_{total} and the mixed flow concentrations $[\text{Glc}]_{\text{m.f.}}$ and $[\text{CN}^-]_{\text{m.f.}}$ are taken from the CSTR experiments; this gives us $[\text{Glc}_{ex}]$ and $[\text{CN}^-_{ex}]$ from the net velocities of reactions 19 and 20:

$$[\text{Glc}_{ex}] = [\text{Glc}]_{\text{m.f.}} - \frac{v_{19\text{net}}}{j_{total}} \tag{6.3}$$

$$[\text{CN}^-_{ex}] = [\text{CN}^-]_{\text{m.f.}} - \frac{v_{20\text{net}}}{j_{total}}. \tag{6.4}$$

(As in table 6.4 the subscript "m.f." denotes the mixed flow concentration).

The extension of the model introduces two additional extreme currents (see table 6.11); we now need four j's to describe all the possible stationary states of a given total flux v_0:

$$\frac{\mathbf{v}}{v_0} = j_1 \cdot \mathbf{E}_1 + j_2 \cdot \mathbf{E}_2 + j_3 \cdot \mathbf{E}_3 + j_4 \cdot \mathbf{E}_4 \tag{6.5}$$

with $j_1 + j_2 + j_3 + j_4 = 1$ and $j_1, j_2, j_3, j_4 \geq 0$. The biochemical interpretation of the four extreme currents is the following:

- $\mathbf{E}_1$: Glycolysis and fermentation
- $\mathbf{E}_2$: Glycerol production
- $\mathbf{E}_3$: Glycolysis, fermentation and glycogen production
- $\mathbf{E}_4$: Glycerol production and formation of lactonitril

This helps us to make an estimate of the values of the four j's. As in the core model, the glycerol production should amount to 17 % (or a little less) of the total flux measured as the production of EtOH and glycerol. This gives us $j_2 + j_4 = 0.17$ and $j_1 + j_3 = 0.83$. According to Betz and Hinrichs (1968), 80–90 % of the ATP produced by glycolysis is used for the production of some storage polyglucoside; expressed in terms of the j's this means that $\frac{j_3}{j_1+j_3} = 0.85$.

It would have been very nice if the measurements of the extracellular ACA and glycerol concentrations could have been used to estimate j_2/j_4, but this is not possible. The reason for this is that the production of glycerol – and presumably ACA – starts at the time of the Glc pulse, while the consumption of ACA starts at the time of the cyanide pulse. There is no way to deduct the two j's from the resulting transient, when the only measurements of the ACA concentrations are from the time 5–7 min after the cyanide pulse. However, we can conclude that j_4 must be quite large compared to j_2, since the ACA concentration is round 5% of the glycerol concentration at this time. Another approach to obtain an estimate of j_2 and j_4 is to make use of the stationarity. From the extreme currents in table 6.11 we have

$$v_{20\text{net}} = v_{24\text{net}} = \frac{v_0}{V_{\text{ratio}}} j_4,$$

and by equating the rate expressions for $v_{20\text{net}}$ and $v_{24\text{net}}$ we obtain

$$j_4 = \frac{V_{\text{ratio}}[\text{CN}^-]_{\text{m.f.}}}{v_0 \left(\frac{1}{j_{\text{total}}} + \frac{1}{k_{24}[\text{ACA}_{ex}]} \right)}$$

which allows us to calculate j_4 (and thereby j_2) from known parameters and concentrations. With typical values from the CSTR experiments this results in $j_4 = 0.04$ and $j_2 = 0.13$. In words this means that round $\frac{1}{4}$ of the ACA produced by the yeast cells reacts with cyanide in the CSTR experiments, while the remaining $\frac{3}{4}$ is removed by the outflow.

With these estimates of j_1, j_2, j_3 and j_4 we have a fair chance of doing the optimization in the same way as described for the core model; now by varying the parameters as indicated in table 6.12.

The calculated eigenvectors of the unstable subspace are used to include the quenching data and the relative phases of the oscillating metabolites in the optimization. Equation 3.36 on page 52 is used along with the left eigenvectors to choose the sets of parameters which fit the quenching data, and the relative phases of the different metabolites – which should match the values given in tables 2.1 and 2.2 – are seen from the right eigenvectors.

In principle, the amplitude and frequency dependencies on the bifurcation parameters (figures 5.14–5.19) could also be used for this validation (Kosek *et al.*, 1994), but we do not do so because of the problems of calibrating the fluorescence measurements mentioned in the previous chapter).

Parameter	Original Value	Comment
$k_d \cdot d_{\text{ACA}}$	–	no estimate
j_{total}	$50 \cdot 10^{-3}$ min$^{-1\dagger}$	varied around this typical value
$[\text{Glc}]_{\text{m.f.}}$	22 mM†	varied around this typical value
$[\text{CN}^-]_{\text{m.f.}}$	4 mM†	varied around this typical value
k_{24}	0.09 mM^{-1} min$^{-1\ddagger}$	kept close to this value
j_1	$j_1 = 0.1245$	varied around this estimate
j_2	–	$j_2 = 1 - j_1 - j_3 - j_4$
j_3	$j_3 = 0.7055$	varied around this estimate
j_4	$j_4 = \frac{V_{\text{ratio}}[\text{CN}^-]_{\text{m.f.}}}{v_0\left(\frac{1}{j_{\text{total}}} + \frac{1}{k_{24}[\text{ACA}_{ex}]}\right)}$	varied around this estimate
v_0	27 mM/min	as in the core model; varied around this estimate

Table 6.12: The variable parameters of the full-size model. †: These parameters can be taken directly from the CSTR experiments. ‡: From Richard *et al.* (1996a), cf. page 64.

Unfortunately, we have not completed this work yet, so the presentation of a full-size model for the glycolytic oscillations in intact yeast cells must await a future paper.

6.3 Modelling Cell Synchronization

At this point, you might be wondering if such a complicated model will be of any use when trying to *understand* the phenomena treated in this thesis. – It might be just as hard to understand what is going on in the model as in the real world. This is true; as long as we use the full model, it is better at describing glycolysis than at explaining it. But, as discussed on page 39, the presence of a Hopf bifurcation allows us to separate the slow and the fast modes of the system, in order to obtain a low-dimensional description, which is nevertheless almost quantitatively correct. Furthermore, the transformation back to the full concentration space can also be calculated, so the biochemical details are not lost. As mentioned, this transformation is done according to the dynamics of the system, and not by intuition as is usually the case when models are simplified. The stable, slow mode which is revealed by the ACA quenching, and seen in the preliminary results from the optimization of the core model, can of course be included in the description. See Ipsen *et al.* (1997) for an example.

In close collaboration with Mads Ipsen and Christian Fenger at UNI-C, Danish Computing Center for Research and Education, we plan to use this approach to investigate the synchronization of the yeast cells in the spirit of Matthews *et al.*. Their work was presented in chapter 4, when equation 4.1 was discussed (starting on page 68). Please refer to these pages when reading this section.

When modelling the cell synchronization, we will explicitly address the question of how the oscillations of the individual cells relate to the macroscopic oscillations. Therefore, we will not restrict the investigation to the order parameter r. Instead, we will calculate the phase distribution, the amplitude distribution, and the mean concentration (which corresponds to the averaged signal which we measure in the experiments), as well as the order parameter.

Since the frequency of the oscillations in the experiments increases with increasing mixed flow glucose concentration (see figure 5.15), we cannot assume $g'' = 0$. Thus, we will model the full version of equation 4.1, which allows for variation of the frequency when the amplitude changes.

The integration of equation 4.1 has already been implemented by Christian Fenger, and I will now briefly discuss some of the preliminary results, which we have obtained. Obviously, the results do not relate explicitly to glycolytic oscillations in yeast cells, but the phase and amplitude distributions resulting from different coupling strengths are useful when discussing the cell synchronization. The parameters of the integrations are the following:

- $N = 12000$ individual oscillators (the behaviour of the system converges when a few thousand oscillators are used)
- d' is varied between 0 and 3, while $d'' = 0$ (simple coupling)
- $\sigma_j = \sigma = 1.467$ and $g_j = 246.6 + 620.4i$ (the oscillations only differ in ω_j)
- ω_j is taken from a Gauss distribution with a mean value of 1.237 and a spread of the same size

Some results of these integrations are shown in figures 6.1–6.6. The plots of the order parameter (upper left panel) and the real part of the mean concentration (lower left panel) both show the time-evolution of the system throughout the integration. The phase and amplitude distributions (upper and lower right panels, respectively) are snap-shots taken at the end of the integration.

At very low coupling strength (figure 6.1), the oscillators are practically uncoupled with phases distributed randomly, and all oscillators oscillating with their intrinsic amplitude. As the coupling strength is increased (figure 6.2), irregular bulk oscillations appear. The bulk amplitude is low due to the very broad phase distribution. The interaction among the oscillators broadens the amplitude distribution, as expected with $g'' \neq 0$.

For some intermediate coupling strengths (figure 6.3), we find that the order parameter r oscillates; in the fixed coordinate system this is seen as torus oscillations. Both the phase and the amplitude distributions have two distinct peaks. If these two sub-populations oscillate at different frequencies, then r will be at its maximum when they coincide, and at its minimum when they are in opposite phases. This is probably the explanation for the bulk torus oscillations.

As the coupling strength is increased further, the interaction between the sub-populations becomes stronger, and consequently they entrain each other. Thus, the order parameter r becomes stable, and the amplitude distribution changes from a double-peak distribution (figure 6.4) into a single-peak distribution (figures 6.5 and 6.6). The phase distribution also changes from a

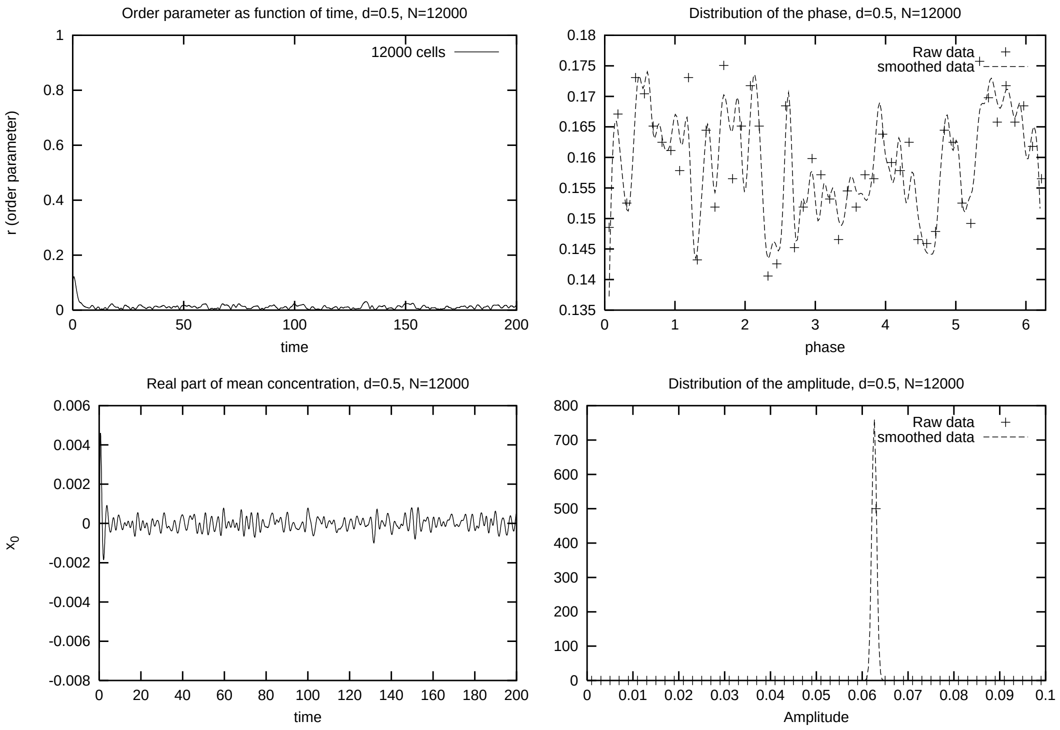

Figure 6.1: Numerical integration of 12000 limit-cycle oscillators with very weak coupling ($d = 0.5$). See text for details. The integration is performed by Christian Fenger.

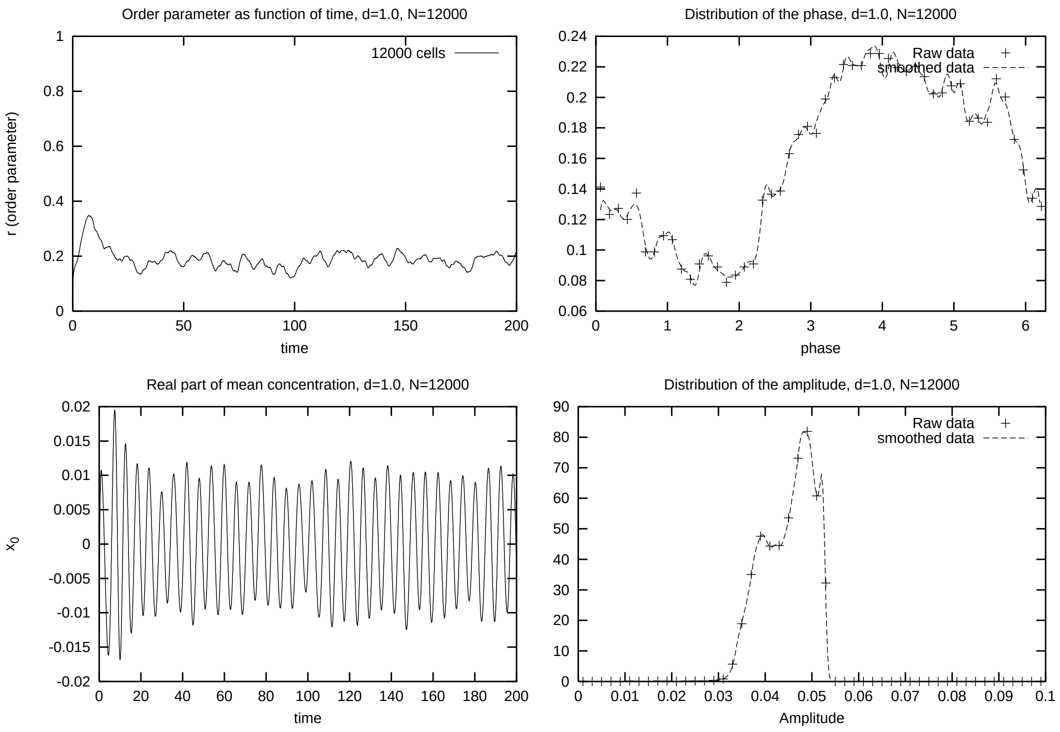

Figure 6.2: Numerical integration of 12000 limit-cycle oscillators with weak coupling ($d = 1.0$). See text for details. The integration is performed by Christian Fenger.

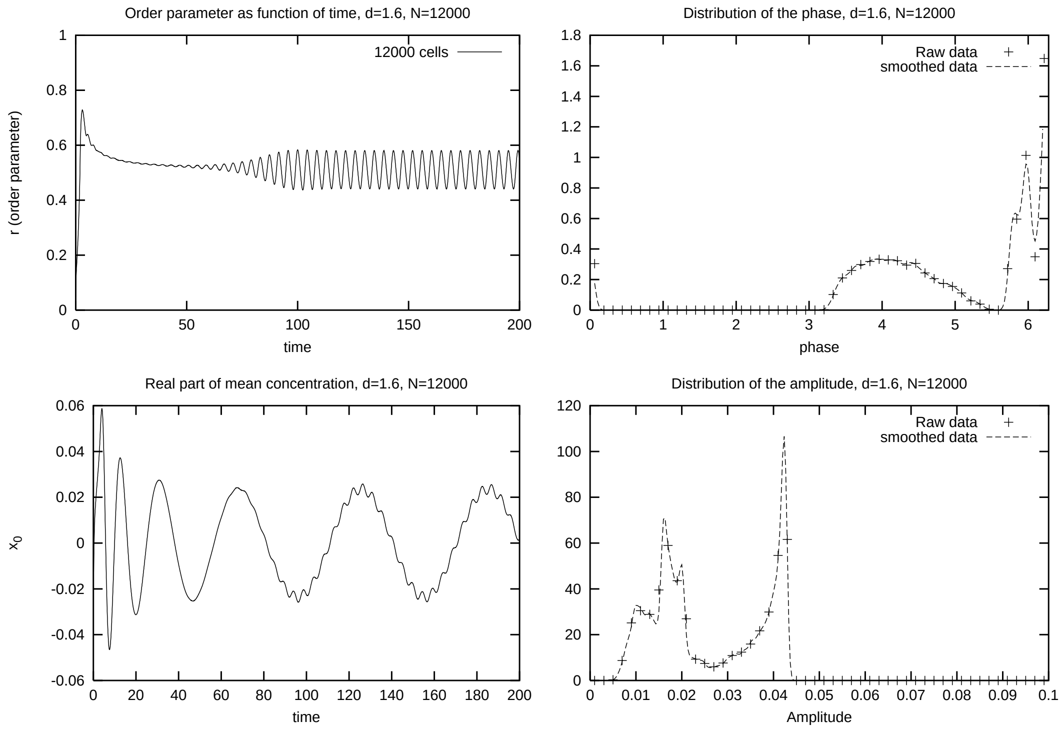

Figure 6.3: Numerical integration of 12000 limit-cycle oscillators with intermediate coupling strength ($d = 1.6$). See text for details. The integration is performed by Christian Fenger.

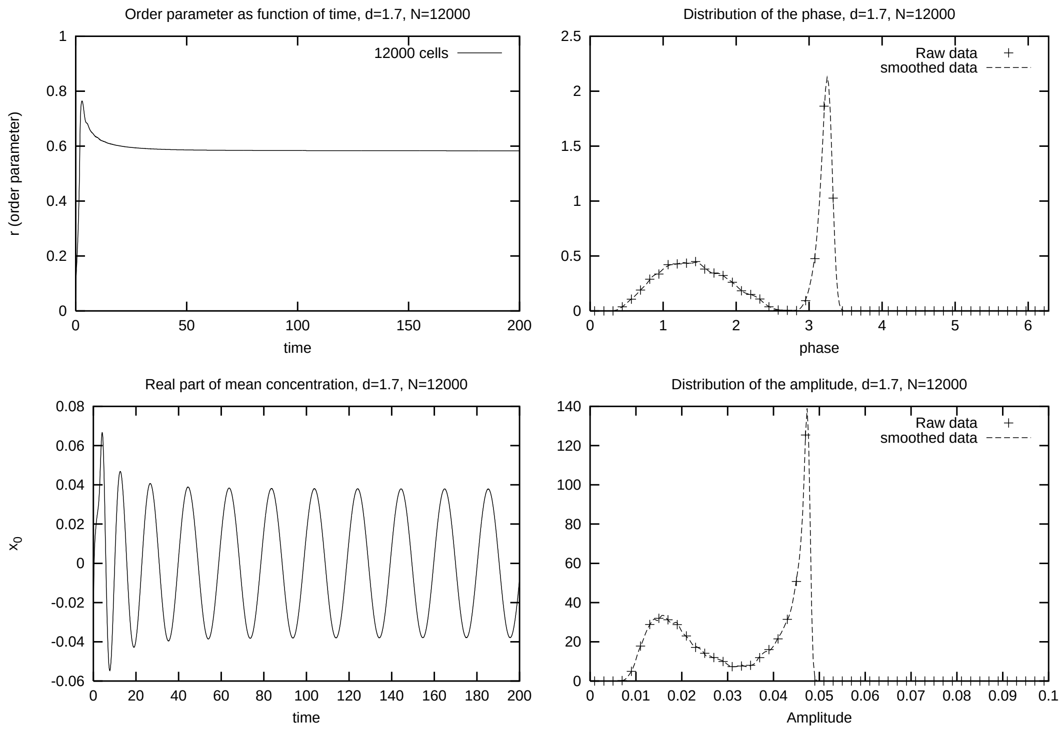

Figure 6.4: Numerical integration of 12000 limit-cycle oscillators with intermediate coupling strength ($d = 1.7$). See text for details. The integration is performed by Christian Fenger.

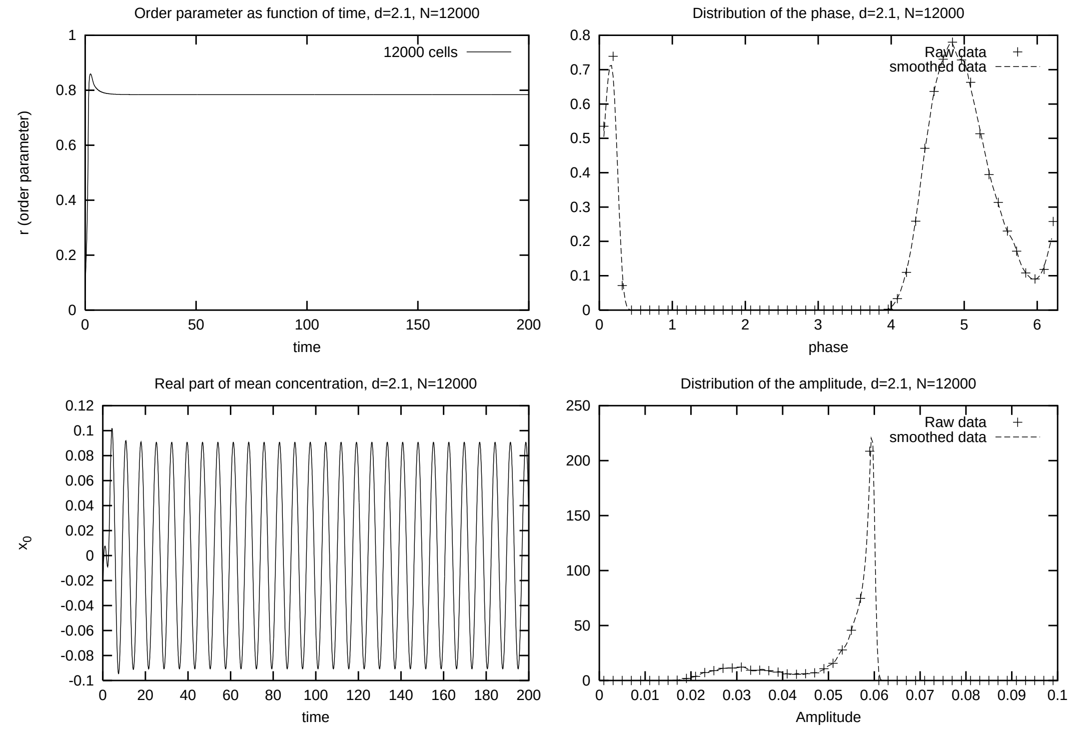

Figure 6.5: Numerical integration of 12000 limit-cycle oscillators with strong coupling ($d = 2.1$). See text for details. The integration is performed by Christian Fenger.

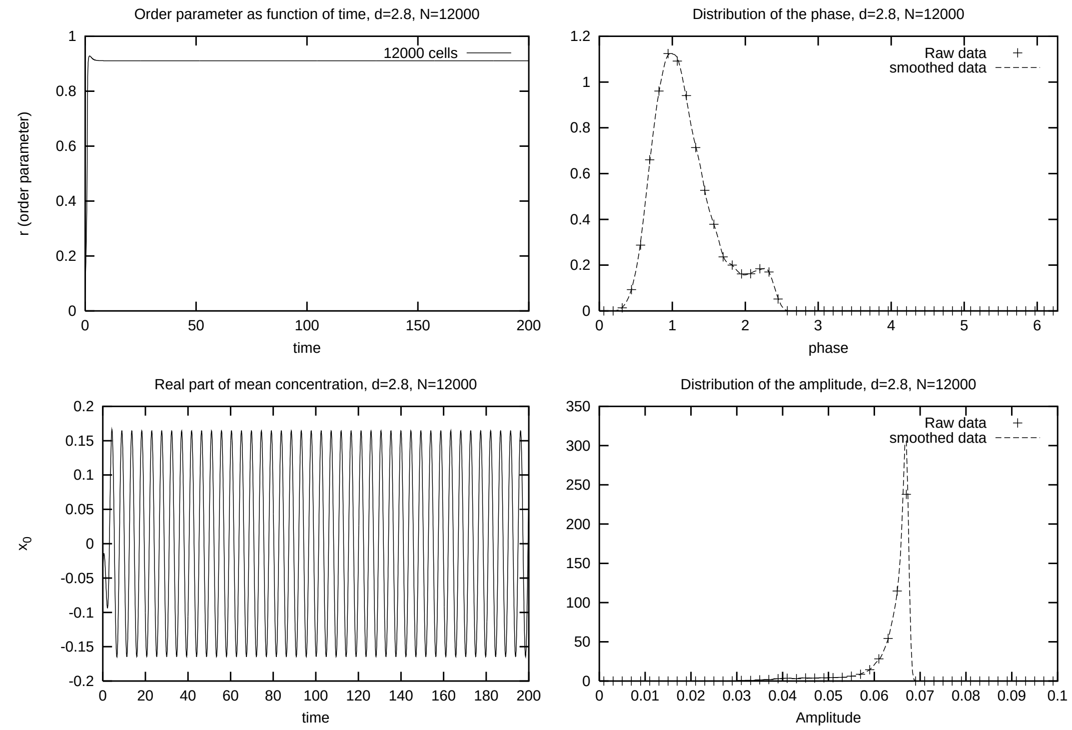

Figure 6.6: Numerical integration of 12000 limit-cycle oscillators with strong coupling ($d = 2.8$). See text for details. The integration is performed by Christian Fenger.

double-peak to a single-peak distribution, but this happens at a higher coupling strength. The phase distribution remains broad (like it is in figure 6.6) in all the simulations we have run (i.e. up to $d = 3$). The period of the bulk oscillations also changes with varying coupling strength; in rough numbers, it increases by a factor 4 when d is increased from 1.7 to 2.8.

We do not know whether these effects will also be seen when the optimized model is used to calculate the parameters for the intgrations. Most likely they will, since similar phenomena are reported by Matthews *et al.* (1991), who use a different set of parameters.

Whether or not such phenomena can be seen in the experiments, depends on the degree of heterogeneity of the yeast cells. I do not know much about this, but one might obtain a relevant estimate from their cell-size distribution. Cells of different sizes will have different surface-to-volume ratios, and this will result in different transport properties. In the scheme presented here, we could formulate this as a distribution in d_j.

The formulation of the all-to-all coupling will probably also have to be changed. As it is now, each cell couples to the average of the concentrations in the other cells. This description is equivalent to an infinitely fast exchange of metabolites across the cell membrane. When the full-size model has been optimized, we can tell from the calculations of the intracellular concentrations of ACA, EtOH and glycerol, and from the calculation of the extracellular Glc concentration, whether or not this is a good description. Thus, further progress on the simulation of the cell synchronization must await the optimization of the extended model.

7
Conclusions and Perspectives

In this thesis I have reported on an experimental study of sustained oscillations in a yeast cell population. As far as I know, this is the first example of a living system being held in a precise dynamical state by using a CSTR.

A Qualitative Description

The results from these experiments can be interpreted in the framework of nonlinear dynamics. The bifurcation analysis shows a clear square-root dependence of the amplitude on the bifurcation parameter. As already discussed, this is the expected behaviour at a supercritical Hopf bifurcation, but it could just as well be caused by a graduate desynchronization of the oscillating yeast cells.

However, the quenchings performed close to the bifurcation point with Glc and ACA show, that the phase space has the geometry of a supercritical Hopf bifurcation. Therefore, the joint conclusion of these two series of experiments is that the onset of the oscillations corresponds to a supercritical Hopf bifurcation. To my knowledge, this is the first direct, experimental demonstration of the presence of a supercritical Hopf bifurcation in a living system.

This means that the dynamics of the biological system can be described by the simple, abstract picture given by nonlinear dynamics. When considering the complexity of the underlying biochemistry, the compartmentation of the yeast cells, and the cell synchronization which takes place, then this is – in my mind – in itself impressive.

As exemplified by the work of Sel'kov (1968) and (Winfree, 1980), the use of nonlinear dynamics in the discussion of glycolytic oscillations is by no means new; concepts like limit cycles and Hopf bifurcations have been used for the *qualitative* explanation of glycolytic oscillations for more than three decades. In spite of this, no detailed biochemical description has emerged from this notion: The science of complexity remains simple, while the "simple" biochemistry remains complicated.

Towards a Quantitative Description

This shows the importance of the quenching experiments. As described in chapter 3, these experiments provide the long sought connection between the qualitative picture given by nonlinear dynamics, and the quantitative details of the underlying biochemistry. In the words of Koshland Jr. (1998), this is a step towards "the era of pathway quantification" where "quantitation and the mathematics of quantitation become part of the arsenal of investigators of metabolic interactions". But there is more to it than just words: The actual implementation of the idea has been outlined in the previous chapter, and we will soon be able to present a comprehensive model of the glycolytic oscillations of the intact yeast cells.

This model will be an explicit mathematical formulation of the present understanding of glycolysis, formulating the accumulated progress of more than a century of research. The biochemical details of such a comprehensive model will be of use when concerned with questions like "how do we produce more ethanol at a lower cost" or "what is supposed to happen if we over-express this enzyme". – Bearing in mind the complexity of cell growth, the later question will probably be rephrased into "what else happened when we over-expressed that enzyme" after the experiment has been performed.

But the strength of such a model lies not only in its detail. The presence of a Hopf bifurcation allows us to distinguish between slow and fast modes of the system. As discussed briefly on page 39, this allows for a low dimensional description of the system, which is nevertheless almost quantitatively correct. Furthermore, the transformation back to the full concentration space can also be calculated, so the biochemical details are not lost.

In short, we get the simple, understandable picture already known from nonlinear dynamics, without loosing the quantitative description. As mentioned at the end of the previous chapter, we will in fact use this strategy to investigate the dynamics of the cell synchronization.

I am sure that the approach presented here could be useful in the quantitative investigation of other complex biological systems such as cytosolic calcium oscillations, the cell communication of the slime mold *Dictyostelium discoideum*, circadian rhythms, or the cell division cycle.

7.1 The CSTR

The experimental prerequisite of the approach discussed above is the availability of an open system. In the experiments presented in this thesis, this is provided by a CSTR setup. This setup should not be confused with the infusion experiments of Hess and Boiteux (1968), where glucose is flowed into the cuvette at a slow and steady rate. Since there is no outflow, this setup is still a closed system, and as such it will only show the dynamics of a transient. The experiments presented by Hess and Boiteux are indeed interesting, but the setup cannot maintain the system at the same dynamical state.

The Importance of an Open System

As demonstrated in figure 5.5, this can be done with the CSTR. Furthermore, the state of the system can be controlled by adjusting the different flow rates; this allows us to investigate phenomena that cannot be investigated in closed systems.

This point is illustrated by the fact that the glucose – and not just acetaldehyde – can quench the oscillations. In the usual setup, which is a closed system, you will not be able to see any effect of a glucose pulse, because this metabolite is added in excess from the start of the experiment. As proposed by Teusink *et al.* (1996b) (cf. page 60), this saturates the glucose transporter which then produces a slow and steady flow of glucose into the cell. This is a prerequisite for the long-lasting oscillations in the usual setup, but at the same time it makes the cells insensitive to glucose perturbations. Thus, one would never have discovered that glucose is a messenger substance, if the yeast cells had not been put into the CSTR. This notion also explains why glucose cannot quench the oscillations when the mixed flow glucose concentration is higher than approximately 24 mM, and why the oscillations are sinusoidal throughout the whole range of mixed flow glucose concentrations. The same argument explains why the amplitude of the oscillations do not change with the mixed flow glucose concentration, when this is above the threshold of 24 mM.

When using the CSTR, it is no longer a prerequisite that the yeast cells can set up their own stable glucose flow. Therefore, we should be able to see glycolytic oscillations in yeast cells irrespectively of the glucose affinity of their glucose transporters. The implications of this are dual: We could use the CSTR to characterize cells differing from the wildtype in their transport properties, or we could use cells with different transport properties to investigate the dynamics in a wider range of glycolytic flux. If this was done, we would expect to see more interesting dynamics, because a wide range of complex dynamics have been reported in CSTR experiments with yeast extracts (Nielsen *et al.*, 1997). Such observations in living cells would be interesting in themselves, but they might also reveal new aspects of the underlying kinetics.

One way of changing the transport properties is to harvest the cells in the exponential growth phase, since the glucose affinity of the transporter is lower at this point (Walsh *et al.* (1994); see also Hess and Boiteux (1968) for an experiment with anaerobically grown yeast cells).

Another way to do such an experiment is to change the sugar from glucose to another sugar. Experimental evidence already exists that fructose (which enters glycolysis at the level of F6P) can produce oscillations with a frequency which differs from that of the glucose induced oscillations. Furthermore, the sensitivity towards variations in the sugar concentration is larger when the oscillations are induced by fructose (Kreuzberg and Betz, 1979). This can be explained by differences in the affinities of the extracellular sugar (Becker and Betz, 1972), just like the growth dependence discussed above. A similar effect is seen when mannose is used (Pye, 1973). (See also Hess and Boiteux (1968) and Kreuzberg (1978)). By pursuing these questions with the new experimental possibilities that the CSTR provides, we will no doubt gain new insights into the ubiquitous metabolic pathway of glycolysis.

The CSTR as a Tool for Cell Biology

The possibility of controlling the exact state of the system in the CSTR, allows us to do detailed studies of the kinetics of the system. One example of this is the bifurcation analysis which I have performed, but it could also be useful without the framework of nonlinear dynamics. For example, one could put the system in different stationary states, and measure the concentrations of all the relevant metabolites in each of these states. For each stationary state tested, this would allow the calculation of a kinetic parameter for each of the reactions involved[1]. Thus, if the measurements are performed at sufficiently many stationary states, this approach will determine all the kinetic parameters of the system.

There are, of course, also some problems related to the CSTR approach. Apart from the minor technical problems of running the CSTR, which were thoroughly discussed in chapter 5, there is one major problem: Large amounts of cell suspension is needed. Evidently, this problem can be overcome when one works with yeast cells. Nevertheless, it puts a strong limitation on the kinds of cell types that can be investigated with the CSTR.

Various other setups exist, which provide an open system. One of these methods, the chemostat, has indeed proved very useful in microbiology. Here, growth medium is flowed into a tank with growing microorganisms, and cells and surplus liquid are flowed out. Most other methods rely on some means of retaining the biological material (e.g. immobilisation of yeast cells in an agarose gel (Brindle and Krikler, 1985), and the use of ultrafiltration membranes to retain the enzymes of a yeast extract (Hocker *et al.*, 1994)). Such setups do not require large amounts of biological material; instead they are technically more difficult to use, than the CSTR presented here. With such setups, there might also be problems of cells growing, aging or being damaged inside the measuring chamber. To a large extent, such problems are circumvented when the cells are included in the flow, because this keeps the cell population in a steady state. You are still faced with the problem of storing the cells, but keeping the cells cold and in some dormant state, does much to solve this problem.

Therefore, our simplistic CSTR approach could very well become an important tool for cell biology, just like the chemostat is for microbiology.

Combining ^{31}P-NMR and the CSTR

Another limitation for the study of *in vivo* kinetics is the difficulties of performing online measurements. Apart from NADH fluorescence, some possibilities exist:

- electrodes have been used to measure CO_2 and pH in yeast extracts (Hess *et al.*, 1969).
- MIMS have been used with yeast extracts Das *et al.* (1990).

[1] See the discussion of equations 6.1 and 6.2 on page 106 for details.

- microcalorimetry has been used with intact cells by Teusink *et al.* (1996b), and with extracts by Grospietsch *et al.* (1995).

- pH has been measured with fluorescent dyes in yeast extracts by Mair and Müller (1996), and in intact yeast cells by Haworth *et al.* (1991) and Aon and Cortassa (1997).

Both electrodes and MIMS are restricted to extracellular measurements, while the microcalorimetry and the pH measurements with fluorescent dyes can give information on the *in vivo* kinetics. However, both methods suffer from the same drawback as does the measurements of NADH fluorescence: Only one parameter is recorded.

What is needed, is detailed information like that obtained with time-averaged ^{31}P-NMR by Brindle and Krikler (1985). In this study, 512 scans were collected with a relaxation delay of 5 s; a total acquisition time of round $\frac{3}{4}$ of an hour. However, we would like such measurements with a time-resolution of seconds.

By utilizing the CSTR setup and the glycolytic oscillations, this can in principle be achieved. In close collaboration with the group of Bjørn Quistorff at the Panum Institute, University of Copenhagen, we are setting up an experiment where the cuvette of the CSTR is placed inside an NMR magnet. The NADH fluorescence is measured continuously through fibre optics, and this signal is used to trigger the NMR scans according to the phases of the oscillations. After the completion of the experiment, the scans obtained at the different phases of the NADH oscillations are averaged separately. Taking 6 scans in each cycle of the oscillations, we should be able to obtain high-resolution time-averaged NMR spectrums with a time-resolution of round 6 s within a couple of hours. The CSTR setup has already been built into the NMR spectrometer, and the NADH fluorescence measurements have been performed through quartz fibre optics. However, the very long tubes needed for the flows of the CSTR causes these flows to fluctuate. This technical problem – which is somewhat reminiscent of that illustrated in figure 5.4 – will hopefully be solved when the completion of this thesis allows me to do more experiments.

Obviously, these ^{31}P-NMR experiments are not genuine online measurements, and they will probably not be as accurate as the enzymatic measurements performed by Richard *et al.* (1996b) on samples of yeast cells. Still, they have the advantage that the open flow system is not disturbed by the removal of sample material. Furthermore, the problem of stopping *all* metabolic processes immediately – which is inherent to all techniques based on sample removal – is circumvented.

7.2 Cell Synchronization

As explained in chapter 4, ACA and cyanide are thought to be important for the cell synchronization. Then, why can cyanide not quench the oscillations?

The answer is simple: The reaction between ACA and cyanide is too slow. This can be seen from some rough calculations. The cyanide is supposed to affect the oscillator through its reaction with ACA_{ex}. So, we want to remove a specific amount of ACA_{ex} at just the right phase. Given a circular limit cycle centered around the unstable stationary point, and a linear approximation of the stable manifold, this amount will be exactly the same as that needed for the quenching with ACA_{ex}, and the phase will be just the opposite of the quenching phase of ACA_{ex} (see inset).

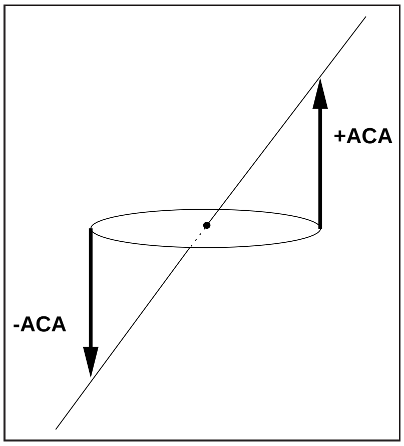

We know that 100 μM ACA_{ex} is needed to quench the oscillations, and we will suppose that $[CN^-_{ex}] = 5$ mM and $[ACA_{ex}] = 0.2$ mM (this is a conservative estimate; according to Richard *et al.* (1996a), $[ACA_{ex}]$ oscillates between 40 μM and 100 μM). Now, if we disregard all other reactions, we can use the integrated rate equation of a second order elementary reaction

$$kt = \frac{1}{[CN^-_0] - [ACA_0]} \ln \frac{[CN^-]/[CN^-_0]}{[ACA]/[ACA_0]}$$

to make some estimates:

- An addition of 100 μM CN^- will need $1\frac{1}{2}$ min to reduce the extracellular concentration of ACA by 100 μM.

- In order to reduce the extracellular concentration of ACA by 100 μM within 10 s, we need to add a cyanide pulse of 46 mM. bifurcation.

Clearly, the reaction between ACA and CN^- is too slow to quench the oscillations with cyanide, without bringing the system on the stable side of the upper cyanide bifurcation. Thus, both the quenching with ACA, and the observation that we cannot quench the oscillations with cyanide, agree perfectly with the synchronization mechanism proposed by the Amsterdam group (Richard *et al.*, 1996a).

A New Perspective on Cell Synchronization

This far, nothing new about the cell synchronization has been concluded. But the finding that *both* Glc and ACA can quench the oscillations has some interesting perspectives.

First of all, it stresses the point made at the end of chapter 4: In contrast to most other known cell synchronization mechanisms, the cell synchronization in yeast cells relies on common metabolites, which are central to the energy metabolism. As a consequence, this mechanism of cell synchronization is inherently difficult to characterize with standard methods like inhibition of receptors or the construction of mutants lacking important parts of the synchronization machinery. – In most cases, this would severely affect the energy metabolism, killing the cells under study.

Secondly, the result clearly shows that this synchronization mechanism, which is based on the ubiquitous glycolytic pathway, could in principle work in all cell types; it can no longer be disregarded as a peculiar consequence of the ethanol fermentation. Once again, the picture given by nonlinear dynamics is helpful. It tells us that the chemical nature of the substance in itself is not important. – What matters is the dynamics which this substance is part of.

The different responses to pyruvate perturbations illustrate this point. The oscillating yeast cells can be phase shifted with this metabolite at pH = 4.6 (Betz and Becker, 1975), but there is only a slow, phase-independent response at pH = 6.8, because pyruvate hardly permeates the cell membrane at this pH. This will be true for all other relevant metabolites as well: They will be able to act as a "synchronizer", provided that they can pass through the cell membrane sufficiently fast. Furthermore, the synchronization will be efficient if the metabolite is present in sufficiently high concentration. This sounds trivial, but as discussed on page 66, this might explain why cells harvested while growing on EtOH do not show bulk oscillations. These cells are believed to have high ADH activity, and this keeps the total amount of ACA too low for efficient synchronization. This notion could be verified experimentally, if bulk oscillations could be induced in these cells by inhibition of ADH (with, e.g., pyrazole (Singlevich and Barboriak, 1971)).

As discussed in chapter 1, the same argument could be used to explain why β-cells, which are responsible for the synchronized secretion of insulin in healthy mammals, have extremely low lactate dehydrogenase activity. Admittedly, this is highly speculative. But, in my mind, the fact that glucose can quench the glycolytic oscillator makes the suggestion by Tornheim (1997), that glycolytic oscillations are responsible for the pulsatory insulin secretion, much more interesting, since this provides a link from the "glucose sensing" to the oscillatory insulin secretion (see also Cunningham *et al.* (1996)).

The Strength of the Synchronization

We have shown how different mechanisms can synchronize the yeast cells, but one question remains: How strong is this synchronization? The phase sensitivity of the quenchings provides a clue. As seen by comparing figures 5.21b and 5.23, the phase interval, in which a given perturbation will stop the oscillations, is quite narrow. This immediately rules out broad phase distributions like that seen in figure 6.2. I also consider it to be very unlikely, that a phase distribution with a double-peak – like those seen in figures 6.4 and 6.5 – can be quenched completely; the oscillators in one of the two sub-populations will still oscillate, when those in the other have been quenched. (However, this should be tested numerically). That leaves us with the strong coupling, where the peak in the phase distribution is even more narrow than that of figure 6.6. However, this is by no means a rigorous argument, and (for reasons discussed in chapter 6) we cannot be sure that the yeast cells will actually behave like the simulations predict.

Therefore, the predictions made by the simulations about the effect of changing coupling strengths, should be tested experimentally. This can in fact be done with the CSTR, since the coupling strength in the experiments can be varied by adjusting the cell density. (The synchronizing substances are diluted when the extracellular volume is increased relative to the intracellular volume). In principle, we only need to add a separate flow with buffer, and then gradually increase the rate of this flow, while we decrease the flow of the cell suspension.

This leaves us with the hope that – someday – this experiment, or some of the other experiments suggested in this chapter, will be performed, and show how the combination of simple experiments and nonlinear dynamics can give new insight into the dynamics of metabolism and cell communication.

A
Abbreviations

This appendix contains an alphabetic listing of the abbreviations used. The listing is divided into enzymes, metabolites and miscellaneous.

Enzymes

ADH	alcohol dehydrogenase
AK	adenylate kinase
ALD	aldolase
ENO	enolase
GAPDH	glyceraldehyde 3-phosphate dehydrogenase
HK	hexokinase
PDC	pyruvate decarboxylase
PFK	phosphofructokinase-1
PFK2	phosphofructokinase-2
PGI	phosphoglucoisomerase
PGK	phosphoglycerate kinase
PGM	phosphoglycerate mutase
PK	pyruvate kinase
TIM	triosephosphate isomerase

Metabolites

2PG	2-phosphoglycerate
3PG	3-phosphoglycerate

ACA	acetaldehyde
acetyl CoA	acetyl coenzyme A
ADP	adenosine 5'-diphosphate
AMP	adenosine 5'-monophosphate
ATP	adenosine 5'-triphosphate
cAMP	cyclic AMP, cyclic adenosine-3',5'-monophosphate
DHAP	dihydroxyacetone phosphate
DNA	deoxyribonucleic acid
DPG	diphosphoglycerate, now called 1,3-bisphosphoglycerate
EtOH	ethanol
F2,6BP	fructose 2,6-bisphosphate
F6P	fructose 6-phosphate
FBP	fructose 1,6-bisphosphate
G6P	glucose 6-phosphate
GAP	glyceraldehyde 3-phosphate
Glc	glucose
mRNA	messenger RNA
NAD^+	nicotinamide adenine dinucleotide (oxidised form)
NADH	nicotinamide adenine dinucleotide (reduced form)
NADPH	nicotinamide adenine dinucleotide phosphate (reduced form)
PEP	phosphoenol pyruvate
P_i	inorganic phosphate
Pyr	pyruvate
RNA	ribonucleic acid
T6P	trehalose 6-phosphate
UTP	uridine 5'-triphosphate

Miscellaneous

a.u.	arbitrary units
BP.	before the present
CSTR	continuous-flow stirred tank reactor
FFT	fast Fourier transform
MCA	metabolic control analysis
MIMS	membrane inlet mass spectroscopy
NMR	nuclear magnetic resonance
OD	optical density

ODE	ordinary differential equations
TCA cycle	tricarboxylic acid cycle
YNB	yeast nitrogen base

B
Materials and Methods

This appendix contains a listing of the materials and instruments used in the experiments.

Chemicals

acetaldehyde	Merck; Acetaldehyd für biochemische Zwecke
glucose	Merck; D(+)-Glucose wasserfrei für biochemische Zwecke
KCN	Merck; Kaliumcyanid pro analysi
K_2HPO_4	Merck; di-Kaliumhydrogenphosphat wasserfrei reinst
KH_2PO_4	Riedel-de Haën; Kaliumdihydrogenphosphat für Analyse
potassium hydrogen phthalate	Fluka; Potassium hydrogen phthalate, MicroSelect; $\geq$ 99.5%(T)
pyruvate	Boehringer Mannheim; prod. No. 128 147
pyruvate ethyl ester	ICN Biomedicals Inc.; cat. No. 156473
YNB	Difco Laboratories; yeast nitrogen base, dehydrated, for classifying yeasts based on carbon assimilation

Cyanide-containing waste is oxidised with potassium permanganate.

Phthalic Acid Buffer; 100 mM, 1 liter

- 20.42 g potassium hydrogen phthalate
- adjust pH to 5.0 with KOH

- H_2O to 1000 ml
- sterilise in autoclave at 1.2 bar, 20 min.

Phosphate Buffer; 100 mM, 1 liter

- 9.42 g KH_2PO_4
- 5.36 g K_2HPO_4
- adjust pH to 6.8 with KOH
- H_2O to 1000 ml
- sterilise in autoclave at 1.2 bar, 20 min.

Growth Medium; 1200 ml for 6000 ml Erlenmeyer flask

- 8.04 g YNB
- 10.80 g glucose
- 1200 ml sterile phtalic acid buffer
- dissolve YNB and glucose in $\frac{1}{10}$ of buffer volume
- sterilise the solution by filtering (0.45μm)
- mix with the rest of the buffer

For precultures, use the above procedure scaled to 50 ml buffer.

Agar Plates

- 2 % glucose
- 2 % peptone
- 1 % yeast extract
- 2 % agar
- sterilise in autoclave at 1.2 bar, 20 min.
- pour into sterile petri dishes before cooling

Methods and Instruments

OD and cell counting

counting chamber	Brand; Thoma, 0.0025 mm^2, depth 0.1 mm
OD measurements	Corning colorimeter 252

Growth and Harvesting

rotary incubator	Gerhardt; Thermoshake, 180 rpm, 30°C
centrifugation	Sorvall; 10 min., 7000 rpm, 4°C, rotor: SLA-3000

Fluorescence Measurements

Hg-lamp	Lamp from a street light with glass bulb removed; custom build housing; adjustable power supply
focusing	quartz lens
excitation filter	Oriel; 365 nm interference filter (fig. B.1)
emission filter	Oriel; 420 nm low pass filter (fig. B.2)
measuring chamber	Custom build, thermostated with water
photomultiplier	RCA 1P28A; sensitive to $200 < \lambda < 660$ nm; stabilised power supply: Oltronix, 900 V
reference	BPX381 phototransistor build into the lamp housing and fitted with an excitation filter
voltmeter	HP 34901A multiplexer board; mounted in a HP 34970A data acquisition switch unit; the sampling interval is 0.5 s

Pumps and Burettes

peristaltic pump	Ismatec; IPC-N-4
tubes (tygon)	Ismatec; ENE-4 (I.D. 0.44 mm) for bubble generation
	Ismatec; ENE-10 (I.D. 0.95 mm) for cell suspension
	Ismatec; ENE-20 (I.D. 1.85 mm) for outflow
burettes	Hamilton; Gastight #1001, 1000 μl for glucose

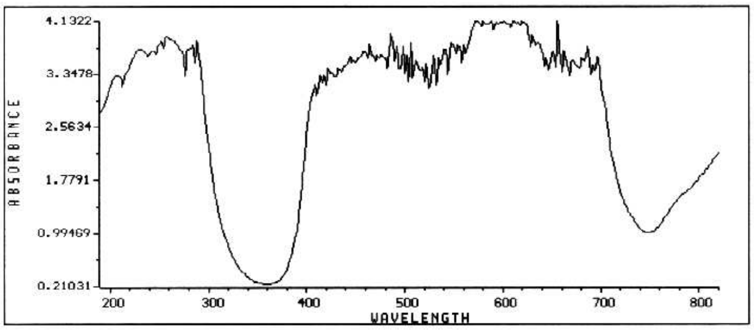

Figure B.1: Absorbance spectrum of the excitation filter.

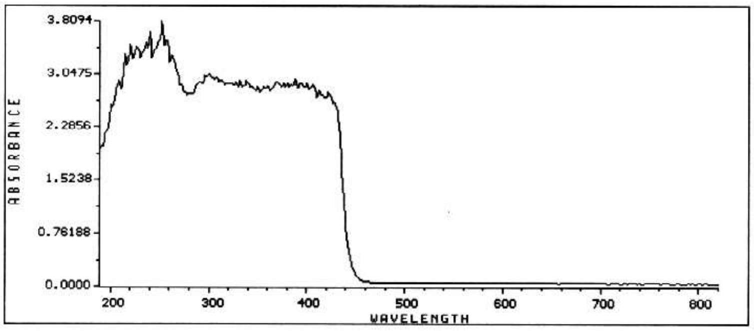

Figure B.2: Absorbance spectrum of the emission filter.

	and cyanide flows; Gastight #1750, 500 μl for perturbations
stepper motors	Airpax; L92211-P2
valves	Furon; 3 way biovalve model 1101437

The peristaltic pump is run at a fixed speed, and the burettes and valves are controlled with custom made electronics and a HP 34907A multifunction board, mounted in a HP 34970A data acquisition switch unit.

Computer

The valves, stepper motors and fluorescence measurements are controlled by a HP Vectra 486 personal computer equipped with a HP82335 HP-IB card, which connects it to the HP 34970A data acquisition switch unit.

Software

YEAST v. 1.3

A pascal program used for data recording and control of burettes and valves. It is a modification and extension of earlier programs written by Preben Graae Sørensen. It uses a graphical interface and a command interpreter written entirely by Preben Graae Sørensen. The entire source code of the program can be found at my website (`http://theochem.ki.ku.dk/~sdd/`). (Hint: The main loop of the program is found close to the end of the listing).

fit.f

This is the fortran program for the data-fitting. It fits the experimental data to a sine function as described on page 81. It comes in two versions: one with sequential non-overlapping windows (`fit.f`), and one with a sliding window (`slidefit.f`). The source codes for both programs are avaliable at `http://theochem.ki.ku.dk/~sdd/`. The two subroutines `CHOLDC` and `CHOLSL` are from Press *et al.* (1992), and the subroutine `BISEC` is a translation of Ole Heilmann's pascal code.

Miscellaneous

filters, 0.45μm	Schleicher & Schuell; FP030/2, ref. No. 462100 (sterile/pyrogene-free)
glucose sticks	Boehringer Mannheim; BM-Test-GP, urine (a glucose-only stick is not for sale in Denmark)

Bibliography

Aldridge, J. & Pye, E. K. (1976), Cell Density Dependence of Oscillatory Metabolism, *Nature* **259**:670–671.

Aon, J. C. & Cortassa, S. (1997), Fluorescent measurement of the intracellular pH during sporulation of *Saccharomyces cerevisiae*, *FEMS Microbiology Letters* **153**:17–23.

Aon, M. A., Cortassa, S., Westerhoff, H. V., Berden, J. A., van Spronsen, E. & van Dam, K. (1991), Dynamic regulation of yeast glycolytic oscillations by mitochondrial functions, *Journal of Cell Science* **99**:325–334.

Aon, M. A., Cortassa, S., Westerhoff, H. V. & van Dam, K. (1992), Synchrony and mutual stimulation of yeast cells during fast glycolytic oscillations, *Journal og General Microbiology* **138**:2219–2227.

Aragón, J. J. & Sols, A. (1991), Regulation of enzyme activity in the cell: effect of enzyme concentration, *FASEB J.* **5**:2945–2950.

Ausubel, F. M., Brent, R., Kingston, R. E., Moore, D. D., Seidman, J. G., Smith, J. A. & Struhl, K. (eds.) (1996), *Current Protocols in Molecular Biology*, vol. 2, chap. 13, John Wiley & Sons.

Azam, F. & Kotyk, A. (1969), Glucose-6-phosphate as regulator of monosaccharide transport in baker's yeast, *FEBS Letters* **2**:333–335.

Babul, J., Clifton, D., Kretschmer, M. & Fraenkel, D. G. (1993), glucose Metabolism in *Escherichia coli* and the Effect of Increased Amount of Aldolase, *Biochemistry* **32**:4685–4692.

Baier, G., Ørsnes, H. & Degn, H. (1999), Complex Dynamics in a Model of Glycolysis is due to Regulation by Fructose-2,6-bisphosphate (submitted).

Bakker, B. (1993), *The Mutual Synchronization of glycolytic Oscillations in intact Yeast Cells*, Master's thesis, E.C. Slater Institute, University of Amsterdam.

Bartholomew, J. W. & Mittwer, T. (1953), Demonstration of Yeast Bud Scars with the Electron Microscope, *J. Bact.* **65**:272–275.

Becker, J.-U. & Betz, A. (1972), Membrane Transport as Controlling Pacemaker of Glycolysis in *Saccharomyces Carlsbergensis*, *Biochim. Biophys. Acta* **274**:584–597.

Benevolensky, S. V., Clifton, D. & Fraenkel, D. G. (1994), The Effect of Increased Phosphoglucose Isomerase on Glucose Metabolism in *Saccharomyces cerevisiae*, *J. Biol. Chem.* **269**:4878–4882.

Betz, A. (1973), Kinetics of Yeast Phosphofructokinase and the glycolytic oscillator, in Chance, B., Pye, E. K., Ghosh, A. & Hess, B. (eds.), *Biological and Biochemical Oscillators*, pp. 221–228, Academic Press, New York.

Betz, A. & Becker, J. U. (1975), Phase Dependent Phase Shifts Induced by Pyruvate and Acetaldehyde in Oscillating NADH of Yeast Cells, *J. interdiscipl. Cycle Res.* **6**:167–173.

Betz, A. & Chance, B. (1965a), Influence of Inhibitors and Temperature on the Oscillations of Reduced Pyridine Nucleotides in Yeast Cells, *Arch. Biochem. Biophys.* **109**:579–584.

Betz, A. & Chance, B. (1965b), Phase Relationship of Glycolytic in Yeast Cells with Oscillatory Metabolic Control, *Arch. Biochem. Biophys.* **109**:585–594.

Betz, A. & Hinrichs, R. (1968), Incorporation of Glucose into an Insoluble Polyglycoside during Oscillatory Controlled Glycolysis in Yeast Cells, *Eur. J. Biochem.* **5**:154–157.

Bier, M., Teusink, B., Kholodenko, B. N. & Westerhoff, H. V. (1996), Control analysis of glycolytic oscillations, *Biophysical Chemistry* **62**:15–24.

Blazquez, M. A., Langunas, R., Gancedo, C. & Gancedo, J. M. (1993), Trehalose-6-phosphate, a new regulator of yeast glycolysis that inhibits hexokinases, *FEBS Lett.* **329**:51–54.

Boiteux, A. & Hess, B. (1973), Control Mechanism of Glycolytic Oscillations, in Chance, B., Pye, E. K., Ghosh, A. & Hess, B. (eds.), *Biological and Biochemical Oscillators*, pp. 243–252, Academic Press, New York.

Boiteux, A., Markus, M., Plesser, T. & Hess, B. (1983), *Biochem. J.* **211**:63.

Brindle, K. & Krikler, S. (1985), ^{31}P-NMR saturation transfer measurements of phosphate consumption in *Saccharomyces cerevisiae*, *Biochim. Biophys. Acta* **847**:285–292.

Cai, J., Pietzsch, M., Theobald, U. & Rizzi, M. (1996), Fast purification and kinetic studies of the glycerol-3-phosphate dehydrogenase from the yeast *Saccharomyces cerevisiae*, *J. Biotechnology* **49**:19–27.

Chance, B., Estabrook, R. W. & Ghosh, A. (1964), Damped Sinusoidal Oscillations of Cytoplasmic Reduced Pyridine Nucleotide in Yeast Cells, *Biochemistry* **51**:1244–1251.

Chance, B., Williamson, G., Lee, I. Y., Mela, L., DeVault, D., Ghosh, A. & Pye, E. K. (1973), Synchronization Phenomena in Oscillations of Yeast Cells and Isolated Mitochondria, in Chance, B., Pye, E. K., Ghosh, A. & Hess, B. (eds.), *Biological and Biochemical Oscillators*, pp. 285–300, Academic Press, New York.

Chou, H.-F., Berman, N. & Ipp, E. (1992), Oscillations of lactate released from islets of Langerhans: evidence for oscillatory glycolysis in β-cells, *Am. J. Physiol.* **262**:E800–E805.

Civelek, V. N., Deeney, J. T., Fusonie, G. E., Corkey, B. E. & Tornheim, K. (1997), Oscillations in Oxygen Consumption by Permeabilized Clonal Pancreatic β-Cells (HIT) Incubated in an Oscillatory Glycolyzing Muscle Extract. Roles of Free Ca^{2+}, Substrates, and the ATP/ADP Ratio, *Diabetes* **46**:51–56.

Cunningham, B. A., Deeney, J. T., Bliss, C. R., Corkey, B. E. & Thornheim, K. (1996), Glucose-induced oscillatory insulin secretion in perifused rat pancreatic islets and clonal β-cells (HIT), *Am. J. Physiol.* **271**:E702–E710.

Das, J., Timm, H., Busse, H.-G. & Degn, H. (1990), Oscillatory CO_2 Evolution in Glycolysing Yeast Extracts, *Yeast* **6**:255–261.

Davis, S. E. C. & Brindle, K. M. (1992), Effect of Overexpression of Phosphofructokinase on Glycolysis in the Yeast *Saccharomyces cerevisiae*, *Biochemistry* **31**:4729–4735.

Duysens, L. N. M. & Amesz, J. (1957), Fluorescence spectrophotometry of reduced phosphopyridine nucleotides in intact cells in the near-ultraviolet and visible region, *Biochim. Biophys. Acta* **24**:19–26.

Edwards, C. H. J. & Penney, D. E. (1988), *Elementary Linear Algebra*, Prentice-Hall, Englewood Cliffs, New Jersey.

Eschrich, K., Schellenberger, W. & Hofmann, E. (1983), Sustained Oscillations in a Reconstituted Enzyme System Containing Phosphofructokinase and Fructose 1,6-Bisphosphatase, *Arch. Biochem. Biophys.* **222**:657–660.

Fell, D. (1997), *Understanding the Control of Metabolism*, Portland Press, London.

Field, R. & Noyes, R. M. (1972), Oscillations in chemical systems. II. Through analysis of temporal oscillation in the bromate-cerium-malonic acid system, *J. Am. Chem. Soc.* .

François, J., van Schaftingen, E. & Hers, H.-G. (1984), The mechanism by which glucose increases fructose 2,6-bisphosphate concentration in *Saccharomyces cerevisiae*, *Eur. J. Biochem.* **145**:187–193.

Frenkel, R. (1968), Control of Reduced Diphosphopyridine Nucleotide Oscillations in Beef Heart Extracts. II. Oscillations of Glycolytic Intermediates and Adenine Nucleotides, *Arch. Biochem. Biophys.* **125**:157–165.

Ghosh, A. & Chance, B. (1964), Oscillations of Glycolytic Intermediates in Yeast Cells, *Biochem. Biophys. Res. Commun.* **16**:174–181.

Ghosh, A. K., Chance, B. & Pye, E. K. (1971), Metabolic Coupling and Synchronization of NADH Oscillations in Yeast Cell Populations, *Arch. Biochem. Biophys.* **145**:319–331.

God (17,000,000,000 years BP.), The Universe, unpublished results.

Goffeau, A., Barrell, B. G., Bussey, H., Davis, R. W., Dujon, B., Feldmann, H., Galibert, F., Hoheisel, J. D., Jacq, C., Johnston, M., Louis, E. J., Mewes, H. W., Y., Y. M., Philippsen, P., Tettelin, H. & Oliver, S. G. (1996), Life with 6000 genes, *Science* **274**:546, 563–567.

Goldbeter, A. (1996), *Biochemical Oscillations and Cellular Rhythms*, Cambridge University Press, Cambridge.

Grospietsch, T., Drong, K. & Lamprecht, I. (1995), Experimental data on the energetic flux during glycolytic oscillations in yeast extracts, *Experientia* **51**:117–120.

Hansen, E. C. (1886), Recherches sur la physiogie et la morphologie des ferments alcoholiques V. Méthodes pour obtenir des cultures pures de *Saccharomyces* et de microorganismes analogues., *Comptes Rendus des Travaux du Laboratorie Carlsberg, Séries Physiologie* **2**:92–105.

Haworth, R. S., Lemire, B. D., Crandall, D., Cragoe Jr., E. J. & Fliegel, L. (1991), Characterisation of proton fluxes across the cytoplasmic membrane of the yeast *Saccharomyces cerevisiae*, *Biochim. Biophys. Acta* **1098**:79–89.

Heinisch, J. (1986), Isolation and characterization of the two structural genes coding for phosphofructokinase in yeast, *Mol. Gen. Genet.* **202**:75–82.

Hess, B. & Boiteux, A. (1968), Mechanism of Glycolytic Oscillation in Yeast, I, *Hoppe-Seyler's Z. Physiol. Chem.* **349**:1567–1574.

Hess, B., Boiteux, A. & Krüger, J. (1969), Cooperation of Glycolytic Enzymes, *Adv. Enzyme Regul.* **7**:149–167.

Hess, B., Kleinhans, H. & Kuschmitz, D. (1973), Component Structure of Oscillating Glycolysis, in Chance, B., Pye, E. K., Ghosh, A. & Hess, B. (eds.), *Biological and Biochemical Oscillators*, pp. 253–267, Academic Press, New York.

Hocker, C. G., Epstein, I. R., Kustin, K. & Tornheim, K. (1994), Glycolytic pH oscillations in a flow reactor, *Biophys. Chem.* **51**:21–35.

Hoffmann, M. (1999), *Glycolyseoscillationer i gærekstrakt*, Master's thesis, University of Copenhagen.

Holtzclaw, H. F. J., Robinson, W. R. & Odom, J. D. (1991), *General Chemistry*, chap. 29, p. 922, D.C. Heath and Company, 9th edn.

Hynne, F., Sørensen, P. G. & Møller, T. (1993a), Complete optimization of models of the Belousov-Zhabotinsky reaction at a Hopf bifurcation, *J. Chem. Phys.* **98**:219–230.

Hynne, F., Sørensen, P. G. & Møller, T. (1993b), Current and eigenvector analyses of chemical reaction networks at Hopf bifurcations, *J. Chem. Phys.* **98**:211–218.

Hynne, F., Sørensen, P. G. & Nielsen, K. (1990), Quenching of chemical oscillations: General theory, *J. Chem. Phys.* **92**:1747–1757.

Ibsen, K. H. & Schiller, K. W. (1967), Oscillations of nucleotides and glycolytic intermediates in aerobic suspensions of Erlich ascites tumor cells, *Biochem. Biophys. Acta* **131**:405–407.

Ipsen, M., Hynne, F. & Sørensen, P. G. (1997), Amplitude Equations and Chemical Reaction-Diffusion Systems, *International Journal of Bifurcation and Chaos* **7**:1539–1554.

Ipsen, M., Hynne, F. & Sørensen, P. G. (1998), Systematic derivation of amplitude equations and normal forms for dynamical systems, *Chaos* **8**:834–852.

Jain, M. K. & Wagner, R. C. (1980), *Introduction to Biological Membranes*, John Wiley & Sons.

von Klitzing, L. & Betz, A. (1970), Metabolic Control in Flow Systems, *Arch. Mikrobiol.* **71**:220–225.

Kosek, J., Sørensen, P. G., Marek, M. & Hynne, F. (1994), Normal Form Analysis of the Belousov-Zhabotinsky Reaction Close to a Hopf Bifurcation, *J. Phys. Chem.* **98**:6128–6135.

Koshland Jr., D. E. (1998), The Era of Pathway Quantification, *Science* **280**:852–853.

Kreuzberg, K. (1978), Interaction of D-Fructose and Fructose 1-Phosphate with Yeast Phosphofructokinase and its Influence on Glycolytic Oscillations, *Biochem. Biophys. Acta* **527**:229–238.

Kreuzberg, K. H. & Betz, A. (1979), Amplitude and Period Length of Yeast NADH Oscillations Fermenting on Different Sugars in Dependence of Growth Phase, Starvation and Hexose Concentratio, *J. interdiscipl. Cycle Res.* **10**:41–50.

Kuramoto, Y. (1975), *Self-entrainment of a populaiton of coupled non-linear oscillators*, vol. 39 of *Lecture Notes in Physics*, pp. 420–422, Springer-Verlag, New York.

Kuramoto, Y. (1984), *Chemical Oscillations Waves and Turbulence*, Springer-Verlag, Berlin.

Lehninger, A. L. (1975), *Biochemistry*, Worth Publishers, 2nd edn.

Lorenzen, T. (1996), *Elaborated quenching analysis of the Ru(bipy)$_3^{2+}$ catalyzed Belousov Zhabotinsky reaction*, Master's thesis, University of Copenhagen.

Luyten, K., Albertyn, J., Skibbe, W. F., Prior, B. A., Ramos, J., Thevelein, J. M. & Hohmann, S. (1995), *Fps1*, a yeast member of the *MIP* family of channel proteins is a facilitator of glycerol uptake and efflux and is inactive under osmotic stress, *EMBO Journal* **14**:1360–1371.

Mair, T. & Müller, S. C. (1996), Travelling NADH and Proton Waves during Oscillatory Glycolysis *in Vitro*, *J. Biol. Chem.* **271**:627–630.

Mathews, C. K. & van Holde, K. E. (1990), *Biochemistry*, The Benjamin/Cummings Publishing Company, Redwood City.

Matthews, P. C., Mirollo, R. E. & Strogatz, S. H. (1991), Dynamics of a large system of coupled nonlinear oscillators, *Physica D* **52**:293–331.

Mihaliuk, E., Skødt, H., Hynne, F., Sørensen, P. G. & Showalter, K. (1999), Normal Modes for Chemical Reactions from Time Series Analysis (submitted).

Nielsen, A. E. (1994), *Kemiske data*, F.A.D.L.'s forlag, 4th edn.

Nielsen, K., Sørensen, P. G. & Hynne, F. (1997), Chaos in Glycolysis, *J. Theor. Biol.* **186**:303–306.

Nielsen, K., Sørensen, P. G., Hynne, F. & Busse, H.-G. (1998), Sustained oscillations in glycolysis: an experimental and theoretical study of chaotic and complex periodic behavior and of quenching of simple oscillations, *Biophysical Chemistry* **72**:49–62.

O'Rourke, B., Ramza, B. M. & Marban, E. (1994), Oscillations of Membrane Current and Excitability Driven by Metabolic Oscillations in Heart Cells, *Science* **265**:962–966.

O'Rourke, B., Ramza, B. M., Romashko, D. N. & Marban, E. (1995), Metabolic Oscillations in Heart Cells, *Adv. Exp. Med. Biol.* **382**:165–174.

Ott, E. (1993), *Chaos in dynamical systems*, Cambridge University Press, Cambridge.

Perko, L. (1996), *Differential Equations and Dynamical Systems*, Springer-Verlag, New York, 2nd edn.

Prentki, M. (1996), New insights into pancreatic β-cell metaboli signaling in insulin secretion, *Eur. J. Endocrinol.* **134**:272–286.

Press, W. H., Teukolsky, S. A., Vetterling, W. T. & Flannery, B. P. (1992), *Numerical Recipes in Fortran*, Cambridge University Press, Cambridge, 2nd edn.

Pye, E. K. (1969), Biochemical mechanisms underlying the metabolic oscillations in yeast, *Can. J. Botany* **47**:271–285.

Pye, K. E. (1973), Glycolytic Oscillations in Cells and Extracts of Yeast – Some Unsolved Problems, in Chance, B., Pye, E. K., Ghosh, A. & Hess, B. (eds.), *Biological and Biochemical Oscillators*, pp. 269–284, Academic Press, New York.

Richard, P., Bakker, B. M., Teusink, B., van Dam, K. & Westerhoff, H. V. (1996a), Acetaldehyde mediates the synchronization of sustained glycolytic oscillations in populations of yeast cells, *Eur. J. Biochem.* **235**:238–241.

Richard, P., Diderich, J. A., Bakker, B. M., Teusink, B., van Dam, K. & Westerhoff, H. V. (1994), Yeast cells with a specific cellular make-up and an environment that removes acetaldehyde are prone to sustained glycolytic oscillations, *FEBS Letters* **341**:223–226.

Richard, P., Teusink, B., Hemker, M. B., van Dam, K. & Westerhoff, H. V. (1996b), Sustained Oscillations in Free-energy State and Hexose Phosphates in Yeast, *Yeast* **12**:731–740.

Richard, P., Teusink, B., Westerhoff, H. V. & van Dam, K. (1993), Around the growth phase transition *S. cerevisiae*'s make-up favours sustained oscillations of intracellular metabolites, *FEBS Letters* **318**:80–82.

Richter, O., Betz, A. & Giersch, C. (1975), The Response of Oscillating glycolysis to Pertubations in the NADH/NAD System: A Comparison Between Experiments and a Computer Model, *BioSystems* **7**:137–146.

Richter, P. H. & Ross, J. (1981), Concentration Oscillations and Efficiency: Glycolysis, *Science* **211**:715–717.

Rizzi, M., Baltes, M., Theobald, U. & Reuss, M. (1997), In Vivo Analysis of Metabolic Dynamics in *Saccharomyces cerevisiae*: II. Mathematical Model, *Biothechnology and Bioengineering* **55**:592–608.

Rizzi, M., Theobald, U., Querfurth, E., Rohrhirsch, T., Baltes, M. & Reuss, M. (1996), In Vivo Investigations of Glucose Transport in *Saccharomyces cerevisiae*, *Biothechnology and Bioengineering* **49**:316–327.

Rost, T. L., Barbour, M. G., Thornton, R. M., Weier, T. E. & Stocking, C. R. (1984), *Botany: a brief introduction to plant biology*, John Wiley & Sons, New York, 2nd edn.

Schaaff, I., Heinisch, J. & Zimmerman, F. K. (1989), Overproduction of Glycolytic Enzymes in Yeast, *Yeast* **5**:285–290.

Sel'kov, E. E. (1968), Self-oscillations in glycolysis. A simple kinetic model, *Eur. J. Biochem.* **4**:79–86.

Sel'kov, E. E. & Betz, A. (1973), On the Mechanism of Single-Frequency Glycolytic Oscillations, in Chance, B., Pye, E. K., Ghosh, A. & Hess, B. (eds.), *Biological and Biochemical Oscillators*, pp. 197–220, Academic Press, New York.

Siegel, G., Malmsten, M., Klüssendorf, D. & Hofer, H.-W. (1997), Vascular Smooth Muscle, a Multiply Feedback-Coupled System of High Versality, Modulation and Cell-Signaling Variability, *Int. J. Microcirc.* **17**:360–373.

Singlevich, T. E. & Barboriak, J. J. (1971), Pyrazole-induced inhibition of yeast alcohol dehydrogenase, *Biochemical Pharmacology* **20**:2087–2089.

Skødt, H. (1999), *Kinetic Spectrometry*, Master's thesis, University of Copenhagen.

Sørensen, P. G. (1999), Chem, a program package for parsing, integration and continuation of chemical reaction dynamics.

Sørensen, P. G., Hynne, F. & Nielsen, K. (1990), Characteristic modes of oscillatory chemical reactions, *J. Chem. Phys.* **92**:4778–4785.

Stemwedel, J. D., Ross, J. & Schreiber, I. (1995), *Formulation of oscillatory reaction mechanisms by deduction from experiments*, vol. LXXXIX of *Advances in Chemical Physics*, pp. 327–388, John Wiley & Sons.

Strogatz, S. H. (1993), *Norbert Wiener's Brain Waves*, vol. 100 of *Lecture Notes in Biomathematics*, Springer-Verlag.

Strogatz, S. H. (1994), *Nonlinear Dynamics and Chaos*, Addison Wesley, Reading, MA.

Svirbely, W. J. & Roth, J. F. (1953), Carbonyl Reactions. I. The Kinetics of Cyanohydrin Formation in Aqueous Solution, *J. Am. Chem. Soc.* **75**:3106–3111.

Termonia, Y. & Ross, J. (1981), Oscillations and control features in glycolysis: Numerical analysis of a comprehensive model, *Proc. Natl. Acad. Sci. USA* **78**:2952–2956.

Teusink, B. (1993), *Glycolytic oscillations in Yeast*, Master's thesis, E. C. Slater Institute, University of Amsterdam.

Teusink, B., Bakker, B. & Westerhoff, H. V. (1996a), Control of frequency and amplitude is shared by all enzymes in three models for yeast glycolytic oscillations, *Biochem. Biophys. Acta* **1275**:204–212.

Teusink, B., Larsson, C., Diderich, J., Richard, P., van Dam, K., Gustafsson, L. & Westerhoff, H. V. (1996b), Synchronized Heat Flux Oscillations in Yeast Cell Populations, *J. Biol. Chem.* **271**:24442–24448.

Teusink, B., Walsh, M. C., van Dam, K. & Westerhoff, H. V. (1998), The danger of metabolic pathways with turbo design, *TIBS* **23**:162–164.

Theobald, U., Mailinger, W., Baltes, M. & Rizzi, M. (1997), In Vivo Analysis of Metabolic Dynamics in *Saccharomyces cerevisiae*: I. Experimental Observations, *Biothechnology and Bioengineering* **55**:305–316.

Tornheim, K. (1997), Are Metabolic Oscillations Responsible for Normal Oscillatory Insulin Secretion?, *Diabetes* **46**:1375–1380.

Tornheim, K. & Lowenstein, J. M. (1973), The Purine Nucleotide Cycle. III. Oscillations in metabolite concentrations during the operation of the cycle in muscle extracts., *J. Biol. Chem.* **248**:2670–2677.

Viola, R. E., Raushel, F. H., Rendina, A. R. & Cleland, W. W. (1982), *Biochemistry* **21**:1295.

Vukojević, V., Sørensen, P. G. & Hynne, F. (1996), Predictive value of a model of the Briggs-Rauscher reaction fitted to quenching experiments, *J. Phys. Chem.* **100**:17175–17185.

Walker, G. M. (1998), *Yeast Physiology and Biotechnology*, John Wiley & Sons, Chichester.

Walsh, M. C., Smits, H. P., Scholte, M. & van Dam, K. (1994), *J. Bacteriol.* **176**:953–958.

Wang, J., Sørensen, P. G. & Hynne, F. (1995), Transient Complex Oscillations in the Closed Belousov-Zhabotinsky Reaction: Experimental and Computational Studies, *Zeitschrift für Physikalische Chemie* **192**:63–76.

Winfree, A. T. (1967), Biological Rhythms and the Behavior of Populations of Coupled Oscillators, *J. Theor. Biol.* **16**:15–42.

Winfree, A. T. (1970), Integrated View of Resetting a Circadian Clock, *J. Theor. Biol.* **28**:327–374.

Winfree, A. T. (1972), Oscillatory Glycolysis in Yeast: The Pattern of Phase Resetting by Oxygen, *Arch. Biochem. Biophys.* **149**:388–401.

Winfree, A. T. (1980), *The Geometry of Biological Time*, Springer-Verlag, New York.

Wolf, J. & Heinrich, R. (1997), Dynamics of two-component biochemical systems in interacting cells; Synchronization and desynchronization of oscillations and multiple steady states, *BioSystems* **43**:1–24.

Wright, B. E. & Albe, K. R. (1994), *J. Theor. Biol.* **169**:231–241.

Wright, B. E., Butler, M. H. & Albe, K. R. (1992), *J. Biol. Chem.* **267**:3101–3105.

Yuan, Z., Medina, M. A., Boiteux, A., Müller, S. & Hess, B. (1990), The role of fructose 2,6-bisphosphate in glycolytic oscillations in extracts and cells of *Saccharomyces cerevisiae*, *Eur. J. Biochem.* **192**:791–795.